Manipulator Control Using Reduced Order Velocity Observers

by

Mile Erlic

B.A.Sc., Queen's University, Kingston, Ontario, Canada
M.A.Sc., University of Victoria, British Columbia, Canada

A DISSERTATION SUBMITTED IN PARTIAL FULFILLMENT
OF THE REQUIREMENTS FOR THE DEGREE OF
DOCTOR OF PHILOSOPHY

in the
Department of Electrical and Computer Engineering

We accept this dissertation as conforming to the required standard

---

Dr. W.-S. Lu, Supervisor, Dept. of Elec. & Comp. Engr.

Dr. P. Agathoklis, Department Member, Dept. of Elec. & Comp. Engr.

Dr. J. S. Collins, Department Member, Dept. of Elec. & Comp. Engr.

Dr. R. Podhorodeski, Outside Member, Dept. of Mechanical Engr.

Dr. D. Wang, External Examiner, University of Waterloo, Dept. of Elec. & Comp. Engr.

ABSTRACT

This thesis is concerned with the investigation of joint velocity observers as they are applied to robot manipulator trajectory control. Often, only displacement sensors are mounted on a robot manipulator. Yet in order to obtain critically damped, or near critically damped response, joint velocity information is also required for use by the controller. Current techniques available for joint velocity estimation include full-order observers and numerical differentiation of the position signals followed by low-pass filtering. The approach which we take uses the knowledge of the robot manipulator's dynamic equation to formulate a reduced-order velocity observer. The observer presented in this thesis is described by a first-order vector differential equation. The reduction in the order of the differential equation improves the observer over its full-order counterparts by simplifying the dynamic response of the observer and reducing the time delay of the estimation.

The proposed observer is adopted to several robot control schemes. For unconstrained motion control, the observer is used to provide velocity estimates for point-to-point proportional-derivative control and for trajectory-tracking model-based control. The observer was originally designed as a non-adaptive estimator. Subsequently, the observer was made adaptive with respect to a manipulator's partially known or completely unknown dynamic parameters by including a gradient adaptation process. In order to account for constrained motion tasks involving interactions of the end-effector with its environment, the observer was modified by including an additional term compensating for contact forces. For the non-adaptive, adaptive and force control cases the dynamic behaviour of the system consisting of the observer, controller and manipulator has been shown to be stable using Lyapunov stability theory.

To verify the theory, simulations were carried out for the non-adaptive observer, adaptive observer and observer used in force control. The simulations showed the effectiveness of the proposed observers even in the presence of noise contained in the position measurements. Experiments were carried out for unconstrained motion control for both the adaptive and non-adaptive cases. The results of these experiments verified the simulations and confirmed the predicted improvement in position control over conventional methods.

Examiners:

Dr. W.-S. Lu, Supervisor, Dept. of Elec. & Comp. Engr.

Dr. P. Agathoklis, Department Member, Dept. of Elec. & Comp. Engr.

Dr. J. S. Collins, Department Member, Dept. of Elec. & Comp. Engr.

Dr. R. Podhorodeski, Outside Member, Dept. of Mechanical Engr.

Dr. D. Wang, External Examiner, University of Waterloo, Dept. of Elec. & Comp. Engr.

Contents

List of Figures

List of Tables

Acknowledgments

The author of this thesis wishes to acknowledge the support received from the Science Council of British Columbia which has made this work possible through its GREAT scholarship program. The support obtained from the Institute for Robotics and Intelligent Systems is also acknowledged. I am most indebted to my supervisor, Dr. Wu-Sheng Lu, for his patience in guiding me through my work. I also appreciate the many technical critiques that I have received from my colleagues, referees and examiners.

Dedication

To my wife Lily and my sons Martin, Jure and Josip.

Chapter 1

Introduction

The control of robot manipulators has been an area of intense research for approximately two decades. The research has proliferated and several branches have developed. Robot control can be roughly divided into position control and force control. In the former the robot end-effector is not constrained by an environment, whereas in the latter the motion of the robot end-effector is constrained in one or more directions. In both position and force control, model-based and non-model based control schemes have been proposed. Controllers have been made adaptive, non-adaptive and robust. For all classes of control a common theme has been the need for displacement and velocity information to obtain critically damped or near critically damped response. Recently, some researchers have presented works which eliminate the need to measure joint velocities yet maintain the advantages held by full state controllers. In this thesis a method is proposed where good tracking results are achieved without using velocity measurements.

Eliminating velocity measurements leads to several benefits. First, the mechanical mounting of an additional set of sensors is eliminated leading to a reduction in costs.

Second, system robustness is improved due to a smaller number of sensors, smaller number of data conversion channels and less wiring - all of which are prone to failure.

In this thesis we propose the reduced-order observer as a means to estimate joint velocities for use in control. The observer uses the nonlinear model of the manipulator together with joint position signals to estimate smooth joint velocities. We also propose an adaptive version of the observer which is used in adaptive control. Additionally, the observer is adapted to force control for applications where the robot comes into contact with its environment.

In what follows a short review on observers and how they are used in control will be given. Since the difference between the observer-controllers proposed in this thesis and those proposed elsewhere is the reduction in the order of the observer, some well established differences between full-order observers and reduced-order observers will be given.

1.1 Background

In the control of a plant or process it is often necessary to have access to all system state variables for suitable feedback regulation [33]. Where it is physically possible and economically justifiable, all the system's states can be measured with commercially available sensors.

Situations arise, however, which inhibit full state measurement. In some applications, the required sensors may be prohibitively expensive. In other applications signals provided by the sensors may be contaminated by electrical noise, quantization 'noise' or other adverse anomalies. It may also occur that the required sensor technology has not yet been developed and direct measurement of the state variables is not physically possible. In all of these situations alternate methods for obtaining some or all system states must be

found.

With the cost of real-time numerical computation on the decrease it is suitable to ask whether numerical techniques may be used for the *estimation* of state variables in lieu of direct measurement. If numerical state reconstruction is feasible then the need for certain sensors may be eliminated, leading to a reduction in overall system costs. In the case where noisy transducers are used, the feasibility of conventional analog and digital filtering must be determined. If filtering leads to unacceptable time delays then alternate approaches must be taken. In this thesis we use a mathematical construction called an *observer* [48] to provide system state estimates, eliminating the need for some sensors and conventional filtering.

An observer is a mathematical construction which uses the inputs and outputs of a system as well as the system's model and a stabilizing term to reconstruct the state variables of the system. It must be noted that the bandwidth of an observation process can be made wider than the bandwidth of the process being observed. This is a positive feature of the observer leading to small or zero delays for the reconstruction of state variables. The implementation of a state observer employs real-time analog or numerical simulation to produce these estimates.

The observer as an engineering concept has wide use and can be applied to mechanical, electrical and chemical processes among others. In this thesis, however, the observer under study is used strictly for robot trajectory control. Hence, we restrict our attention to observers and controllers (observer-controllers) as they are applied to robot manipulator position and force control problems.

The state variables of a manipulator undergoing trajectory tracking consist of the joint displacements and joint velocities. As a consequence, a robot having n joints has $2n$ state variables. The joint displacements can be measured with a variety of sensor technologies including potentiometers, hall-effect sensors and optical encoders. The signals obtained

with these sensors are of relatively high standard and filtering is typically not required.

The most common device available for direct measurement of joint velocities is the tachogenerator. These sensors produce in addition to the actual velocity signal an appreciable noise component. One may consider analog or digital finite impulse response (FIR) or infinite impulse response (IIR) filters to smooth the tachogenerator signal; however, in so doing phase delays may be introduced leading to possibly unstable tracking.

Manipulator trajectory tracking requires that the measurements obtained with the displacement and velocity sensors be used in a feedback regulator. A variety of feedback regulators can be used. Whether the feedback regulators are model based [8] non-model based [5], [59], [42], adaptive [17], [58], [46] or non-adaptive they all require the full state of the system in their feedback loops. The accuracy of control nearly always depends on the magnitude of gains used. The higher the gains - the lower the tracking errors. If signals provided by sensors are inherently noisy then large feedback gains lead to control signals having large amounts of chatter. In the case of a robot manipulator, the control signal is the torque applied to the actuators.

If the actuator torques chatter, several outcomes may be encountered. One possible outcome is that the energy of chatter is sufficiently small and the robot actuators absorb the energy in much the same way as a low-pass filter. Alternately, the energy generated may be large enough to excite some of the natural frequencies of the robot structure. The unstable behaviour might subsequently lead to unacceptable transient performance or catastrophic electrical or mechanical failure.

Since the position signals generated by optical encoders, potentiometers and hall effect sensors are typically smooth, high position gains can be applied in the feedback loop of a regulator. Direct measurement of joint velocities with tachogenerators, on the other hand, leads to much noise and large velocity gains in the feedback loop are not

possible. One may incorrectly assume that differentiation of high standard position signals would lead to *clean* velocity estimates for use in feedback. Yet it is a well known fact that the differentiation of signals which contain even the smallest quantities of noise can lead to derivatives containing large noise energy. Hence the differentiation of optical encoder, potentiometer or hall effect sensor signals may lead to noisy and unusable velocity estimates.

In the two sections which follow we outline the concepts of the full-order observer and reduced-order observer for linear systems. Examples of the two observers are provided as they are applied to a linear servo-actuator.

1.1.1 Full-Order Observers for Linear Systems

A single-input single-output plant or system can be modeled as a linear process described by the following first-order vector differential equation

$$\dot{x} = Ax + bu \tag{1.1a}$$

$$y = cx \tag{1.1b}$$

where $x \in \Re^n$ is the state of the system, $y \in \Re$ is the output and $u \in \Re$ is the input. Equation (1.1) is a state-space representation of the system. To stabilize the system one can use a closed-loop state feedback controller, i.e.

$$u = -k^T x \tag{1.2}$$

Application of (1.2) to the system leads to

$$\dot{x} = \left(A + bk^T\right)x$$

which can always be made stable if (A,b) is controllable [33]. Sometimes it is not possible to measure all the states of a system directly. In these situations an alternate technique must be found in order to make feedback regulation possible. One technique available to accomplish this is through linear state observers [44], [45].

In simple terms an observer is a mathematical constructions which simulates a process in real-time and by so doing can provide a regulator with state information for use in feedback control even though some of the states cannot be measured directly. The notion of observability detects for conditions in which it is mathematically feasible to reconstruct the full system state. If a system (c,A) is observable, then the state of the system can be found by on-line state reconstruction [33]. Assuming an observable system, the following full-order state observer can help provide estimates of the system's state

$$\dot{\hat{x}} = A\hat{x} + bu + l\left[y - c\hat{x}\right] \qquad , \qquad \hat{x}(0) = \hat{x}_0 \tag{1.3}$$

The estimate of the state $x \in \Re^n$ is given by $\hat{x} \in \Re^n$. The difference between the observed states and the actual states is obtained by subtracting (1.3) from the system model (1.1), i.e.

$$\dot{\tilde{x}} = (A - lc)\tilde{x} \quad , \qquad \tilde{x}(0) = x_0 - \hat{x}_0$$

where $\tilde{x} = x - \hat{x}$ is the observer error. The asymptotic stability of the state matrix $A - lc$ is guaranteed by proper selection of the observer gain $l \in \Re^n$ in (1.3).

The implementation of the full state observer is accomplished by integrating (1.3), i.e.

$$\hat{x}(t) = \hat{x}(t_0) + \int_{t_0}^{t} A\hat{x}(t) + bu(t) + l[y(t) - c\hat{x}(t)]dt$$

A recursive discrete formulation of the observer is given as follows

$$\hat{x}(i) = [I + \Delta(A - lc)]\hat{x}(i-1) + \Delta[bu(i-1) + ly(i-1)]$$

where Δ is the integration time interval.

Example 1.1: ***Nicosia and Tomei's Observer applied to a linear servo-actuator***

For this example we investigate the construction of a full-order state observer for a linear servo-actuator. The observer output provides joint position and velocity estimates. The observer presented here is a special case of the full-state manipulator velocity observer in [47].

The open-loop dynamic equation for a linear servo-actuator is given by

$$m\ddot{q} + b\dot{q} = u \tag{1.4a}$$

where m is the effective mass, b is the viscous friction coefficient and u is the input torque. The linear velocity of the actuator is denoted by $\dot{q}$. A state-space representation of (1.4a) is given by

$$\begin{bmatrix} \dot{x}_1 \\ \dot{x}_2 \end{bmatrix} = \begin{bmatrix} 0 & 1 \\ 0 & c/m \end{bmatrix} \begin{bmatrix} x_1 \\ x_2 \end{bmatrix} + \begin{bmatrix} 0 \\ 1/m \end{bmatrix} u \tag{1.4b}$$

where $x_1 = q$ is the position and $x_2 = \dot{q}$ is the velocity. For observer gain $l^T = \begin{bmatrix} k_d & k_p \end{bmatrix}$, the full-state observer is given by

$$\begin{bmatrix} \dot{\hat{x}}_1 \\ \dot{\hat{x}}_2 \end{bmatrix} = \begin{bmatrix} 0 & 1 \\ 0 & c/m \end{bmatrix} \begin{bmatrix} \hat{x}_1 \\ \hat{x}_2 \end{bmatrix} + \begin{bmatrix} 0 \\ 1/m \end{bmatrix} u + \begin{bmatrix} k_d \\ k_p \end{bmatrix} \left(y - \begin{bmatrix} 1 & 0 \end{bmatrix} \begin{bmatrix} \hat{x}_1 \\ \hat{x}_2 \end{bmatrix} \right)$$

A block diagram representation of the full-order observer is shown in Fig. 1.1 below.

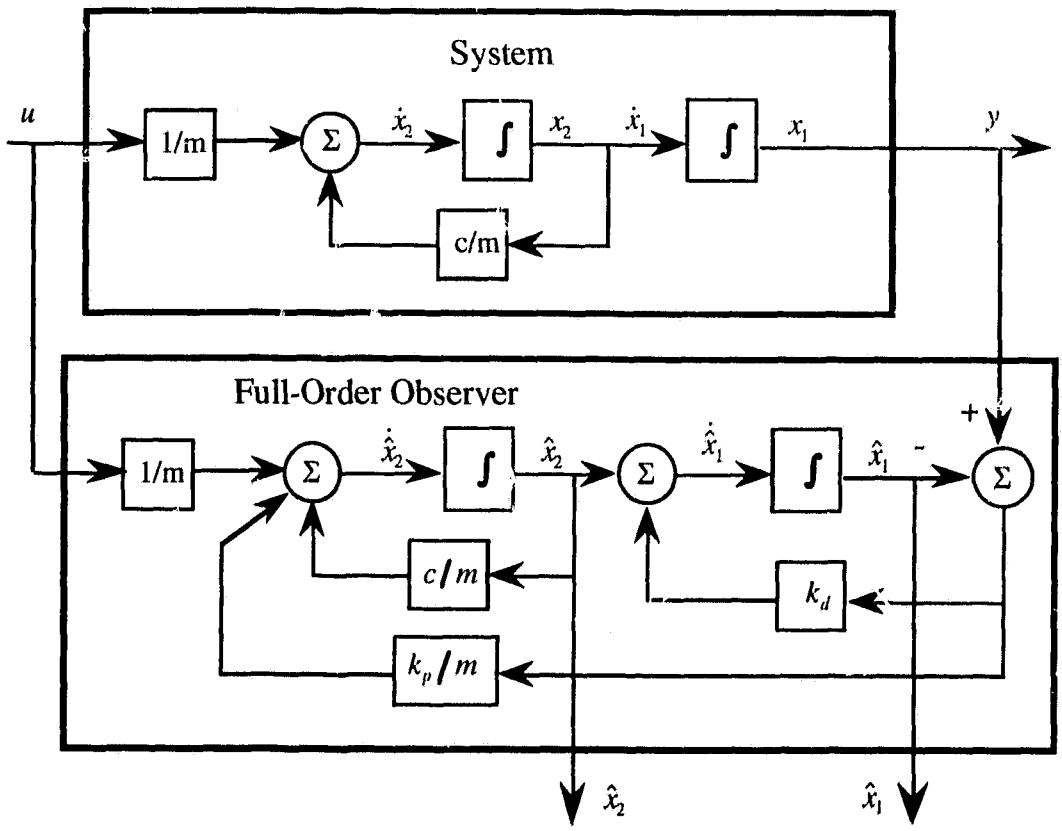

Fig. 1.1: A full-order observer for a linear servo-actuator

1.1.2 Reduced-Order Observers for Linear Systems

Often an observation process is not required to estimate the full state of a system

because some of the states are measured directly. In these situations it may be possible to implement a *reduced-order* observer. This class of observer is a well known matter for linear systems [33] and shall be presented here for completeness.

A linear system can be represented by the following partitioned state-space representation

$$\begin{bmatrix} \dot{x}_n \\ \dot{x}_r \end{bmatrix} = \begin{bmatrix} a_{nn} & c_r \\ b_r & A_r \end{bmatrix} \begin{bmatrix} x_n \\ x_r \end{bmatrix} + \begin{bmatrix} g_n \\ g_r \end{bmatrix} u \tag{1.5}$$

$$y_r = c_r x_r \qquad , \qquad y = x_n$$

where x_n represents states which can be measured and x_r represents states which cannot be measured. The reduced-order observer is based on formulation (1.5) and is given by

$$\dot{\hat{x}}_r = A_r \hat{x}_r + b_r x_n + g_r u + l_r \left(y_r - c_r \hat{x}_r \right) \tag{1.6}$$

In (1.6) quantity y_r is not directly available since it depends on states x_r – a quantity which cannot be measured. However, we can employ from (1.5) the relationship $y_r = \dot{y} - a_{nn} x_n - g_n u$, leading (1.6) to

$$\dot{\hat{x}}_r = A_r \hat{x}_r + b_r x_n + g_r u + l_r \left(\dot{y} - a_{nn} x_n - g_n u - c_r \hat{x}_r \right) \tag{1.7}$$

Implementation of the reduced-order observer is done through integration of (1.7) giving us

$$\hat{x}_r(t) = \hat{x}_r(t_0) + l_r\left[y(t) - y(t_0)\right] \int_{t_0}^{t} b_r x_n + g_r u - l_r\left(a_{nn}x_n + g_n u + c_r \hat{x}_r\right)dt \tag{1.8}$$

A recursive, discrete formulation of (1.8) is given by

$$\hat{x}_r(i) = \left[I + \Delta\left(A_r - l_r c_r\right)\right]x_r(i-1) + l_r\left[y(i) - y(i-1)\right] + \Delta\left[b_r - l_r a_{nn}\right]x_n(i-1) + \Delta\left[g_r - l_r g_n\right]u(i-1)$$

Example 1.2: ***A Reduced-Order Observer applied to a linear servo-actuator***

In this example the linear servo-actuator dynamics described by (1.5) is considered as a candidate for a reduced-order observer. Carrying out modeling with regard to equations (1.4), (1.5) and (1.7), the reduced-order velocity observer for the servo-actuator is given by

$$\dot{\hat{x}}_r = \frac{c}{m}\hat{x}_r + \frac{1}{m}u + l_r\left(\dot{q} - \hat{x}_r\right) \tag{1.9}$$

Implementation of the observer is obtained by integrating (1.9), i.e.

$$\hat{x}_r(t) = \hat{x}_r(t_0) + l_r\left[q(t) - q(t_0)\right] + \int_{t_0}^{t}\left(\frac{c}{m} - l_r\right)\hat{x}_r(t) + \frac{1}{m}u(t)\,dt$$

A discrete implementation of the observer is given by

$$\hat{x}_r(i) = \left[I + \Delta\left(\frac{c}{m} - l_r\right)\right]\hat{x}_r(i-1) + l_r\left[q(i) - q(i-1)\right] + \frac{\Delta}{m}u(i-1)$$

A block diagram of the system and reduced-order observer is shown in Fig. 1.2 below.

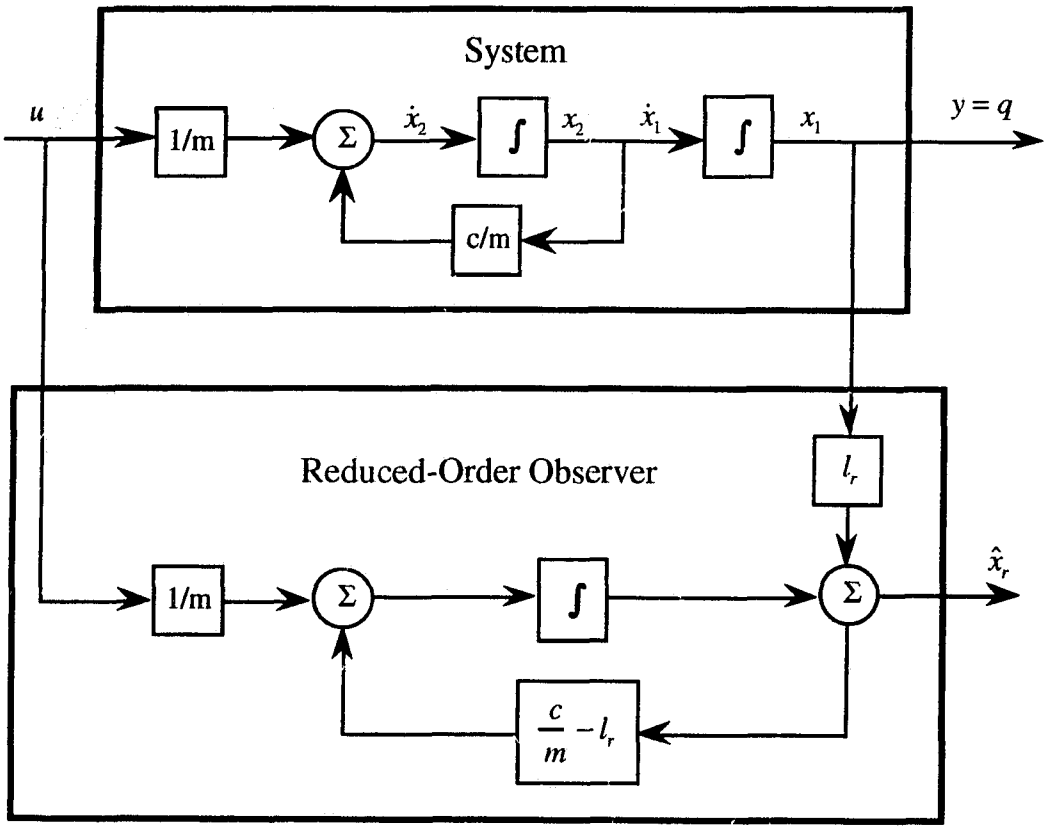

Fig. 1.2: A reduced-order observer for a linear servo-actuator

1.2 Existing Velocity Observers for Manipulators

1.2.1 Non-Adaptive Observers

The design of feedback controllers for robots undergoing unconstrained motions has received a considerable amount of attention in the past two decades. The control problem is complicated by the nonlinear dynamics of a manipulator. As a result a great deal of effort has been spent to help guarantee stable robot operation and control.

The research activity can be grouped roughly into (i) robust non-model based control

(ii) model-based control and (iii) variable structure control. Representative research results in these areas can be found in [5], [59], [42] for non-model based control, [8] for model based control and [56] for variable structure control. The design methods employed vary but the Lyapunov approach, small gain theory and passivity theories are among the more popular methods used. In the early work on robot controllers it was assumed that a clean joint velocity signal would be available for use in control. It was only after experiments were conducted that researchers discovered that the magnitude of the velocity gains used was limited by the noise present in the velocity measurements [58], [36]. As a result the need for filtering, observer implementation or other signal conditioning techniques [9], [64] was established .

The original work on observers for linear systems was written by Luenberger [44] in 1964. Later, systems theory investigators established theoretical results on nonlinear observers. Some of the nonlinear observers employed a nonlinear state variable transformation [39],. [62], [63], [67], [52], [1], [40], [72], [73], [10], [61], [65] yet other methods used sliding surfaces [57]. As far as robotics was concerned, a theoretical foundation had been laid for the design of nonlinear observers for manipulators.

The estimation of a manipulator's joint velocities is a specific application of nonlinear observers. Several velocity observers for rigid-link manipulators were developed in [12], [13], [74], [16], [47] and [11]. In [12], [13] and [74] sliding observers were used which use switching terms in their implementations. A result of the switching terms is chattering in the observed velocity leading possibly to the excitation of the manipulator's unmodelled higher frequency dynamics. In [16], [47], [11] and [47] smooth observers were proposed which produce locally stable observation errors. These use a state-space approach which yields an observer with second order dynamics.

In this thesis a new velocity observer is proposed [21]. A major distinction between the existing velocity observers and the observer proposed here is that in the latter the joint

positions are treated as known variables. Hence the observer can be formulated as first order differential equations without introducing an additional state-space formulation. This is, in spirit, a nonlinear counterpart of the reduced-order observer which is a well understood matter for linear systems [33, p. 28].

1.2.2 Adaptive Observers

Adaptive control has been an area of interest in control theory since the late fifties [34], [69]. A comprehensive list of references can be found in [54], [2]. The need for adaptive control arises because most systems involve a model of considerable complexity for which the system parameters are only partially known or not known at all. Traditional controller design procedures require knowledge of the plant parameters. If the plant parameters are not known then off-line identification needs to be applied. When the parameters have been found they can be used in traditional non-adaptive controller designs. However, most processes have a model whose parameters vary during operation. This is the case for robot manipulators which may handle different tools and payloads leading to changes in the dynamics parameters. In these kind of situations on-line adaptive control must be employed.

Two differing approaches to adaptive control have evolved – these are self tuning control and model-based adaptive control. In self tuning control a non-model based feedback regulator such as a PD-Controller has its gains adjusted according to an established set of performance indices. In model reference adaptive control the model of the system is incorporated into the control strategy. The adaptive process *seeks* the model parameters of the system and uses these to improve the controller. Both self-tuning control and model-based control have been applied to nonlinear systems in general and to robot manipulator control in particular. In this thesis the approach taken to develop the

proposed observers and associated controllers is model-based in nature.

For robot manipulators whose dynamics parameters are perfectly known, the best model-based control method available is the computed torque controller, first proposed in [8]. This controller compensates exactly for the nonlinear dynamics of a robot manipulator and introduces a specified second-order linear dynamics. But, the performance of the computed torque controller depends on a precise knowledge of the dynamic parameters. To obtain these an identification procedure must be followed [4], [30], [6].

Identification is a complex and time consuming endeavor and dynamic parameters are not always available for commercial manipulators. Even for the popular manipulator such as the PUMA-560, for which the dynamic parameters have been accurately determined [6], performance degradation can be expected for variable payloads.

In order to overcome the limitations of the computed torque controller in the presence of unknown parameters and changing loads, controllers using adaptive mechanisms have been proposed [37], [58], [41], [17], [32], [46], [55], [38]. Reviews on adaptive control for manipulators are given in [29] and [49]. In [37], [58], [41], [17], [32], Lyapunov analysis and the special properties of the manipulator dynamics (Section 2.3) are adopted to design controllers which identify the manipulator's link or load parameters. Non-model based adaptive controllers are presented in [46], [55], [38].

The concept of the observer was used to estimate manipulator joint velocities in [11] and [47] where state-space approaches were used that yield observers with second-order dynamics. In [21] a reduced-order manipulator velocity observer was proposed which has first-order dynamics. In these papers, observers have been proposed which assume an exact knowledge of the manipulator's dynamic parameters. In order to accommodate for cases where dynamic parameters are only partly known or are not known at all, an adaptive mechanism is required. In [14] and [15] adaptive observer-controllers have been

proposed that use variable structure compensation. Even though most of the high frequency switching is restricted to the numerical implementation of the observer, the switching might excite unmodeled higher frequency dynamics. In [22], [23] a reduced-order adaptive velocity observer is presented for manipulator trajectory tracking control.

1.2.3 Observers in Force Control

Applying robot manipulators to constrained motion tasks is arguably the most important current challenge in robot control. A popular technique in force control is impedance control [25], [26], [27], [28] in which the robots nonlinear dynamics is replaced by a specified mechanical impedance in Cartesian space. In the hybrid position/force control scheme position and force control is decoupled [24], [51] and separate controllers are designed for each. Other force control techniques are discussed in [50], [71], [53], [66], [70], [68], [43], and [31]. The more sophisticated force controllers require position, velocity and force information for proper operation.

Few velocity observers have been designed for use in force control. In [3] a full-order velocity observer has been designed which employs a nonlinear transformation. For this thesis, the observer reported for motion control in the work of this thesis in [21] has been adopted for constrained motion force control by including an extra term compensating for the end-effector force.

1.3 Objective and Contributions of This Thesis

The objective of this thesis is to provide an improved technique for obtaining manipulator joint velocities that can be used subsequently in manipulator control. The reduced-order velocity observer for manipulators was designed and has been theoretically

evaluated and practically implemented. The objectives of the thesis study were met, leading to the following thesis contributions:

1. A new model-based reduced-order observer is designed for use by a robot manipulator in point-to-point control and in trajectory tracking control. The distinction between the observer developed in this thesis and previous model-based observers is the reduction in the order of the observer leading to improved observer error dynamics and position error dynamics. Conditions for the asymptotic stability of the dynamic system consisting of the observer, controller and robot dynamics are determined and a region of attraction for the observer and controller errors is found using Lyapunov stability analysis.

2. An adaptive version of the proposed reduced-order observer-controller has been designed. The adaptive observer-controller uses the regressor formulation of the robot dynamics to estimate the unknown or partially known dynamic parameters of the manipulator. The updated parameters are injected into the observer and controller to improve the observer velocity estimate and the trajectory-tracking control. A Lyapunov analysis provides local conditions for asymptotic stability of the observer and tracking-error dynamics.

3. The non-adaptive observer-controller is modified for use in constrained motion force control tasks. A Lyapunov stability analysis proves the local asymptotic stability of the observer dynamics, trajectory-tracking control dynamics. The force tracking is also asymptotically stable.

4. Experiments are conducted to verify the theory and implementation of the non-adaptive and adaptive observer-controllers. The experiments are performed on a PUMA-560 manipulator. The second and third joints of the manipulator are actuated and all other joints are held fixed leading to an equivalent two-degree-of-freedom planar manipulator. The observer-controllers were successfully implemented using an IBM compatible 80486 machine at a control update frequency of 250Hz.

5. Simulation studies are carried out for the non-adaptive observer-controller, adaptive observer-controller and observer-controller modified for constrained motion force control. The results of the simulation studies show that the proposed reduced-order observer-controls outperform equivalent control strategies which use the filtered velocity estimates provided by numerical differentiation. The reduced amount of noise in the velocity signals and smaller phase delays allows for larger controller velocity and position gains. Larger gains, as a consequence, lead to smaller tracking errors while incurring less chatter in the control torques.

1.4 Organization of This Thesis

Chapter 2 deals with some preliminary material which is useful to the understanding of the proposed observers and controllers which are presented in latter chapters. The approach taken for the observer and controller designs is model based. Accordingly the understanding of the assumed robot dynamic model is critical and a detailed explanation of the electro-mechanical actuator dynamics, transmission dynamics and rigid-link dynamics has been included. Some simplifying assumptions regarding the dynamic model of the robot have been made.

The dynamic model of the robot is originally developed with respect to a set of

generalized joint coordinates. The manipulator dynamics is then expressed with respect to a set of end-effector Cartesian coordinates which are a useful framework from which to study manipulator force control. The regressor formulation of the dynamics is reviewed and a simple example is given. The regressor formulation of the dynamics is an integral component in the design and application of adaptive observers and controllers. Chapter 2 also outlines a set of useful properties inherent to the dynamic equation of a robot. These set of properties is used in the Lyapunov design process leading to the observers and controllers proposed in this thesis.

Chapter 3 presents a proposed non-adaptive observer which gives smooth estimates of a robot manipulator's joint velocities. The observer is initially presented as a stand alone-velocity estimator. Assuming that the actual joint velocities are bounded it is shown that the proposed observer leads to locally asymptotically stable joint velocity estimates. The observer is them employed to provide a PD-Controller with joint velocities for point-to-point position control. The overall result is a system whose set-point position errors and velocity observation errors tend to zero asymptotically as long as the initial tracking errors and observation errors belong to a predefined region of attraction. The observer is used to provide joint velocity estimates for a model-based trajectory-tracking controller. The theoretical results present a system with locally asymptotically stable observation and tracking errors. Simulations and experiments are presented to support the theoretical findings.

In Chapter 4 an adaptive version of the velocity observer is given. The observer is adaptive with respect to the dynamic parameters of the robot. The observer cooperates with an adaptive controller to generate a control signal which leads to locally asymptotically stable trajectory tracking. A theorem is given which provides sufficient conditions for system stability. Stability is guaranteed if the initial observer, trajectory tracking and parameter estimation errors lie within an acceptable bound. Simulations and

experiments are performed to validate the theoretical findings.

Chapter 5 is concerned with force control. The controller developed in this chapter uses a velocity signal which is generated by a reduced-order observer. The observer is an adaptation of the one given in Chapter 3 where an additional term compensating for the contact force is included in the observer formulation. Stability analysis shows that end-effector Cartesian tracking-errors are asymptotically stable and that actual contact forces approach those which are desired. Simulations provide additional verification of the usefulness of the proposed constrained motion observer-controller.

Chapter 6 concludes the findings of this thesis and discusses possible research topics in robot manipulator control for the future emphasizing control techniques which require fewer sensors than traditional methods.

Chapter 2

Preliminaries

In this chapter, some preliminary topics are covered which will help in the understanding of observer and controller designs in later Chapters. The chapter begins with the detailed derivation of the robot manipulator dynamic equation. The dynamic equation is represented in the standard closed formed format made possible by Lagrangian and Newton-Euler derivations. The dynamics are also expressed using the Regressor formulation and in Cartesian coordinates where an end-effector force is included. Several useful properties of the manipulator dynamics are presented.

2.1 Derivation of the Manipulator Dynamic Model

The dynamics of a rigid link robot manipulator can be thought to consist of two parts: (i) the dynamics of the rigid links and (ii) the dynamics of the actuators. In this section and also in this thesis we restrict our attention to the class of robots having rigid links, direct current (dc) servomotor actuation and gears and belts for transmission.

Since the algorithms introduced by this thesis are classified as model-based algorithms and are based on the dynamic equations which describe manipulator motions and are classified as model-based algorithms, the modeling process of the manipulator dynamics is especially important. Since the model employed by the observer and the controller algorithms in this thesis assume a simplified structure, the simplifying assumptions adopted will be stated clearly. We begin our investigation by introducing the dynamics of a dc servomotor.

2.1.1 Actuator Dynamics

The equivalent electric circuit for a dc-servomotor is shown in Fig. 2.1. The voltage applied to the armature of a dc-servomotor is given by $v(t)$, the armature inductance is l_a, the resistance is r_a, and the back *emf* voltage is given by $v_b = k_b\dot{\theta}_m$ where k_b is the back *emf* constant and $\dot{\theta}_m$ is the angular velocity of the armature and therefore the angular velocity of the motor's output shaft. The current which passes through the armature of the motor is denoted by i_a.

By completing a voltage loop for the circuit shown in Fig. 2.1 the electrical dynamics of the motor is obtained, i.e.

$$v = l_a\frac{di_a}{dt} + r_a i_a + k_b\dot{\theta}_m \tag{2.1}$$

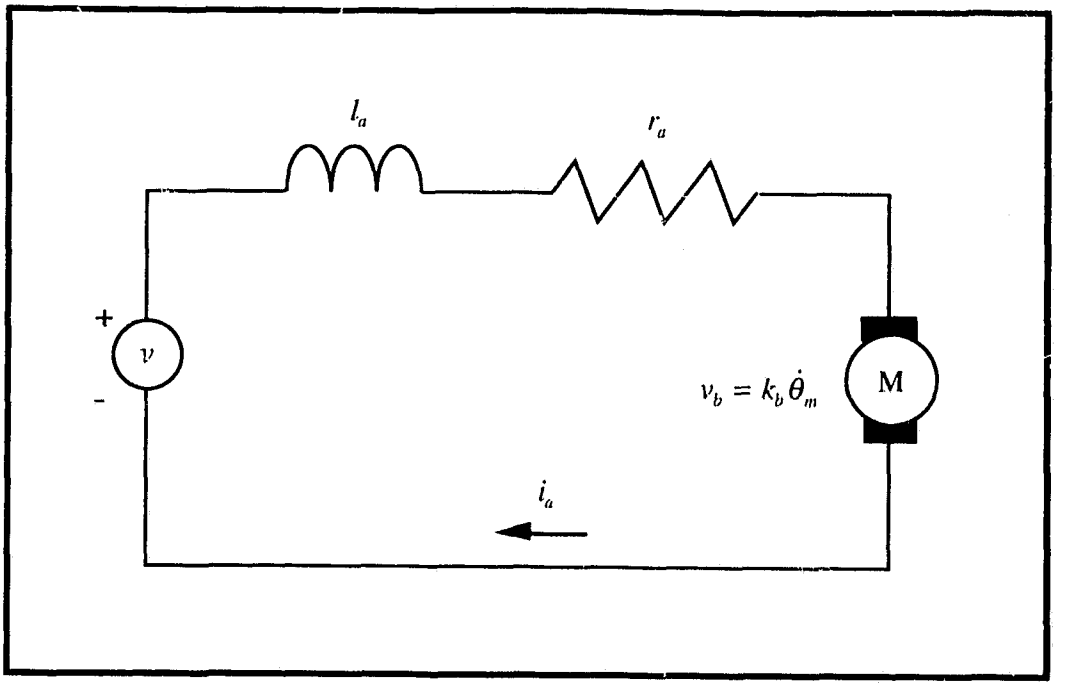

Fig 2.1: Equivalent Electric Circuit for a DC-Servomotor.

The mechanical dynamics of the system is derived by noting that the electro-magnetic interaction between the stator and armature of the motor leads to a torque applied to the armature according to

$$\tau_m = k_t i_a \tag{2.2}$$

where τ_m is the torque applied to the armature of the motor and k_t is the torque constant. The complete dynamics of the motor can now be derived by summing all torques acting on the armature and equating those to the product of armature inertia and acceleration, i.e.

$$\tau_m - k_f \dot{\theta}_m - \tau_l = j_a \ddot{\theta}_m \tag{2.3}$$

where j_a is the armature inertia $k_f\dot{\theta}_m$ is the opposing torque due to viscous friction and τ_l, is the load torque applied directly to the output shaft of the motor.

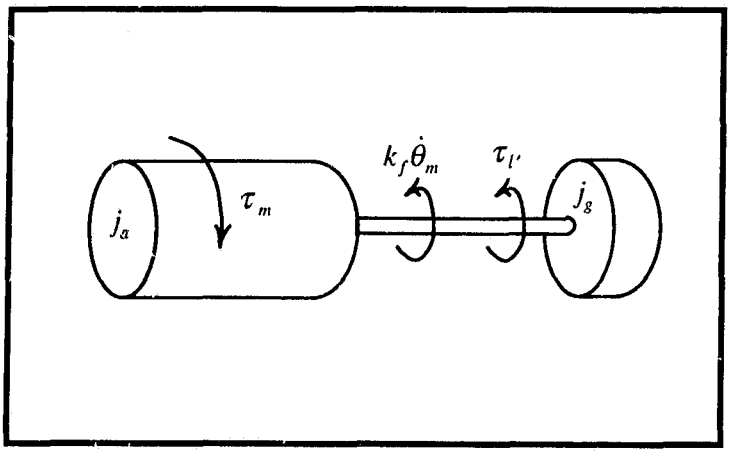

Fig. 2.2: Mechanical Dynamics of a DC-Servomotor.

An important assumption which will be made here is that the term $l_a \frac{di_a}{dt}$ in (2.1) represents an electrical transient which is an order of magnitude quicker than the dynamics of the mechanical system. This leads to the simplified expression

$$v = r_a i_a + k_b \dot{\theta}_m \tag{2.4}$$

In practice the term $l_a \frac{di_a}{dt}$ leads to inductive voltage spikes. These voltage spikes occur whenever abrupt torque disturbances are registered by the armature of the motor. Contemporary motor drive circuits are designed to attenuate these voltage spikes through means of electronic suppressers [35].

We can now employ (2.2) with (2.3) and (2.4) to derive the differential equation of the motor dynamics, i.e.

$$j_a\ddot{\theta}_m + \left(k_f + \frac{k_b k_t}{r_a}\right)\dot{\theta}_m = \frac{k_t}{r_a}v(t) - \tau_l, \tag{2.5}$$

For an n degree-of-freedom manipulator n motors are required. Therefore n equations such as (2.5) formulate the following n dimensional vector equation describing the set of motor dynamics

$$J_a\ddot{\theta}_m + \left(K_f + R_a^{-1}K_b K_t\right)\dot{\theta}_m = R_a^{-1}K_t v(t) - \tau_l, \tag{2.6}$$

Typical dc-servomotors are manufactured as low torque high speed actuators. In robotics, however, the opposite is usually required – high torque low speed actuation. A dc-servomotor can be used to produce higher torques and lower speeds by placing a gear reduction on the motor's output shaft.

2.1.2 Rigid Link Dynamics

The rigid-link dynamic equation of a manipulator is a well known matter [19], [7], [60]. Several formulations can be used to derive the second order equation including the Newton-Euler and the Lagrangian formulations. Both formulations can provide a closed form expression for the dynamics. The rigid link dynamic equation is given by the following vector differential equation

$$\tau_l = M(q)\ddot{q} + C(q,\dot{q})\dot{q} + V\dot{q} + g(q) \tag{2.7}$$

where $q \in \Re^n$ is the generalized vector of joint displacements, $M(q) \in \Re^{n\times n}$ is the rigid link inertia matrix, $C(q,\dot{q})\dot{q} \in \Re^n$ is the vector of Coriolis and centripetal forces, $V \in \Re^{n\times n}$

is a viscous friction coefficient matrix, $g(q) \in \Re^{nx1}$ is a vector of gravitational forces and the vector of joint torques is $\tau_l \in \Re^{nx1}$.

The manipulator dynamic model used throughout this thesis includes actuator, gear and link dynamics. By adding the effect of gear inertia and $\theta_m = Nq$ we get

$$H(q)\ddot{q} + C(q,\dot{q})\dot{q} + F\dot{q} + g(q) = \tau \tag{2.8}$$

where $H(q) = \left(J_a + J_g\right)N^2 + M(q)$, $F = \left(K_f + R_a^{-1}K_bK_t\right)N^2 + V$ and $\tau = NR_a^{-1}K_tv(t)$.

The two assumptions which have been made in the formulation of the dynamics are (i) that the electrical transient due to the armature inductance is small compared to the mechanical time constants of the system and (ii) that the stiffness of the gears and gear shafts is large. These lead to a simplified dynamics given in (2.8).

2.1.3 End-Effector Forces and Cartesian Dynamics

The dynamic equation of an n degree-of-freedom manipulator operating in m-dimensional Cartesian space and subject to external end-effector forces is given by

$$H(q)\ddot{q} + C(q,\dot{q})\dot{q} + F\dot{q} + g(q) = \tau - J^T(q)F_{ext} \tag{2.9}$$

The external force F_{EXT} is distributed among the joints by means of the mapping $\tau_{ext} = J^T(q)F_{ext}$ where the matrix $J(q) \in \Re^{mxn}$ is known as the Jacobian matrix [19 pp. 179].

Several relationships mapping the manipulator's generalized joint space coordinates to the end-effector coordinates will now be given. Forward kinematic equations define the Cartesian end-effector pose for given joint angles and displacements , i.e. $x = \text{kin}(q)$

where $x \in \Re^m$ is the Cartesian pose consisting of position and orientation three tuples and q is the vector of joint displacements. The relationship between the generalized joint velocities and end-effector velocities is given by $\dot{x} = J(q)\dot{q}$ and the relationship between end-effector accelerations and joint space accelerations is given by $\ddot{x} = J(q)\ddot{q} + \dot{J}(q)\dot{q}$. The mappings above are called the kinematic functions and they are summarized as follows:

$$x = \text{kin}(q) \tag{2.10a}$$

$$\dot{x} = J(q)\dot{q} \tag{2.10b}$$

$$\ddot{x} = J(q)\ddot{q} + \dot{J}(q,\dot{q})\dot{q} \tag{2.10c}$$

Assuming the manipulator is not in a mathematically singular configuration, we can write

$$q = \text{invkin}(x) \tag{2.11a}$$

$$\dot{q} = J^{-1}(q)\dot{x} \tag{2.11b}$$

$$\ddot{q} = J^{-1}(q)\left[\ddot{x} - \dot{J}(q,\dot{q})J^{-1}(q)\dot{x}\right] \tag{2.11c}$$

which are the set of inverse kinematic equations.

A nonlinear change of coordinates using (2.11) can transform the manipulator dynamic equation given in (2.8) from joint space to end-effector space, i.e.

$$H_x(q)\ddot{x} + C_x(q,\dot{q})\dot{x} + F_x(q)\dot{x} + g_x(q) = J^{-T}\tau - F_{ext}$$

where

$$H_x(q) = J^{-T}H(q)J^{-1}$$

$$C_x(q,\dot{q}) = J^{-T}\left[C(q,\dot{q}) - H(q)J^{-1}\dot{J}\right]J^{-1}$$

$$F_x(q) = J^{-T}FJ^{-1}$$

$$g_x(q) = J^{-T} g(q)$$

and $J(q)$ full rank has been assumed. Physically $J(q)$ full rank implies (i) that the dimension of the operational variables is equal to that of the generalized variables and (ii) that the manipulator does not lose any motion degrees of freedom due to the configuration of its joints.

2.2 The Regressor Formulation

The dynamics of a robot manipulator is given in (2.9). This formulation is useful in (i) the design of model based trajectory controllers and (ii) in simulation of manipulator motions to obtain $q(t), \dot{q}(t)$ and $\ddot{q}(t)$ for a given torque trajectories $\tau(t)$. The formulation (2.12), although useful in control and simulation, is not practically suited for applying adaptive manipulator control strategies. To accommodate adaptive techniques another formulation is required and it is called the regressor formulation.

The regressor formulation allows for the separation of a manipulator's dynamics into a matrix of functions which multiplies a vector of dynamic parameters as follows

$$H(q)\ddot{q} + C(q,\dot{q})\dot{q} + g(q) = Y(q,\dot{q},\ddot{q})a \tag{2.12}$$

where the regressor matrix is denoted by $Y(q,\dot{q},\ddot{q}) \in \Re^{n \times p}$ and $a \in \Re^p$ is a vector containing p lumped dynamic parameters.

In order to demonstrate the construction of the manipulator regressor, we will investigate the model of a simple manipulator shown in Fig. 2.3.

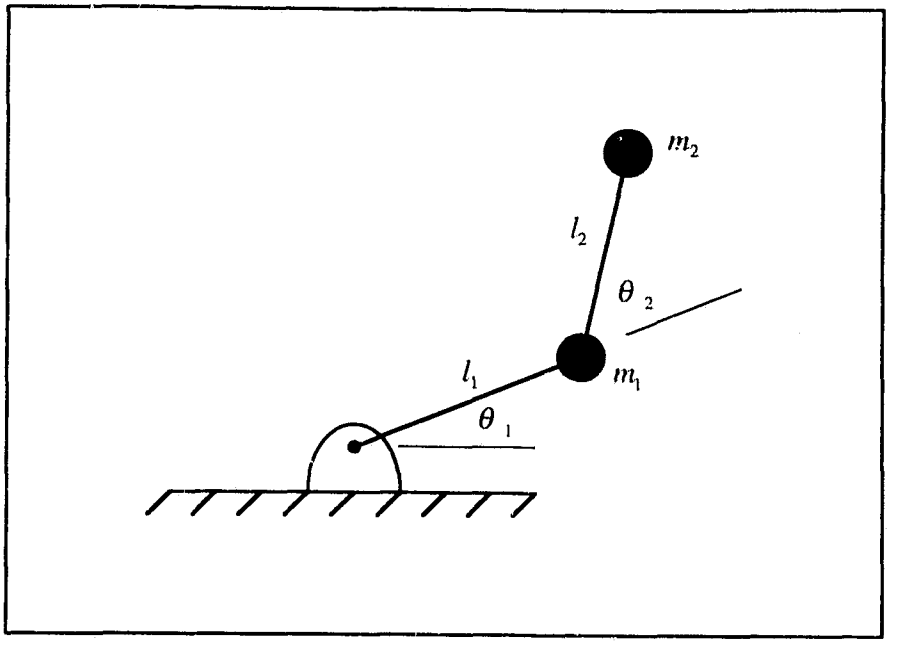

Fig. 2.3: Two Degree-of-freedom planar manipulator

The manipulator consists of two links and two revolute joints. It is assumed that the manipulator shown is actuated by an instantaneous source of joint torques and that friction is negligible. The link's masses are concentrated at the distal end of the links. The closed-form dynamic equation of this manipulator is then given by

$$\tau_1 = m_1 l_1^2 \ddot{\theta}_1 + m_2 l_1^2 \ddot{\theta}_1 + m_2 l_2^2 \left(\ddot{\theta}_1 + \ddot{\theta}_2\right)$$
$$+ m_2 l_1 l_2 \left[c_2\left(2\ddot{\theta}_1 + \ddot{\theta}_2\right) - s_2\left(2\dot{\theta}_1\dot{\theta}_2 + \dot{\theta}_2^2\right)\right] + (m_1 + m_2) g l_1 c_1 + m_2 g l_2 c_{12}$$

and

$$\tau_2 = m_2 l_2^2 \left(\ddot{\theta}_1 + \ddot{\theta}_2\right) + m_2 l_1 l_2 \left(c_2 \ddot{\theta}_1 + s_2 \dot{\theta}_1^2\right) + m_2 g l_2 c_{12}$$

for joints one and two respectively and the notation $s_2 = \sin(\theta_2)$, $c_{12} = \cos(\theta_1 + \theta_2)$ etc. is used. These two equations can be arranged in the usual way and represented as

$$H(q)\ddot{q} + C(q,\dot{q})\dot{q} + g(q) = \tau$$

where $q = \begin{bmatrix}\theta_1 & \theta_2\end{bmatrix}^T$, $\tau = \begin{bmatrix}\tau_1 & \tau_2\end{bmatrix}^T$ and

$$H(q) = \begin{bmatrix} m_1 l_1^2 + m_2\left(l_1^2 + l_2^2 + 2l_1 l_2 c_2\right) & m_2\left(l_2^2 + l_1 l_2 c_2\right) \\ m_2\left(l_2^2 + l_1 l_2 c_2\right) & m_2 l_2^2 \end{bmatrix}$$

$$C(q,\dot{q}) = m_2 l_1 l_2 s_2 \begin{bmatrix} -\dot{\theta}_2 & -\left(\dot{\theta}_1 + \dot{\theta}_2\right) \\ \dot{\theta}_1 & 0 \end{bmatrix}$$

$$g(q) = \begin{bmatrix} m_1 g l_1 c_1 + m_2 g\left(l_1 c_1 + l_2 c_{12}\right) & m_2 g l_2 c_{12} \end{bmatrix}^T$$

The dynamic formulation of primary interest in this section is the regressor formulation. Its construction is accomplished by extracting the dynamic parameters from the matrix equation above and placing them in a vector as follows

$$\begin{aligned} a^T &= \begin{bmatrix} a_1 & a_2 & a_3 & a_4 & a_5 & a_6 \end{bmatrix} \\ &= \begin{bmatrix} m_1 l_1^2 & m_2 l_1^2 & m_2 l_2^2 & m_2 l_1 l_2 & (m_1 + m_2) g l_1 & m_2 g l_2 \end{bmatrix} \end{aligned}$$

The vector a then post multiplies the regressor matrix

$$Y(q,\dot{q},\ddot{q}) = \begin{bmatrix} \ddot{\theta}_1 & \ddot{\theta}_1 & \ddot{\theta}_1 + \ddot{\theta}_2 & c_2\left(2\ddot{\theta}_1 + \ddot{\theta}_2\right) + s_2\left(\dot{\theta}_2^2 + 2\dot{\theta}_1\dot{\theta}_2\right) & c_1 & c_{12} \\ 0 & 0 & \ddot{\theta}_1 + \ddot{\theta}_2 & c_2\ddot{\theta}_1 + s_2\dot{\theta}_1^2 & 0 & c_{12} \end{bmatrix}$$

to give

$$Y(q,\dot{q},\ddot{q})a = \tau$$

which is the regressor formulation.

The regressor formulation is useful in adaptive control because the regressor

$Y(q,\dot{q},\ddot{q}) \in \Re^{n\times p}$ is a matrix whose elements are known functions of time. The parameter vector $a \in \Re^{p}$, on the other hand, can be known, not known at all or just partially known. If the parameters are not known at all or just partially known, an adaptive routine can use the structure of the regressor formulation to obtain estimates of the unknown parameters. A recursive estimation algorithm can be used for this.

Let us now consider the case where some of the parameters are known and others are not. In particular, for the example given let us assume that mass m_1 has been determined and that link lengths l_1 and l_2 have been measured. However, since the mass of the distal end of link two may vary due to end-effector tool changeovers and the grasping of various payloads, we consider m_2 to be an unknown variable.

In this case, the regressor formulation can be written as

$$Y(q,\dot{q},\ddot{q}) = Y_k(q,q,q)a_k + Y_u(q,q,q)a_u = \tau$$

where

$$Y_k = \begin{bmatrix} \ddot{\theta}_1 + g l_1 c_1 \\ 0 \end{bmatrix}$$

with $a_k = m_1$ and

$$Y_u = \begin{bmatrix} l_1^2\ddot{\theta}_1 + l_2^2\left(\ddot{\theta}_1 + \ddot{\theta}_2\right) + l_1 l_2 c_2\left(2\ddot{\theta}_1 + \ddot{\theta}_2\right) - l_1 l_2 s_2\left(2\dot{\theta}_1\dot{\theta}_2 + \dot{\theta}_2^2\right) + g\left(l_1 c_1 + l_2 c_{12}\right) \\ l_2^2\left(\ddot{\theta}_1 + \ddot{\theta}\right) + l_1 l_2\left(c_2\ddot{\theta}_1 + s_2\dot{\theta}_1^2\right) + g l_2 c_{12} \end{bmatrix}$$

with $a_u = m_2$.

2.3 Properties of the Manipulator Dynamics

The manipulator dynamic equation has properties that are useful in the analysis and design of the proposed observer and control strategies. These are summarized in the

following two sections. Section 2.3.1 presents these properties for the joint space formulation of the dynamics and Section 2.3.2 presents the same for the Cartesian space dynamics.

2.3.1 Properties of a Manipulator's Dynamics in Joint Space [47]

Property 1. The manipulator inertia matrix is positive definite, symmetric and bounded, i.e.,

$$m_l \le \|H(q)\| \le m_u \qquad m_l, m_u > 0, \ \forall q \in \Re^n$$

Property 2. The 2-norm of $C(q,x)$ is bounded, i.e.,

$$\|C(q,x)\| \le m_c \|x\| \qquad m_c > 0 \ , \forall q, x \in \Re^n \tag{2.13}$$

Property 3. The matrix of Christoffel symbols, $C(q,x)$ satisfies

$$C(q,x)\xi = C(q,\xi)x \quad \forall q, x, \xi \in \Re^n$$

where the matrix of Christoffel symbols is uniquely defined in [60].

Property 4. $\dot{H}(q) - 2C(q,x)$ is skew symmetric, i.e.,

$$\xi^T \left(\dot{H}(q) - 2C(q,x)\right)\xi = 0 \qquad \forall \xi \in \Re^n$$

Property 5. The manipulator dynamic equation is linear in its parameters of interest, i.e.,

$$H(q)\psi + C(q,\xi)\xi + F\xi + g(q) = Y(q,\xi,\psi)a \tag{2.14a}$$

$$H(q)\psi + C(q,x)\xi + F\xi + g(q) = Y(q,\xi,x,\psi)a \tag{2.14b}$$

$\forall q,\xi,x,\psi \in \Re^n$ and $\forall a \in \Re^p$ where p is the number of dynamic parameters. Matrix Y in (2.14) is known as the manipulator regressor [58].

2.3.2 Properties of a Manipulator's Dynamics in Cartesian Space

Property 6. The manipulator inertia matrix is positive definite, symmetric and bounded, i.e.,

$$m_l \le \|H_x(q)\| \le m_u \qquad m_l, m_u > 0, \ \forall q \in \Re^n$$

Property 7. The 2-norm of $J^{-T}C(q,J^{-1}\dot{x})J^{-1}$ is bounded, i.e.,

$$\left\|J^{-T}C(q,J^{-1}\dot{x})J^{-1}\right\| \le m_c\|\dot{x}\| \qquad m_c > 0\ ,\ \forall q,\dot{x} \in \Re^n$$

Property 8. $\dot{H}_x(q) - 2C_x(q,\dot{q})$ is skew symmetric, i.e.,

$$\xi^T\left(\dot{H}_x(q) - 2C_x(q,x)\right)\xi = 0 \quad \forall \xi \in \Re^n$$

Chapter 3

A Non-Adaptive Velocity Observer

3.1 Introduction

In this section a non-adaptive velocity observer is presented. The observer is introduced as a nonlinear first-order differential equation of joint velocity estimates. The digital implementation of the observer is then addressed and made clear. Simulation and experimental studies show the practical usefulness of the observer when it is used in simple PD-control and in more involved model-based control.

3.2 The Observer

3.2.1 Observer Formulation

The dynamic equation of a robot manipulator as given in (2.8) can be reordered to solve for the joint accelerations explicitly, i.e.,

$$\dot{x} = H^{-1}(q)\left[\tau - C(q,x)x - Fx - g(q)\right] \tag{3.1}$$

where $x = \dot{q}$ and $\dot{x} = \ddot{q}$. One can view (3.1) as a first order nonlinear differential equation in x where q is assumed to be a known function of time and τ is the input. The proposed observer has a structure similar to (3.1) and its differential equation is given by

$$\dot{\hat{x}} = \psi(q,\hat{x},\tau) + K\tilde{x} \tag{3.2a}$$

$$\psi(q,\hat{x},\tau) = H^{-1}(q)\left[\tau - C(q,\hat{x})\hat{x} - F\hat{x} - g(q)\right] \tag{3.2b}$$

where $\hat{x}$ is the velocity estimate which is *observed*. The term $\tilde{x} = x - \hat{x}$ is the error between the observed velocity and the actual velocity, and $K > 0$ is a diagonal gain matrix used to stabilize the observer. The observer as it is presented in (3.2) seems non-implementable because it contains the term $x = \dot{q}$, the actual velocity which is not available. It will be shown later in Section 3.2.2, however, that the numerical integration of (3.2) leads to an implementable realization of the observer.

3.2.2 Implementation of the Observer

In order to realize the observer as a function of time we must integrate (3.2a) over the interval $[t_0, t]$. By doing this and using the estimated initial condition $\hat{x}(t_0)$ we obtain the integral equation

$$\hat{x}(t) = \hat{x}(t_0) + K\left[q(t) - q(t_0)\right] + \int_{t_0}^{t}\left[\psi(q,\hat{x},\tau) - K\hat{x}(t)\right]dt \tag{3.3}$$

The integral equation (3.3), which is equivalent to (3.2) together with initial condition $\hat{x}(t_0)$, defines the observer to be studied further in this thesis. The signal $\hat{x}(t)$, which is

the solution to this vector integral equation, is called the output of the observer or more commonly, the observed velocity.

If the manipulator starts from rest, the initial estimate of the joint velocity vector can be made exact with the assignment $\hat{x}(t_0)=0$ where t_0 is the time when the robot begins motion. If the robot does not start from rest a guess of the initial velocity is made which is denoted by $\hat{x}(t_0)$. Although it is very likely that these initial estimates are not accurate, it will be shown in Section 3.2.3 that the observer being developed here is locally asymptotically stable as long as the errors of the initial velocity estimate belong inside a region of attraction.

Smooth joint velocity estimates can be obtained for a robot manipulator by programming the proposed velocity observer on a microprocessor with a discrete implementation of the integral equation (3.3). If the sampling period of the microprocessor controller is Δ then numerical integration of (3.3) using Euler's first method leads to

$$\hat{x}(i)=\hat{x}(i-1)+K[q(i)-q(i-1)]+\Delta[\psi(i-1)-K\hat{x}(i-1)] \tag{3.4a}$$

where

$$\psi(i-1)=H^{-1}(q(i-1))[\tau(i-1)-C(q(i-1),\hat{x}(i-1))\hat{x}(i-1)-F\hat{x}(i-1)-g(q(i-1))] \tag{3.4b}$$

and i represents the time at $t=i\Delta$. Equations (3.4a) and (3.4b) represent a recursive equation easily written as software computer code.

3.2.3 Stability of the Observer

The dynamics of the observer error is obtained by subtracting (3.2) from (3.1) and

applying property 3 of Section 2.3.1, resulting in

$$H(q)\dot{\tilde{x}} = -C(q,x)\tilde{x} - C(q,\hat{x})\tilde{x} - F\tilde{x} - H(q)K\tilde{x} \tag{3.5}$$

The observer error tends to zero asymptotically as long as the initial velocity estimate $\hat{x}_0$ is within a region of attraction. If this is the case then it is said that equation (3.5) is locally asymptotically stable. The stability of (3.5) is stated formally in the following theorem and a proof can be found in Appendix 3.A.

Theorem 1: For a given $K > 0$, $\tilde{x}(t) \to 0$ exponentially if $\|x(t)\| \le m_v$,

$$\underline{\sigma} > m_c m_v + \beta - m_f$$

where $\underline{\sigma} = \lambda_{\min}\left(KH(q) + H(q)K\right)/2$, $\beta > 0$ is a fixed arbitrary constant, $m_f = \lambda_{\min}(F)$, m_c is given in (2.13), and the initial estimation error $\tilde{x}(0)$ belongs to the ball B_v defined by

$$B_v = \left\{ \tilde{x}(0) \in \Re^n : \|\tilde{x}(0)\| < \frac{1}{m_c}\sqrt{\frac{m_l}{m_u}}\left(\underline{\sigma} + m_f - m_c m_v - \beta\right) \right\}$$

where $m_l = \lambda_{\min}\left(H(q)\right)$ and $m_u = \lambda_{\max}\left(H(q)\right)$.

Remark: The region of attraction B_v, can be made arbitrarily large by increasing the size of K. This makes the stability of the system errors *practically* global.

3.3 Point-to-Point Control Using the Observer

3.3.1 Proportional-Derivative Control

The main motivation behind the development of the velocity observer is the use of its output $\hat{x}(t)$ in control. In this section we study the use of the proposed observer in point-to-point control. Here $q_d \equiv$ constant and the position error is defined as $\tilde{q} = q - q_d$. As such, the joint velocity errors and accelerations can be expressed as $\dot{\tilde{q}} = \dot{q}$ and $\ddot{\tilde{q}} = \ddot{q}$. The proposed controller is a simple PD-controller where actual velocities are replaced by the velocities estimated by the observer (3.5) and gravity compensation is included, i.e.,

$$\tau := -K_p\tilde{q} - K_d\hat{x} + g(q) \tag{3.6}$$

3.3.2 Stability of the Observer and Proportional-Derivative Controller

The dynamics of the control error is derived by subtracting the control torque (3.6) from the dynamic equation (2.8) along with the relationships $\dot{\tilde{q}} = \dot{q} = x$ and $\ddot{\tilde{q}} = \ddot{q}$. The resulting expression is given by

$$H(q)\ddot{\tilde{q}} = -\left(C(q,x)\dot{\tilde{q}} + F\dot{\tilde{q}} + K_d\left(\dot{\tilde{q}} - \tilde{x}\right) + K_p\tilde{q}\right) \tag{3.7}$$

A theorem relating initial conditions, gains and the local asymptotic stability of the observer error (3.5) and the control error (3.7) will be given in the following theorem. The proof to this theorem is located in Appendix 3.B.

Theorem2: For given $K>0$, $K_p=K_p^T>0$, $K_d=k_dI>0$, $\tilde{x}(t),\tilde{q}(t),\dot{\tilde{q}}(t)\to 0$ as $t\to\infty$ if

$$\underline{\sigma}>\frac{k_d^2}{4\left(k_d+m_f\right)}-m_f+\beta$$

and the initial error estimate $e^T(0)=\left[\tilde{x}^T(0)\quad \dot{\tilde{q}}^T(0)\quad \tilde{q}^T(0)\right]$ belongs to the ball B defined by

$$B_1=\left\{\|e(0)\|\in\Re^{3n}:\|e(0)\|<\frac{1}{m_c}\sqrt{\frac{p_l}{3p_u}}\left(\underline{\sigma}+m_f-\frac{k_d^2}{4\left(k_d+m_f\right)}\right)\right\}$$

where $\beta>0$ is a fixed constant, $p_l=\lambda_{\min}(P)$, $p_u=\lambda_{\max}(P)$ with $P=\mathrm{diag}\left(H(q),H(q),K_p\right)$ and $\underline{\sigma}=\lambda_{\min}\left(KH(q)+H(q)K\right)/2$.

3.4 Trajectory Control Using the Observer

3.4.1 The Trajectory Tracking Controller

The velocity signal generated by the proposed observer can also be used in trajectory tracking control. In this section a trajectory tracking controller is presented where it is shown that the resulting position and velocity tracking errors as well as the velocity observer errors tend to zero asymptotically. The trajectory controller is defined as

$$\tau:=H(q)\ddot{q}_d+C(q,\hat{x})\dot{q}_d+F\dot{q}_d+g(q)-K_d\left(\hat{x}-\dot{q}_d\right)-K_p\tilde{q} \tag{3.8}$$

where $\tilde{q}=q-q_d$ is the position tracking error.

3.4.2 Stability of the Observer Plus Trajectory Controller

The dynamics of the position and velocity trajectory errors is obtained by subtracting the control torque (3.8) from the manipulator dynamics (2.8) and by using property 3 of the manipulator dynamics leading to

$$H(q)\ddot{\tilde{q}} = -\left[C(q,x) + K_d + F\right]\dot{\tilde{q}} - \left[C(q,\dot{q}_d) - K_d\right]\tilde{x} - K_p\tilde{q} \tag{3.9}$$

A theorem relating the controller gains, observer gain, initial conditions and the stability of (3.5) and (3.9) will be given presently and the proof to this theorem can be found in Appendix 3.C.

Theorem 3: For given $K > 0$, $K_p = K_p^T > 0$, $K_d = k_d I > 0$, $\tilde{x}(t), \tilde{q}(t), \dot{\tilde{q}}(t) \to 0$ as $t \to \infty$ if

$$\underline{\sigma} > m_c m_d + \frac{\left(k_d + m_c m_d\right)^2}{4\left(k_d + m_f\right)} + \beta - m_f$$

and the initial error estimate $e^T(0) = \left[\tilde{x}^T(0) \quad \dot{\tilde{q}}^T(0) \quad \tilde{q}^T(0)\right]$ belongs to the ball B defined by

$$B = \left\{ \|e(0)\| \in \Re^{3n} : \|e(0)\| < \frac{1}{m_c}\sqrt{\frac{p_l}{3p_u}}\left(\underline{\sigma} + m_f - m_c m_d - \frac{\left(k_d + m_c m_d\right)^2}{4\left(k_d + m_f\right)} \right) \right\}$$

where $\beta > 0$ is a fixed constant, $p_l = \lambda_{\min}(P)$, $p_u = \lambda_{\max}(P)$ with $P = \mathrm{diag}\left(H(q), H(q), K_p\right)$ and $\underline{\sigma} = \lambda_{\min}\left(KH(q) + H(q)K\right)/2$.

3.5 Robot Model and Test Trajectory

3.5.1 The Model

The simulations and experiments considered in this section concern the planar manipulator consisting of the second and third links of the PUMA-560. The dynamic equation of this manipulator is defined by

$$H(q)=\begin{bmatrix} i_{m1}+h_0+2h_1\cos(q_2) & h_2+h_1\cos(q_2) \\ h_2+h_1\cos(q_2) & i_{m2}+h_2 \end{bmatrix}$$

$$C(q,\dot{q})=h_1\sin(q_2)\begin{bmatrix} -\dot{q}_2 & -(\dot{q}_1+\dot{q}_2) \\ \dot{q}_1 & 0 \end{bmatrix}$$

$$F=\begin{bmatrix} f_1 & 0 \\ 0 & f_2 \end{bmatrix} \text{ and } g(q)=\begin{bmatrix} g_1\cos(q_1)+g_2\cos(q_1+q_2) \\ g_2\cos(q_1+q_2) \end{bmatrix}$$

The numerical values of the dynamic parameters were obtained from [6] and are given by: $h_0=2.08\ Kgm^2$, $h_1=0.373\ Kgm^2$, $h_2=0.336\ Kgm^2$, $g_1=37.2\ Nm$, $g_2=8.47\ Nm$, $i_{m1}=4.71\ Kgm^2$ and $i_{m2}=0.83\ Kgm^2$. The friction coefficients f_1 and f_2 were obtained with an integral recursive least squares identification algorithm whose results gave us $f_1=27.6\ Kgm/s$ and $f_2=4.54\ Kgm/s$. These parameters were used for the simulations performed in this section. They were also used in the experimental implementation of the proposed observer and trajectory controller.

3.5.2 The Test Trajectory

In trajectory control the objective is to track a *desired* joint displacement history as closely as possible. For our study the following desired trajectories for joints one and two

were used.

$$q_{1d}(t)=\begin{cases}-2.232t^5+16.74t^4-33.51t^3+0.1333t^2+90 & 0\le t\le 3\\ -2.232\zeta^5+16.74\zeta^4-33.51\zeta^3+0.1333\zeta^2+90 & 3<t\le 6\end{cases} \quad (3.10a)$$

$$q_{2d}(t)=\begin{cases}2.963t^5-22.22t^4+44.44t^3 & 0\le t\le 3\\ 2.963\zeta^5-22.22\zeta^4+44.44\zeta^3 & 3<t\le 6\end{cases} \quad (3.10b)$$

where t and $\zeta=(6-t)$ are in seconds and $q_{1d}(t)$ and $q_{2d}(t)$ are in degrees. Fifth order polynomial trajectories were employed to obtain non-constant displacement, velocity and acceleration trajectories. Computations of (3.10) are provided to the controller as set points every 12 ms. Graphs of these trajectories are shown in Figs. 3.7a and 3.8a for joints one and two respectively. The range of the joint motions and the maximum velocities and accelerations for these trajectories is provided in Table 3.1.

	Joint 1	**Joint 2**
$q_{d\max}$ (deg)	90	120
$\dot{q}_{d\max}$(deg/s)	56.3	75.0
$\ddot{q}_{d\max}\left(\text{deg}/s^2\right)$	57.8	77.0

Table 3.1: Maximum Absolute Displacements, Velocities and Accelerations for the Desired Trajectory

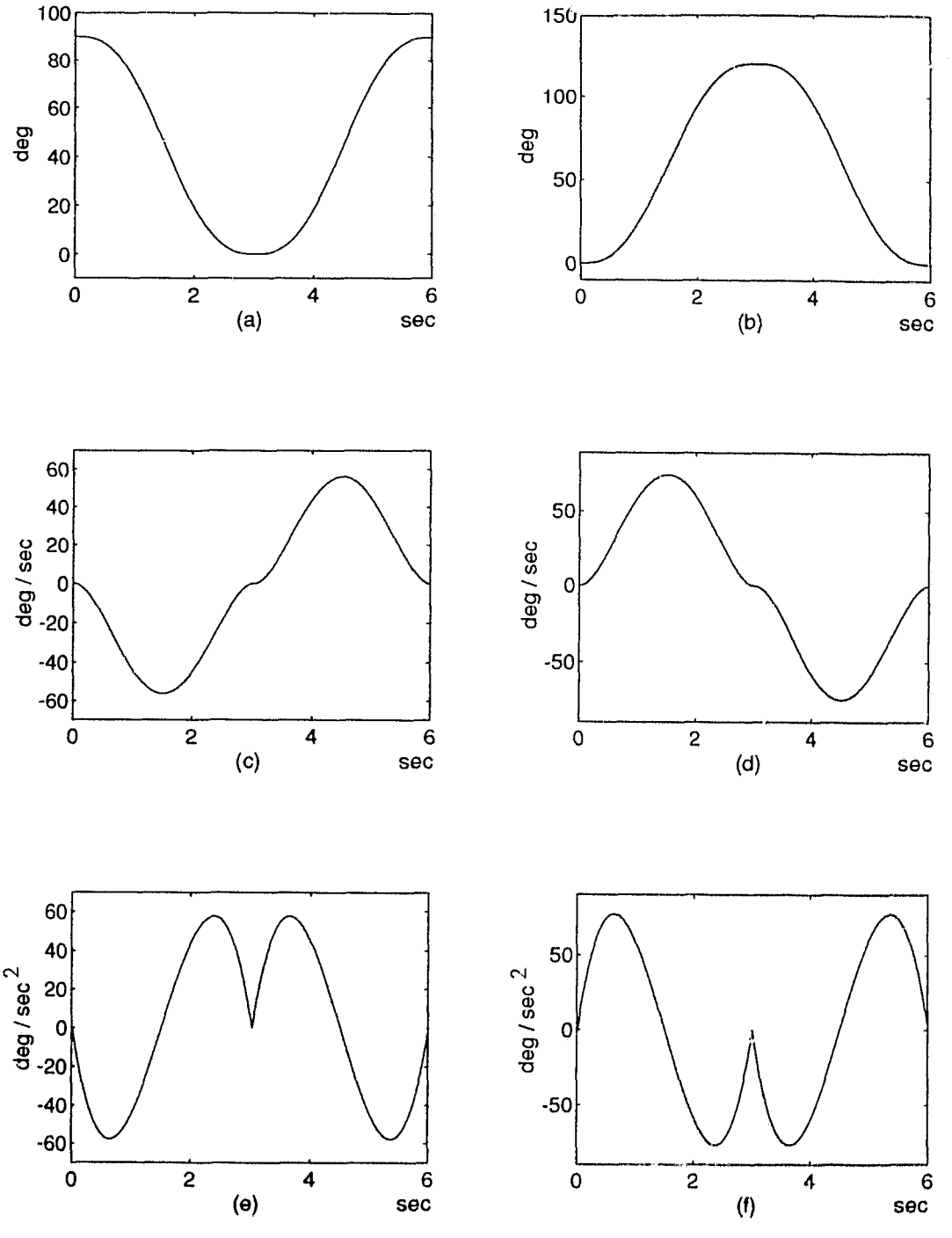

Fig. 3.1: Desired test trajectory (a) joint one position trajectory (b) joint two position trajectory (c) joint one velocity trajectory (d) joint two velocity trajectory, (e) joint one acceleration (f) joint two acceleration.

3.6 Simulation of the Proposed Observer-Controller

In this section, simulations are carried out for two different PD-controllers. One of them obtains its velocity estimate from numerically differentiated filtered position signals. The other one obtains its velocity estimates from the output of the observer proposed in (3.5). The results of the simulation study are provided in Sections 3.6.2 for a PD-Controller using a velocity obtained through filtering. Results for the controller using the observed velocity estimates is provided in 3.6.3. In the next section criteria will be established for our simulation study.

3.6.1 Performance Criteria Adopted for the Simulation Study

In Appendix A, data is presented which shows the levels of measurement noise present in sensors equipped on a certain industrial robot manipulator. The amount of noise in these measurements restricts the magnitude of gains which can be used in controllers. It was found that the factor limiting control accuracy most is chatter in the applied control torque. Large amounts of chatter result from large feedback gains multiplying the noise present in sensor signals.

In order to limit this unwanted and possibly destabilizing behaviour, a restriction was placed on the amount of allowable chatter in the joint torques and hence on the position and velocity gains used. For the simulations the allowable chatter in the control torques was not allowed to exceed 2% of the maximum joint torques available to each of the joints. For the two PUMA-560 joints considered having $\tau_{max} = [\pm 156 \quad \pm 63.3]^T$ Nm the chatter was restricted to $\tau_{chatter} < [6.2 \quad 2.5]^T$ Nm.

3.6.2 PD-Control Using Numerical Differentiation for Joint Velocities

In order to employ a PD-Controller which receives its velocity estimates from numerically differentiated position data, it was necessary to smooth the position signal with a lowpass filter. The noise contained in the position measurements is quantified in Appendix A. Without filtering numerical differentiation would have led to noisy velocity estimates resulting in excessive chattering in the control torque. To alleviate this problem the following filter and PD-controller were used

$$q_f(t) = q_f(t_0) - K_f \int_{t_0}^{t} \left(q_f(\lambda) - q_n(\lambda)\right) d\lambda \tag{3.11a}$$

$$\tau := -K_p(q_n - q_d) - K_d \dot{q}_f + g(q_n) \tag{3.11b}$$

In (3.11a) q_f is the filtered position signal, q_n is the noisy position signal and K_f is a matrix of filter coefficients. For the controller (3.11b), K_p and K_d are the proportional and derivative gain matrices. The digital implementation of (3.11a) is achieved with

$$q_f(i) = q_f(i-1) - \Delta K_f\left[q_f(i-1) - q_n(i-1)\right] \tag{3.11c}$$

where Δ is the sampling period. According to the constraints imposed on chatter in the control torques, the PD gains were optimized and the following filter coefficients and gains were used: $K_f = \text{diag}(20,20)$, $K_p = \text{diag}(200,150)$ and $K_d = \text{diag}(28.3,24.5)$. The sampling period was taken as $\Delta = 4$ ms. The initial joint angles of the robot were at $q^T = [90 \quad 0]$ deg. A set-point was then specified at $q_d^T = [140 \quad -60]$ deg and a response to this step ensued.

The step response is shown in Fig. 3.3a for joint one and in Fig. 3.4a for joint two.

The resulting joint velocities are shown in Figs. 3.3b and Fig. 3.4b and the control torques for joints one and two are shown in Figs. 3.3c and 3.4c respectively.

In our observations it was found that large K_p would introduce under damped behaviour without sufficiently large K_d. But a large K_d would lead to excessive chattering in the control torque. If one narrowed velocity signal bandwidth with sufficiently small filter gain K_f, an unacceptable delay would result as shown in 3.3b and 3.4b. Accordingly, an upper bound on K_p and K_d depended on the amount of acceptable chatter in the control torque and a limitation on the filter bandwidth arose due to unacceptably large delays.

3.6.3 PD Control Using Velocities Obtained from the Proposed Observer

Now we discuss the simulation of the PD-Controller which used velocity estimates received from the proposed observer. The results of the simulation for this case are shown in Figs. 3.5 and 3.6. The following Observer and controller gains were used: $K = \text{diag}(20,20)$, $K_p = \text{diag}(500,300)$, and $K_d = \text{diag}(75,35)$. The gains were optimally chosen to maximize speed of response while adhering to the constraint imposed on the magnitude of chatter in the torque control signal. Gain selection was done as follows: The position gain was increased until underdamped behaviour was observed. The velocity gain would then be increased to eliminate oscillations. Increases in the velocity gain led to increased noise (chatter) in the control torque. The position and velocity gains were alternately increased until the maximum allowable chatter in the torque signals was observed. The sampling period was taken as $\Delta = 4$ ms.

Note by comparing Fig. 3.3 to 3.5 for joint one and Fig. 3.4 to 3.6 for joint two, that a quicker response is achieved with the method using an observer while producing less

chatter in the control torques. Also, note that the initial observer error was set at $\tilde{x}^T = [-5 \quad 5]$ deg purposely. The dynamic response of the observer error is shown in Fig 3.5d for joint one and 3.6d for joint two. The velocity estimates provided by the observer are better than those obtained by numerically differentiating filtered position signals, i.e. compare Fig 3.3c and Fig. 3.5c for joint one and Fig 3.4c and Fig. 3.6c for joint two.

3.6.4 Trajectory Control Using Numerical Differentiation to Obtain Joint Velocities

In this section, results obtained from the computed torque controller will be presented. The controller obtains its velocity estimates from numerically differentiated filtered position signals as in Section 3.6.2. The position filter used is given in (3.11a) and the computed torque controller is calculated according to

$$\tau := H(q_n)\left[\ddot{q}_d - K_d\left(\dot{q}_f - \dot{q}_d\right) - K_p\left(q_n - q_d\right)\right] + C\left(q_n, \dot{q}_f\right)\dot{q}_d + F\dot{q}_f + g(q_n)$$

where $q_d(t)$ is the desired trajectory. The controller gains $K_p = \text{diag}(80,100)$, $K_d = \text{diag}(18,20)$ and filter coefficient matrix $K_f = \text{diag}(10,20)$ were selected to minimize position and velocity errors while adhering to the constraints with regard to allowable chatter in the control torques. Simulation results for position and velocity tracking are shown in Figs. 3.7 and 3.8. The initial position errors were set at $\tilde{q} = [-5 \quad -5]^T$ deg. The resulting position error trajectories are shown in Figs. 3.7b and 3.8b for joints one and two respectively. The 1-norm position and velocity tracking errors are given in Table 3.2

	Joint 1	**Joint 2**
$\|q - q_d\|_1$ (deg)	0.59	0.32
$\|\dot{q} - \dot{q}_d\|_1$ (deg/s)	0.96	0.55

Table 3.2: 1-Norm of the Trajectory Tracking Errors – CT Control

The velocity tracking errors are shown in Figs. 3.7d and 3.8d. The control torques required to produce these results are shown in Figs. 3.7e and 3.8e. The amount of chatter in these signals was acceptable according to the criteria introduced in Section 3.6.1. The difference between the actual and estimated joint velocities can be seen in Fig. 3.9.

3.6.5 Trajectory Control Using Velocities Obtained from the Proposed Observer

The results obtained with the proposed observer-controller will now be presented. The proposed method used the following observer and controller gains: $K = \text{diag}(2.0,1.5)$ $K_p = \text{diag}(1000,300)$, and $K_d = \text{diag}(120,30)$. Position tracking results are shown in Figs. 3.10a and 3.11a for joints one and two respectively.

The position tracking errors are shown in Figs. 3.10b and 3.11b. The velocity tracking errors are shown in Figs. 3.10d and 3.11d. The control torques produced with the proposed method are shown in Figs. 3.10e and 3.11e. The comparison of the observed velocity estimates to the actual velocities can be seen in Fig. 3.12. The quantitative measure of the tracking quality is given in Table 3.3 for the angular and velocity tracking errors.

	Joint 1	**Joint 2**
$\|q - q_d\|_1$ (deg)	0.011	0.015
$\|\dot{q} - \dot{q}_d\|_1$ (deg/s)	0.12	0.20

Table 3.3: 1-Norm of the Trajectory Tracking Errors – Observer-Control

The graphical results shown in Figs. 3.5-3.9 reveal that smaller position and velocity tracking errors can be achieved with the proposed method while reducing the amount of chatter in the control torques.

3.6.6 Simulation Showing the Stability of the Observer Error

To verify the convergence of the proposed observer, computer simulation was employed since *actual* velocities could not be obtained experimentally. For the simulation, the planar manipulator of Section 3.5.1 was used, where the position measurements were assumed perfectly smooth. The observer given in (3.2) and the point-to-point controller described in (3.6) were used for the simulation. The position, velocity and observer gains used were as follows: $K_p = [1000 \quad 750]^T$, $K_d = [200 \quad 150]^T$, and $K = [100 \quad 100]^T$. Results for two different sampling frequencies were obtained in order to underscore the effect of integration step size on observer convergence. The sampling frequencies used were $f = 250$ Hz and $f = 4000$ Hz which correspond to time intervals $\Delta = 4$ ms and $\Delta = 0.25$ ms respectively.

Fig. 3.17 shows observer simulation results for the first joint of our manipulator. Figs. 3.17a and 3.17b correspond to an integration step $\Delta = 0.25$ ms and Figs. 3.17c and 3.17d correspond to a step of $\Delta = 4$ ms. Note the improvement of the velocity estimate with decrease in the integration step.

3.7 Experiments Using the Observer-Controller

To make the observer-controller experiments possible, the stock UNIMATE COMPUTER/CONTROLLER was modified so we could implement our algorithms at higher sampling frequencies [20]. With these modifications, we were able to compute our observer-controllers at a frequency of 250 Hz.

3.7.1 Point-to-point Control

The point-to-point control experiment described here uses the proposed observer and PD-controller. The initial and desired joint positions as well as the sampling period were the same as those in the simulation. The gains employed were chosen as $K_p = [1000 \quad 750]^T$, $K_d = [200 \quad 150]^T$, and $K = [100 \quad 100]^T$. This section also provides results for a step response using the PD-controller which obtains its velocity by numerically differentiating position data.

A comparison of experimental results for these two methods is shown in Figs. 3.13 and 3.14. Note that the position response for the proposed method is quicker and the applied joint torques have less chatter. Position responses are shown in Figs. 3.13a and 3.13b for joint one and Figs. 3.14a and 3.14b for joint two. The velocity responses for the two methods differ considerably as is shown in Figs. 3.13c and 3.13d for joint one and Figs. 3.14c and 3.14d for joint two. For the PD-controller using numerical differentiation, a noisy velocity signal results. This is evident in Fig. 3.13d for joint one and it is especially evident in Fig. 3.14d for joint two.

The noisy velocity signals produced by numerical differentiation lead to control torques which exhibit large amounts of chattering. This is shown in Fig. 3.13f and 3.14f where extremely large amounts of chattering are present at joint two and saturation

occurs frequently. The relatively smooth control torques obtained with the proposed observer plus controller shown in Figs. 3.13c and 3.14c are preferred.

3.7.2 Trajectory Tracking Control

For the trajectory tracking controller experiments the controller of (3.8) was employed to track the fifth order trajectory polynomial given in (3.10). The gains used for the controller were $K_p = \text{diag}(500\,,\,500)$ and $K_d = \text{diag}\left(2\sqrt{500}\,,\,2\sqrt{500}\right)$. For the observer, gains $K = \text{diag}(100\,,\,100)$ were chosen. Set points of the desired trajectory were made available to the controller every 12 ms and the observer and controller were computed at the frequency $f = 250$ Hz Results of position and velocity tracking are shown in Figs. 3.15 and 3.16.

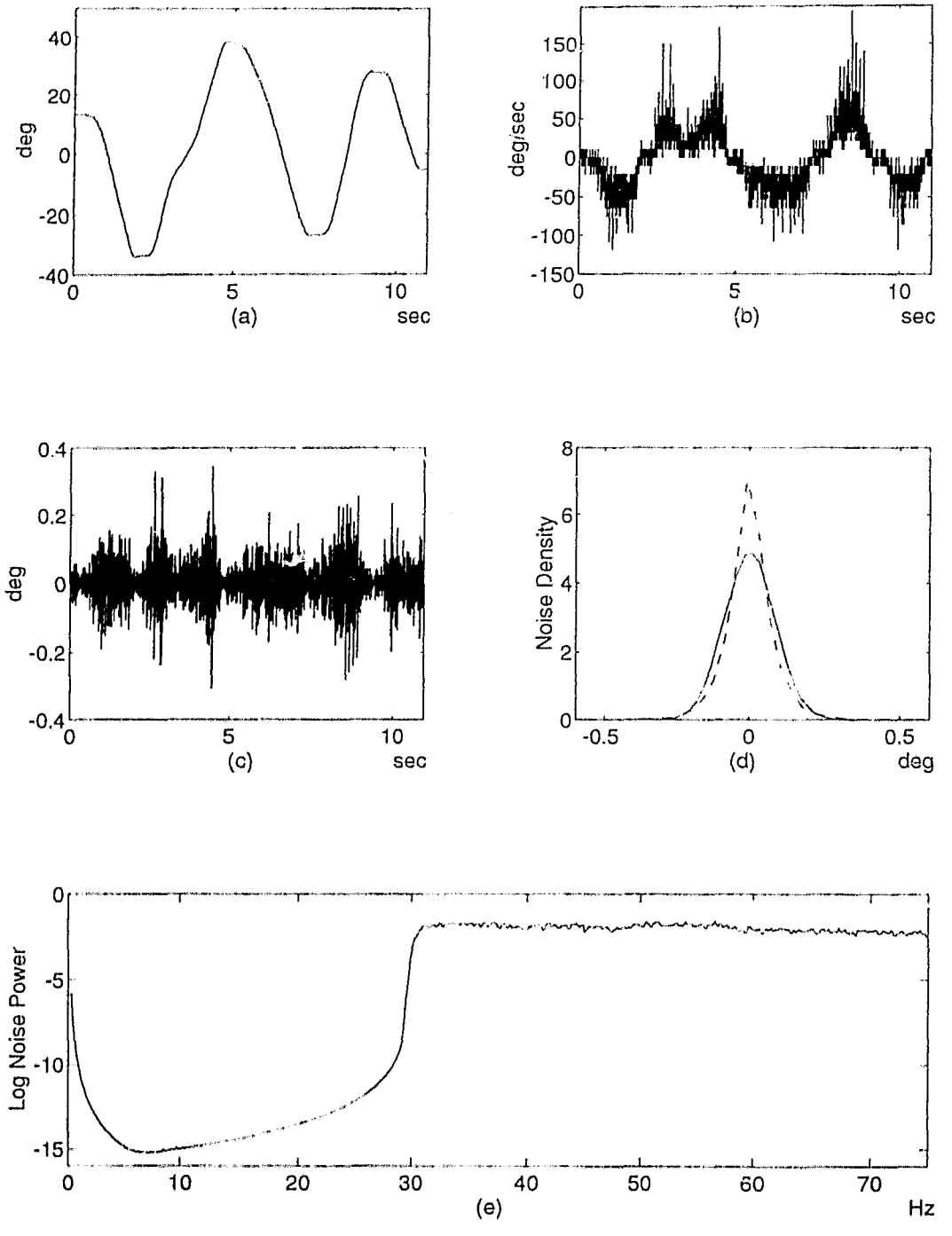

Fig. 3.2: Experimental data from the GE Arm: (a) measured position trajectory, joint one, (b) velocity using differentiation, joint one, (c) noise in the position signal, (d) distribution density of the noise, (e) spectral noise power (dB).

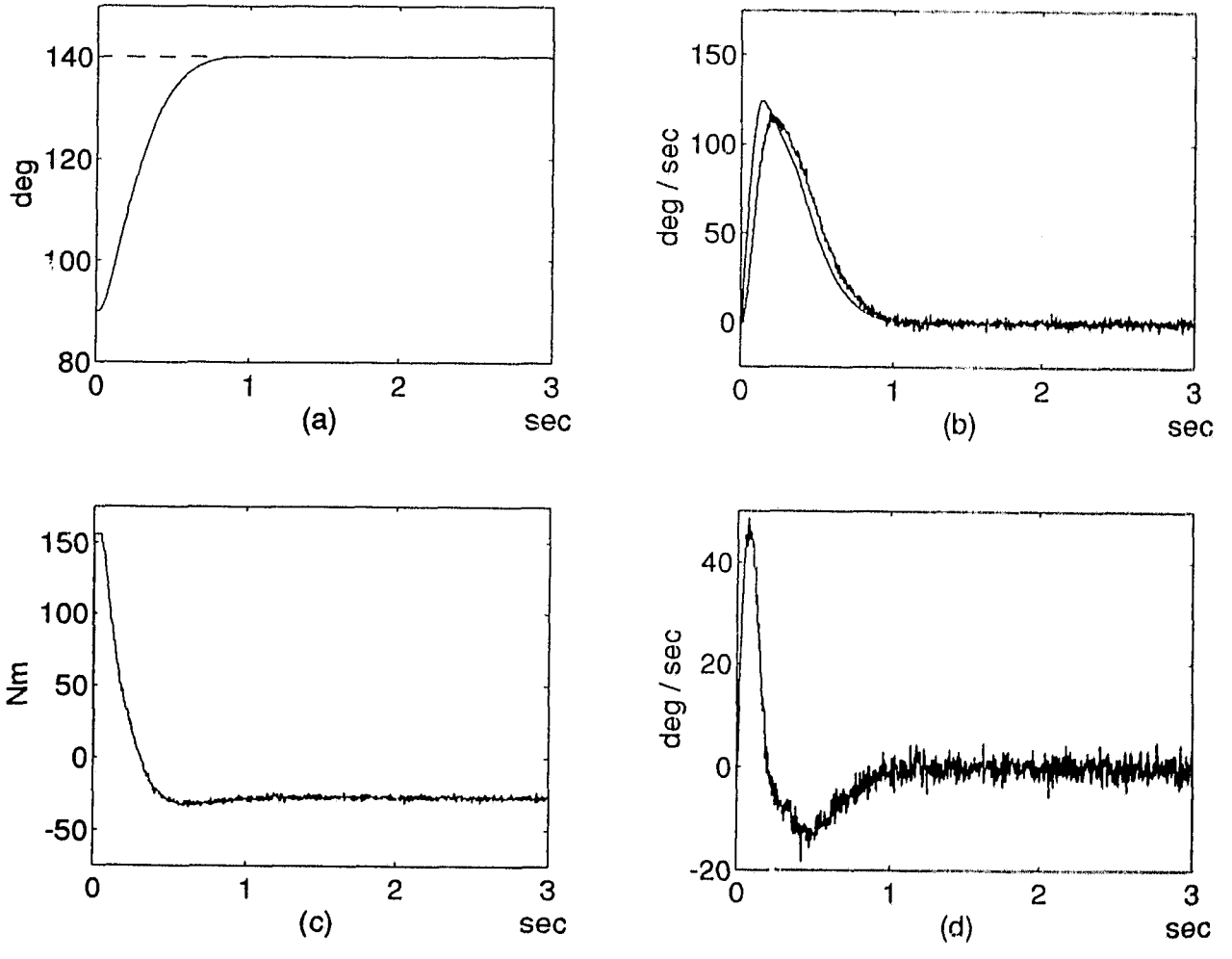

Fig. 3.3: Simulation: Numerical Differentiation + PD Control: joint one step response (a) position response (b) actual (smooth) vs. estimated velocity (c) applied torque (d) estimated velocity error.

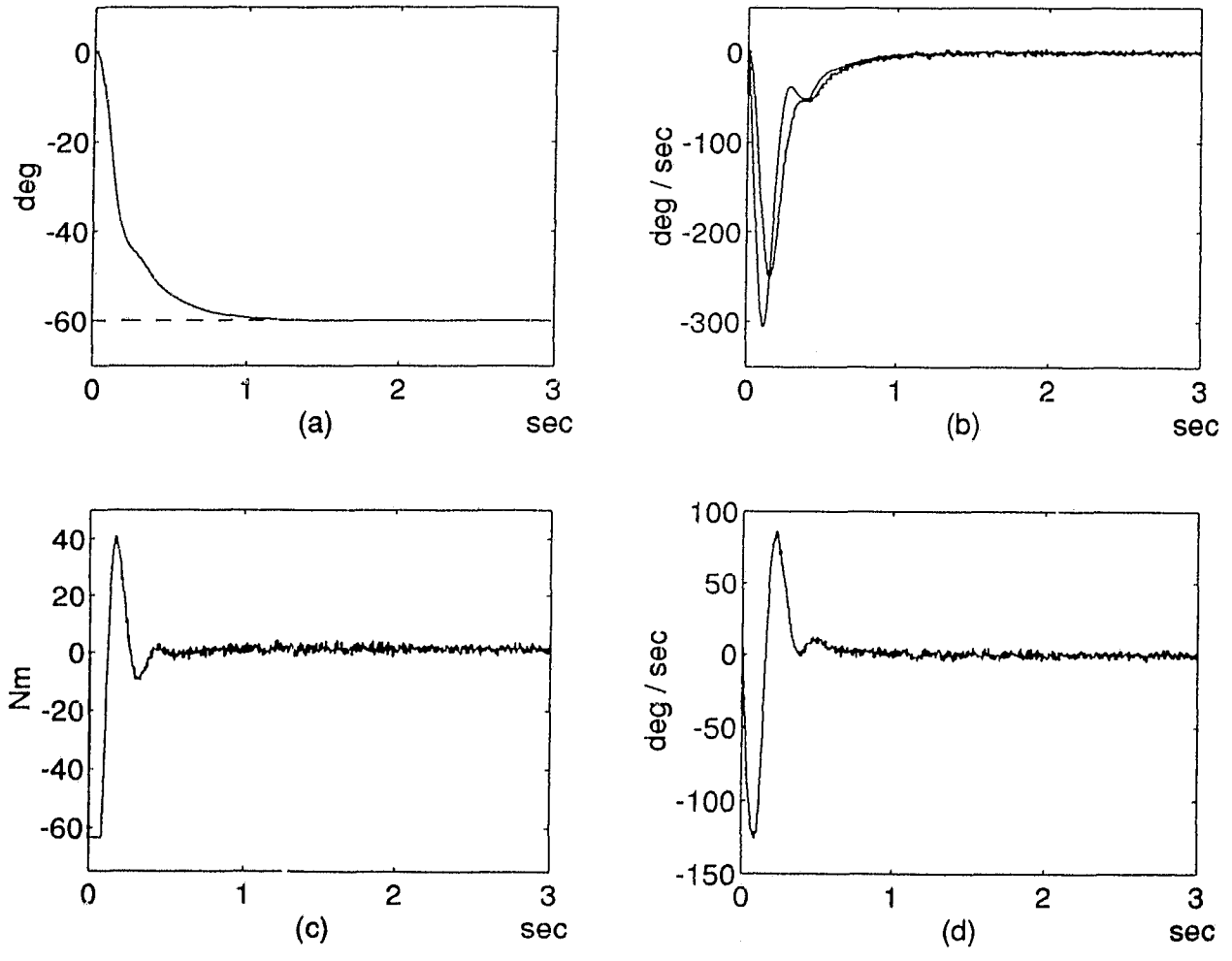

Fig. 3.4: Simulation: Numerical Differentiation + PD Control: joint two step response (a) position response (b) actual (smooth) vs. observed velocity (c) applied torque (d) estimated velocity error.

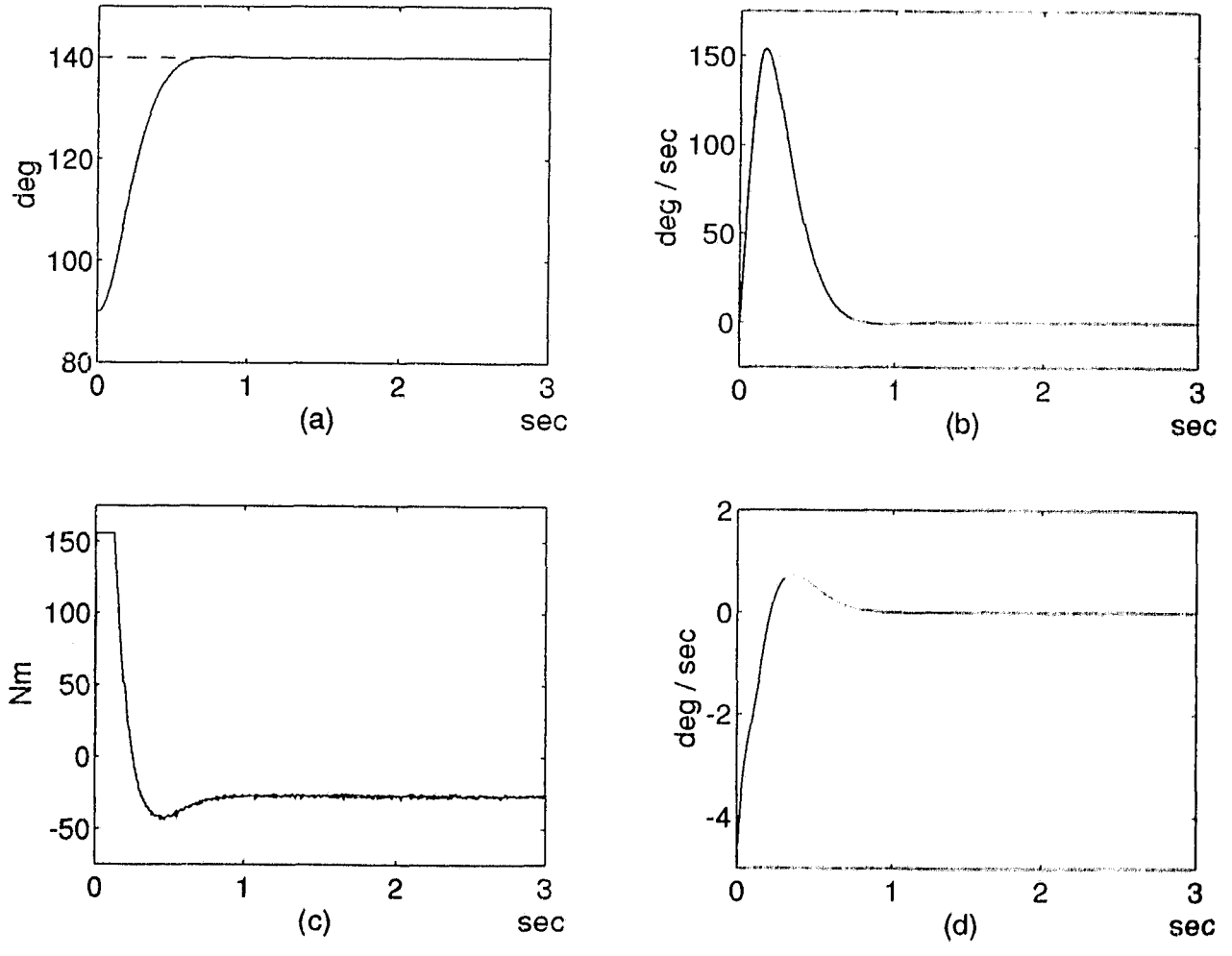

Fig. 3.5: Simulation: Observer + PD Control: joint one step response (a) position response (b) actual vs. observed velocity (c) applied torque (d) velocity observer error.

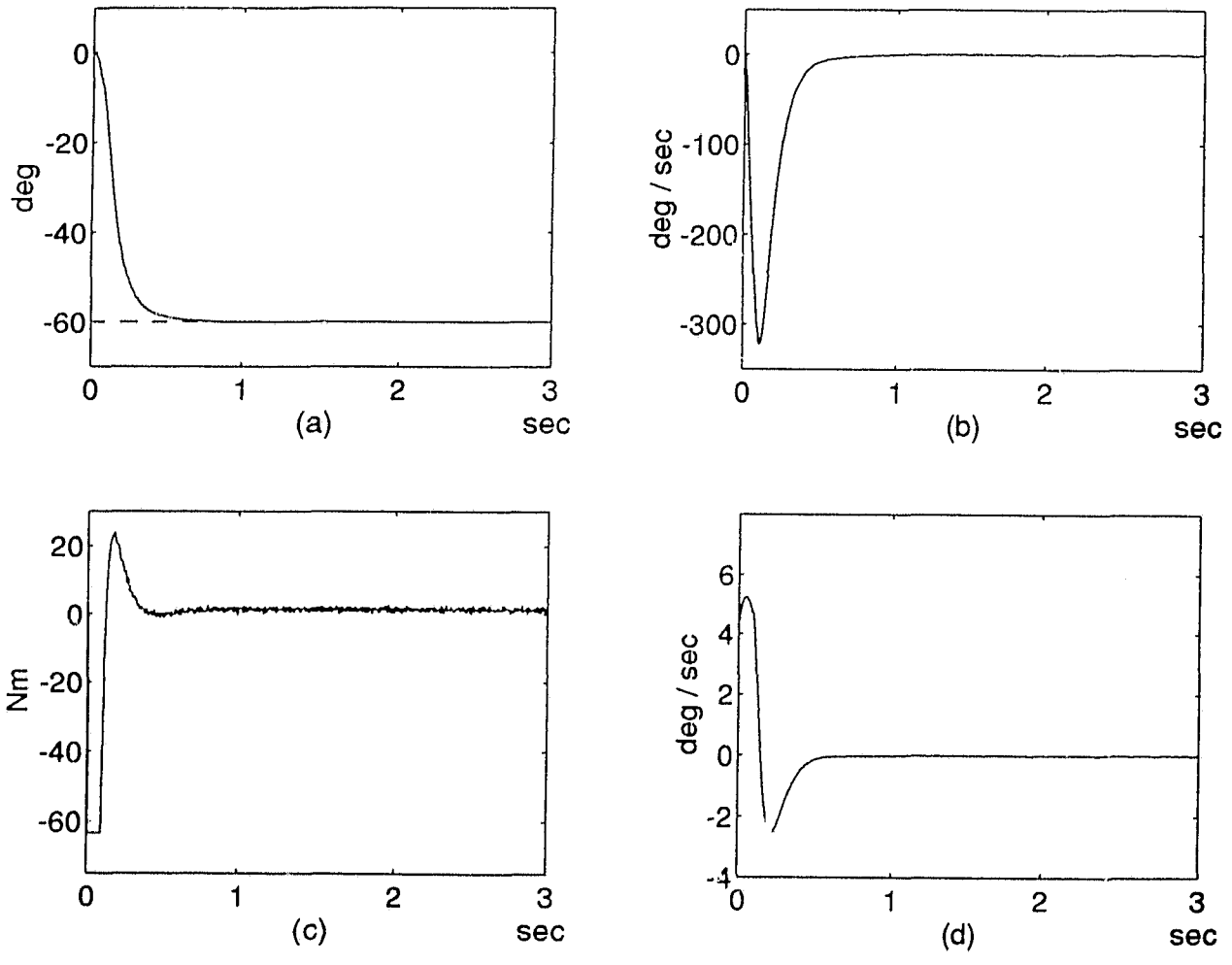

Fig. 3.6: Simulation: Observer + PD Control: joint two step response (a) position response (b) actual vs. observed velocity (c) applied torque (d) velocity observer error.

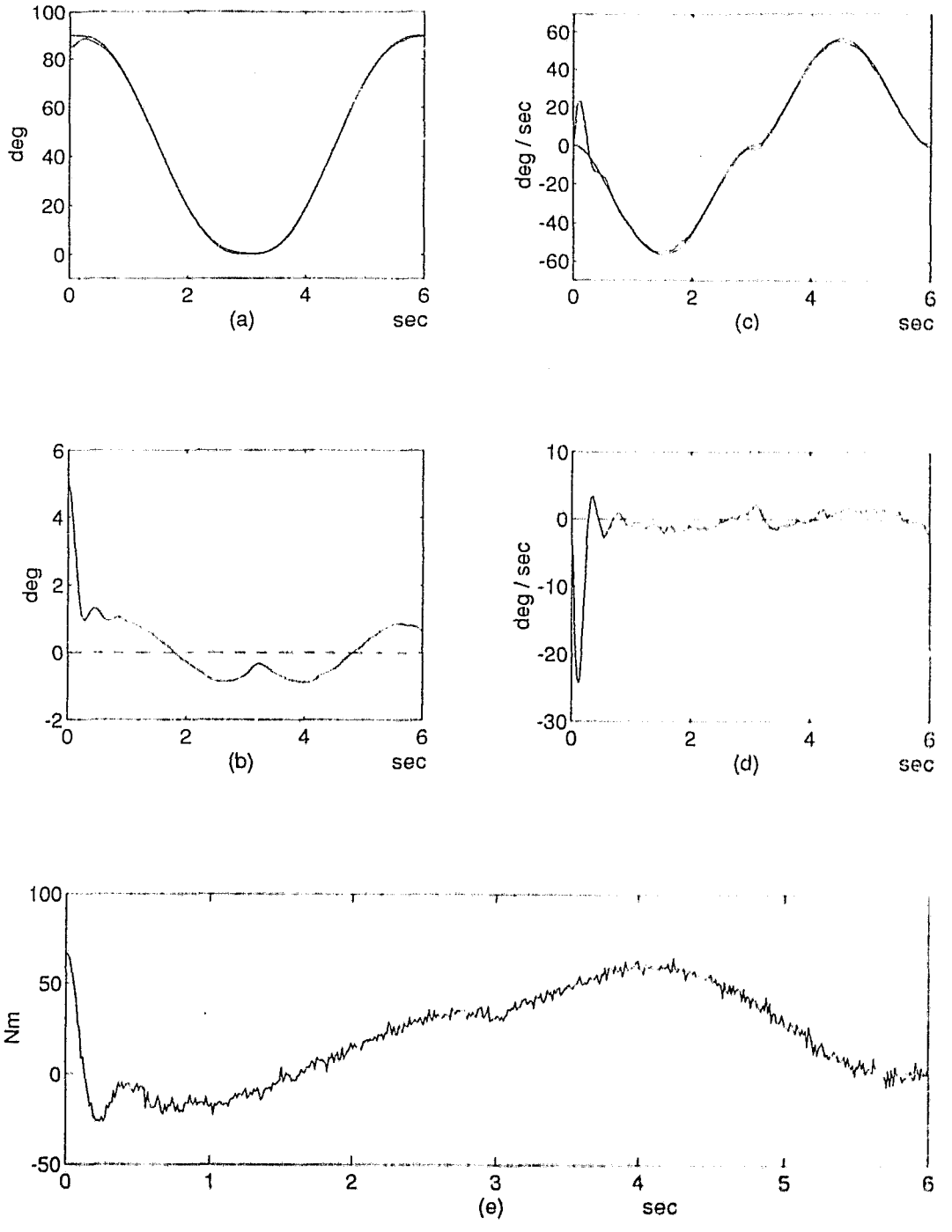

Fig. 3.7: Simulation: Numerical Differentiation + Computed Torque Control: joint one (a) desired vs. actual position (b) position error (c) desired vs. actual velocity (d) velocity error (e) applied torque.

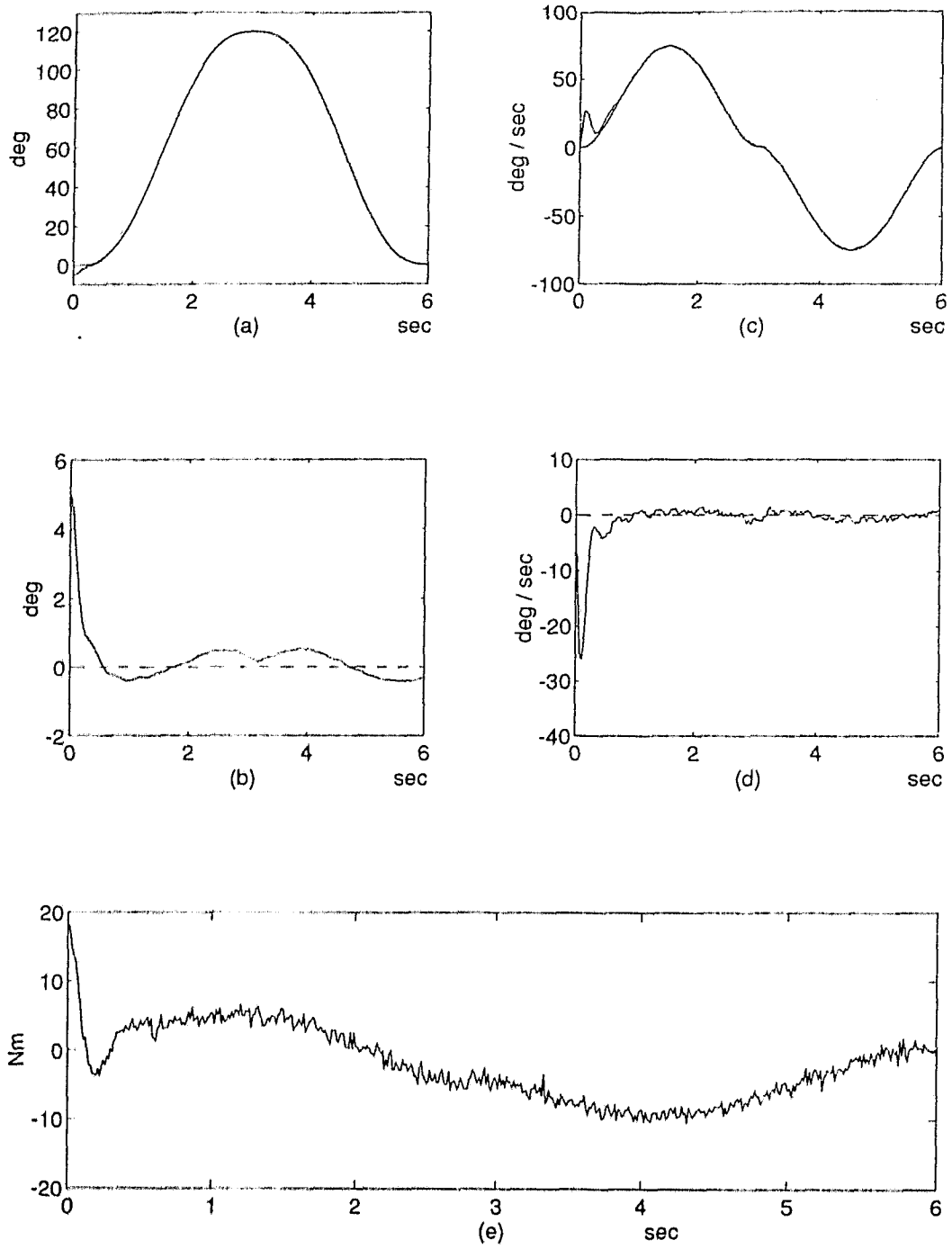

Fig. 3.8: Simulation: Numerical Differentiation + Computed Torque Control: joint two (a) desired vs. actual position (b) position error (c) desired vs. actual velocity (d) velocity error (e) applied torque.

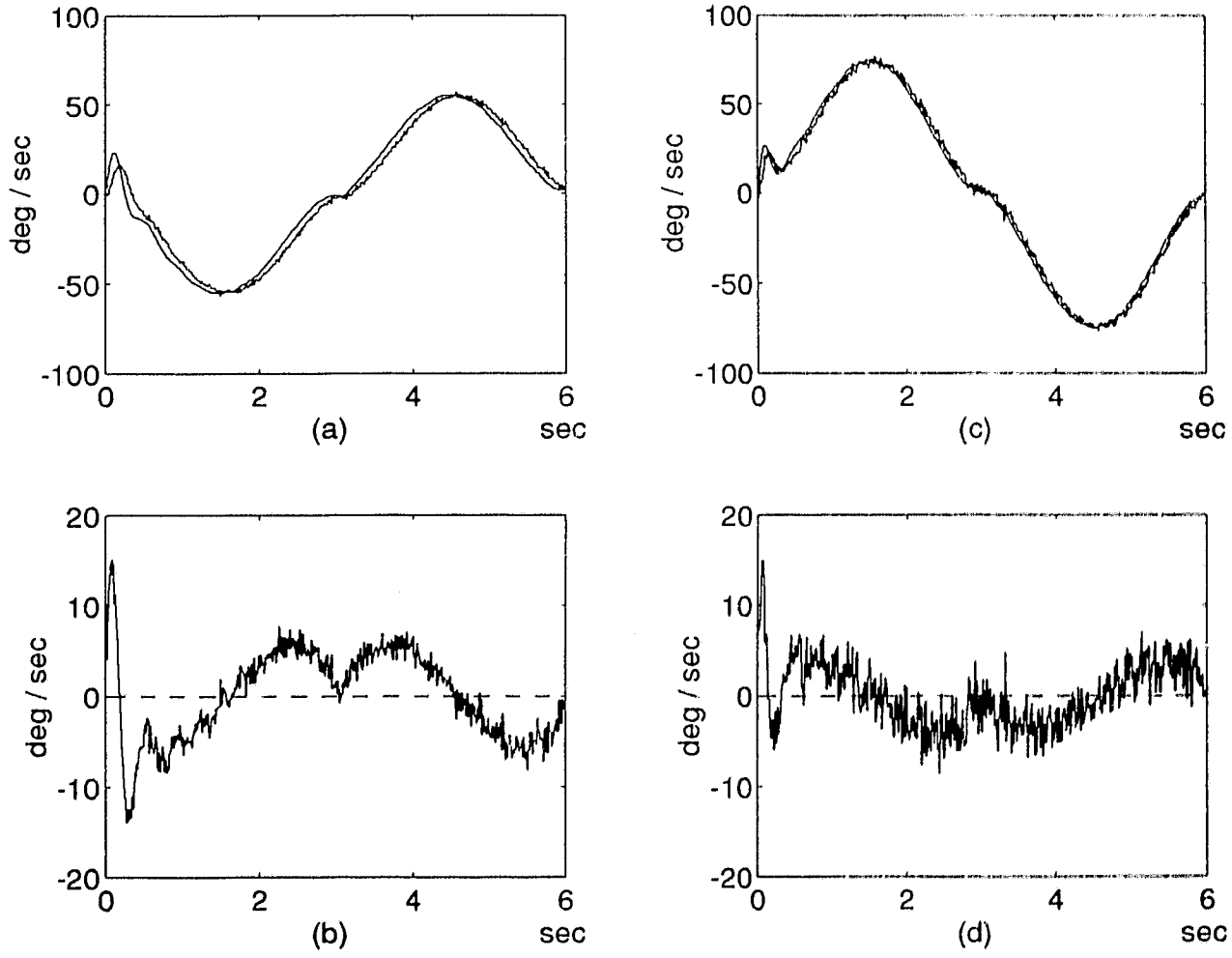

Fig. 3.9: Simulation: Numerical Differentiation + Computed Torque Control: velocity estimation errors (a) actual vs. estimated velocity, joint one (b) joint one velocity estimate error (c) actual vs. estimated velocity, joint two (d) joint two velocity estimate error.

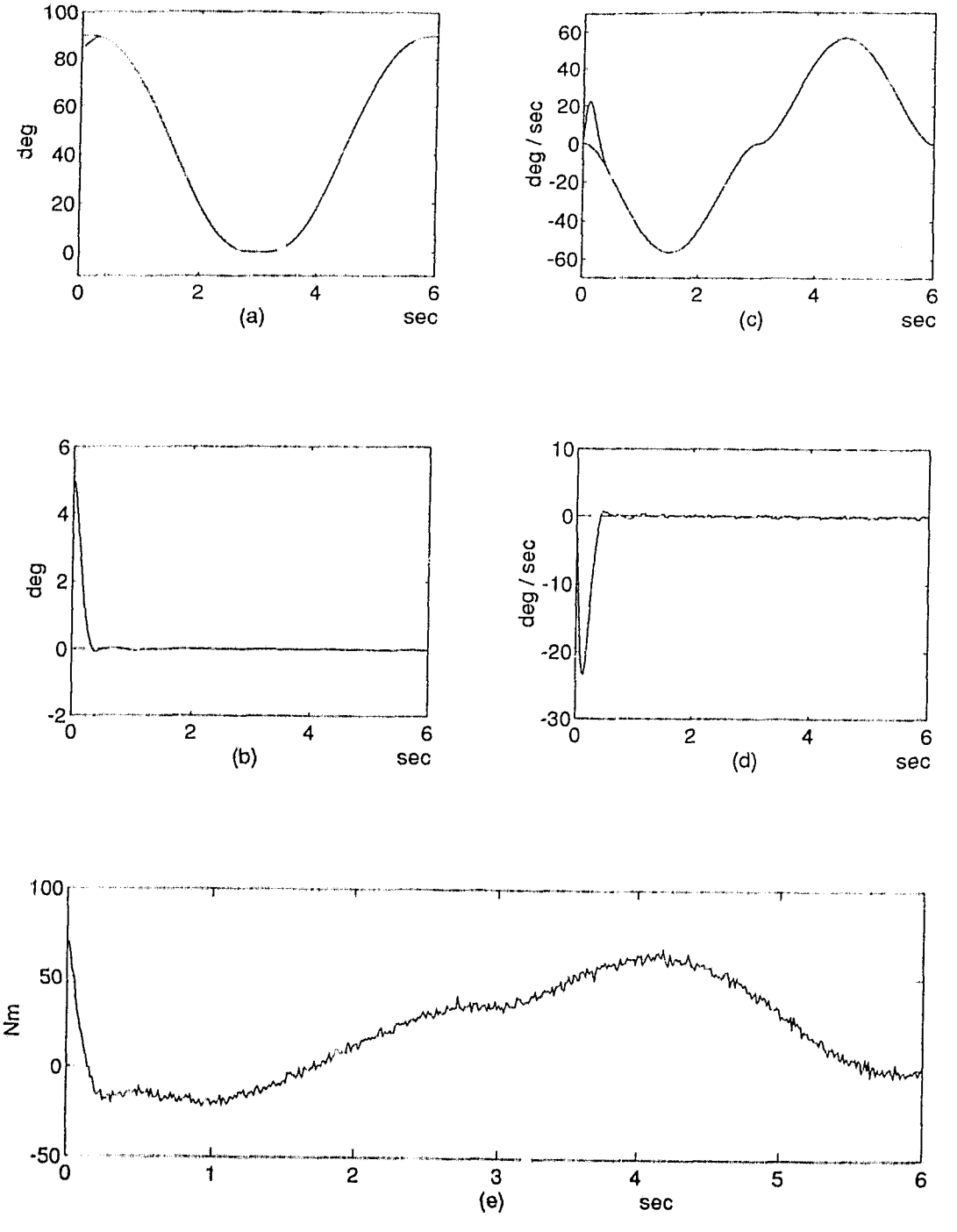

Fig. 3.10: Simulation: Observer + Trajectory Controller: joint one (a) desired vs. actual position (b) position error (c) desired vs. actual velocity (d) velocity error (e) applied torque.

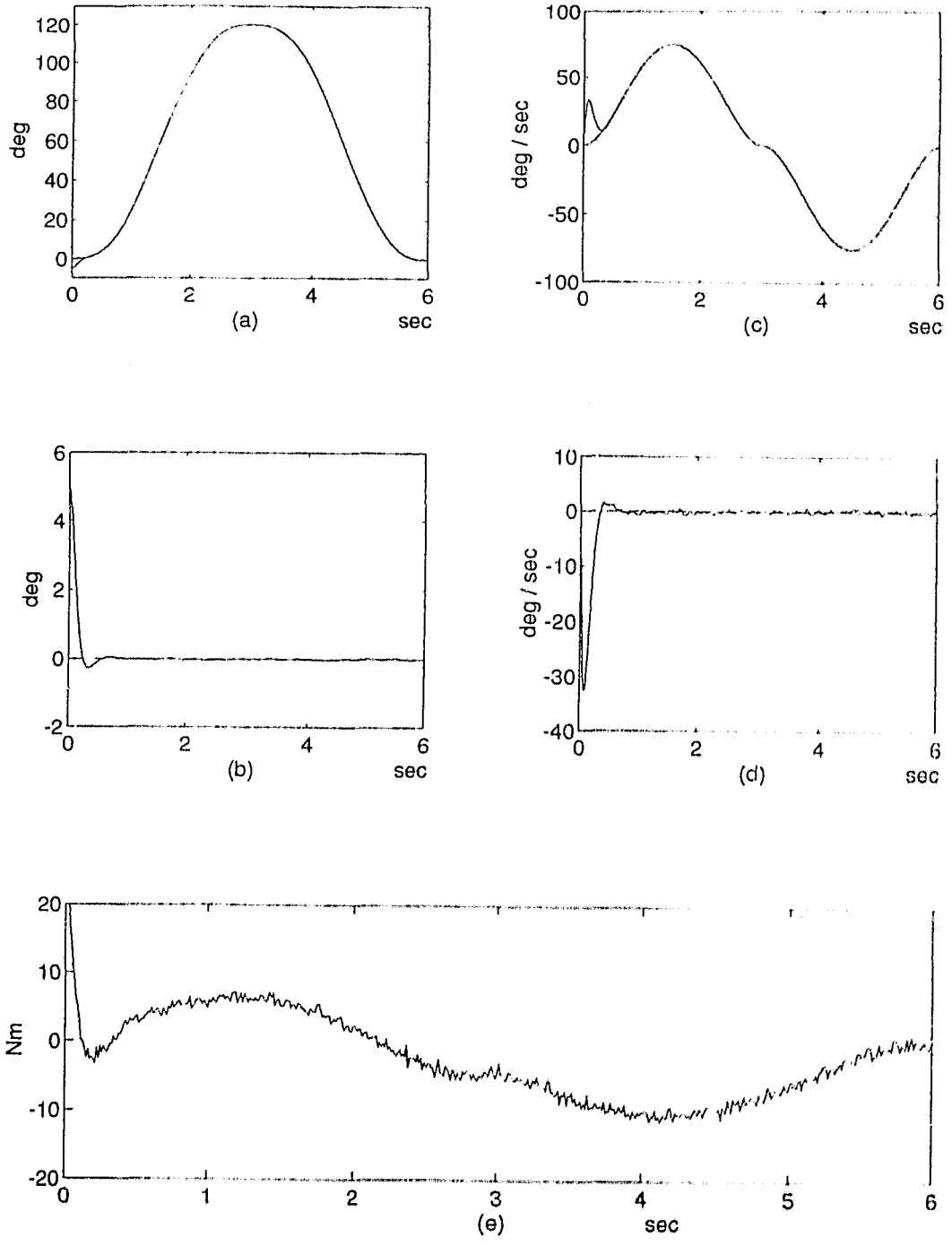

Fig. 3.11: Simulation: Observer + Trajectory Controller: joint two (a) desired vs. actual position (b) position error (c) desired vs. actual velocity (d) velocity error (e) applied torque.

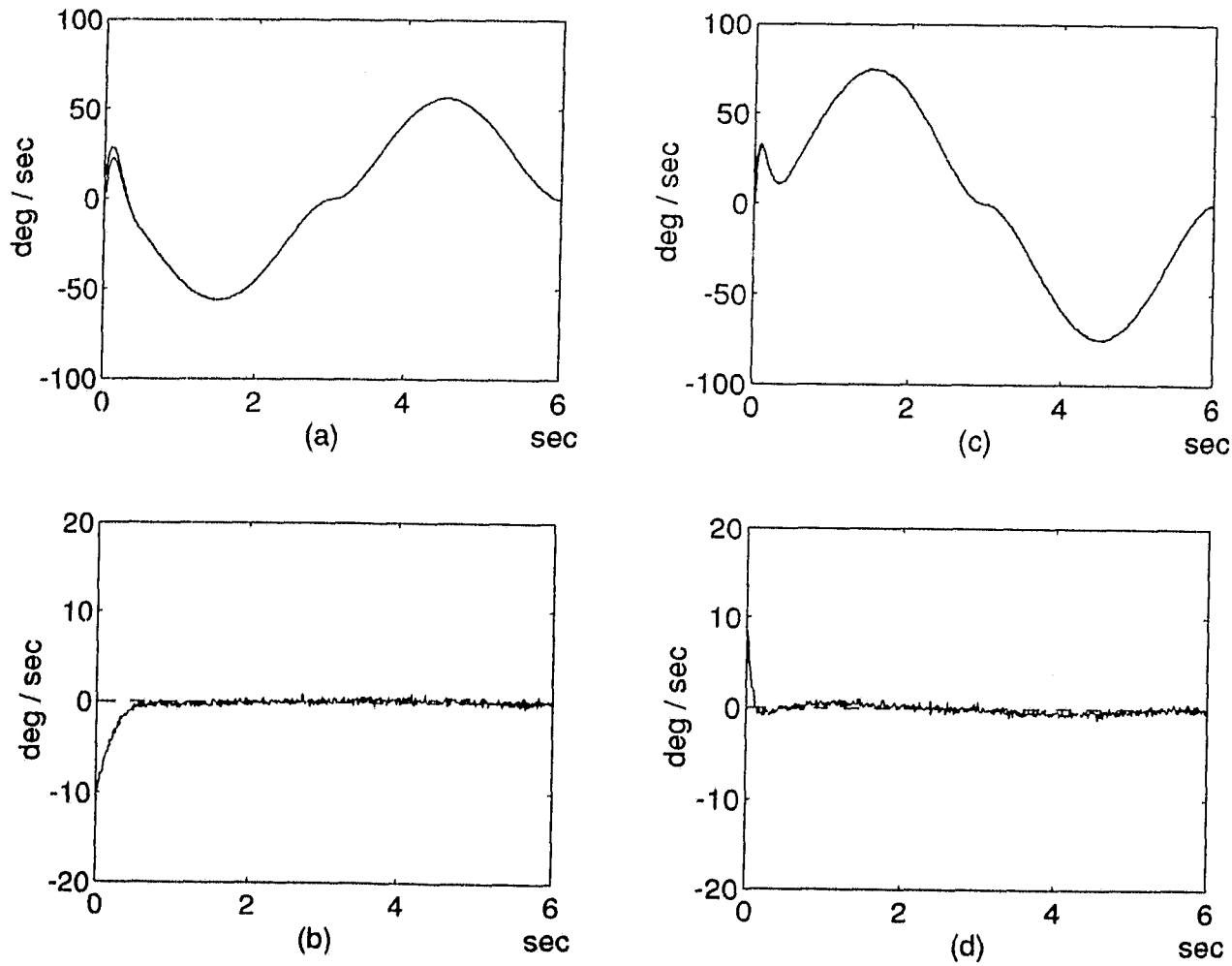

Fig. 3.12: Simulation: Observer + Trajectory Controller: observer errors (a) actual vs. observed velocity, joint one (b) joint one observer error (c) actual vs. observed velocity, joint two (d) joint two observer error.

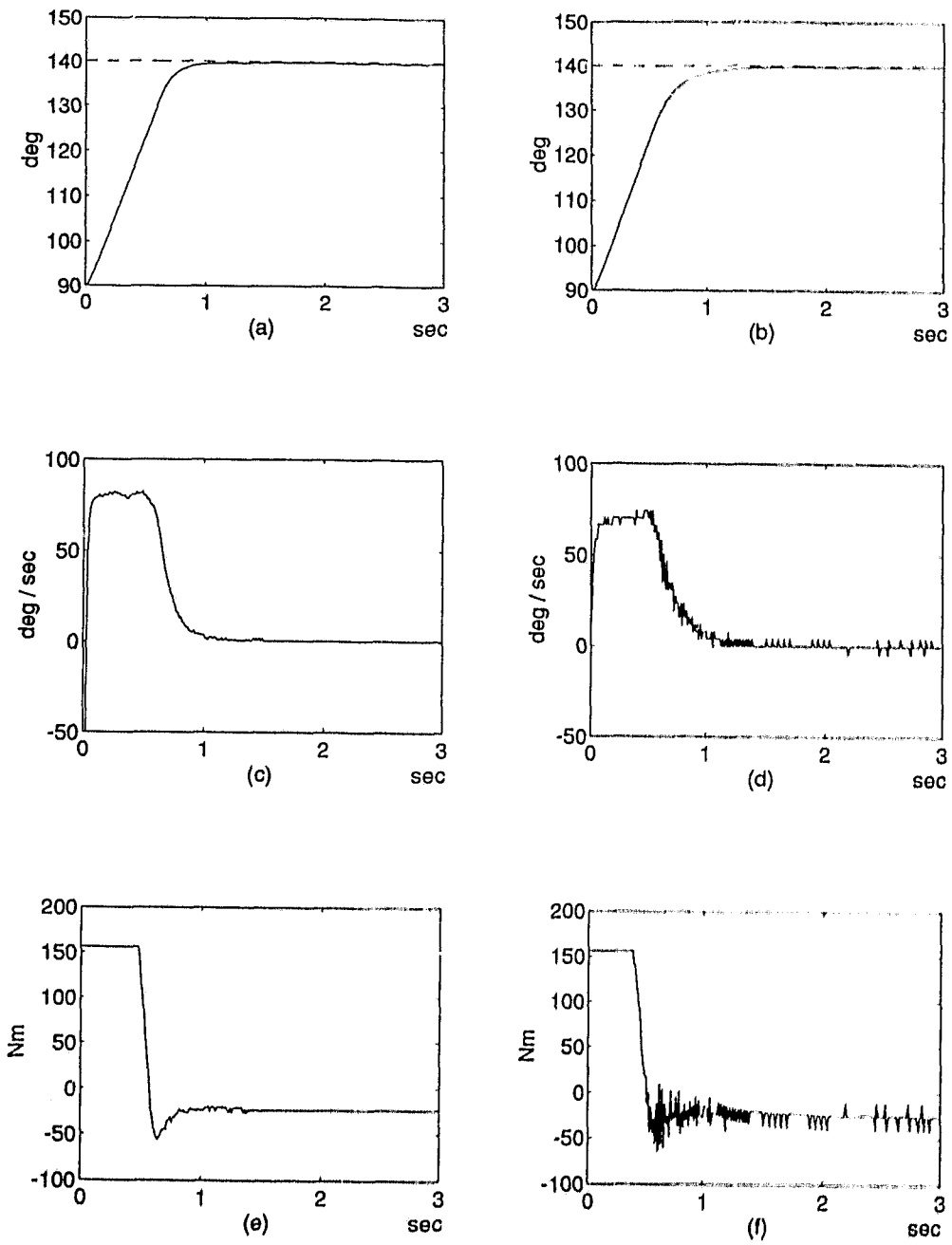

Fig. 3.13: Experiment: joint one step response (a) position response, using observer, (b) position response, using differentiation, (c) velocity response, using observer, (d) velocity response, using differentiation, (e) applied torque, using observer, (f) applied torque, using differentiation.

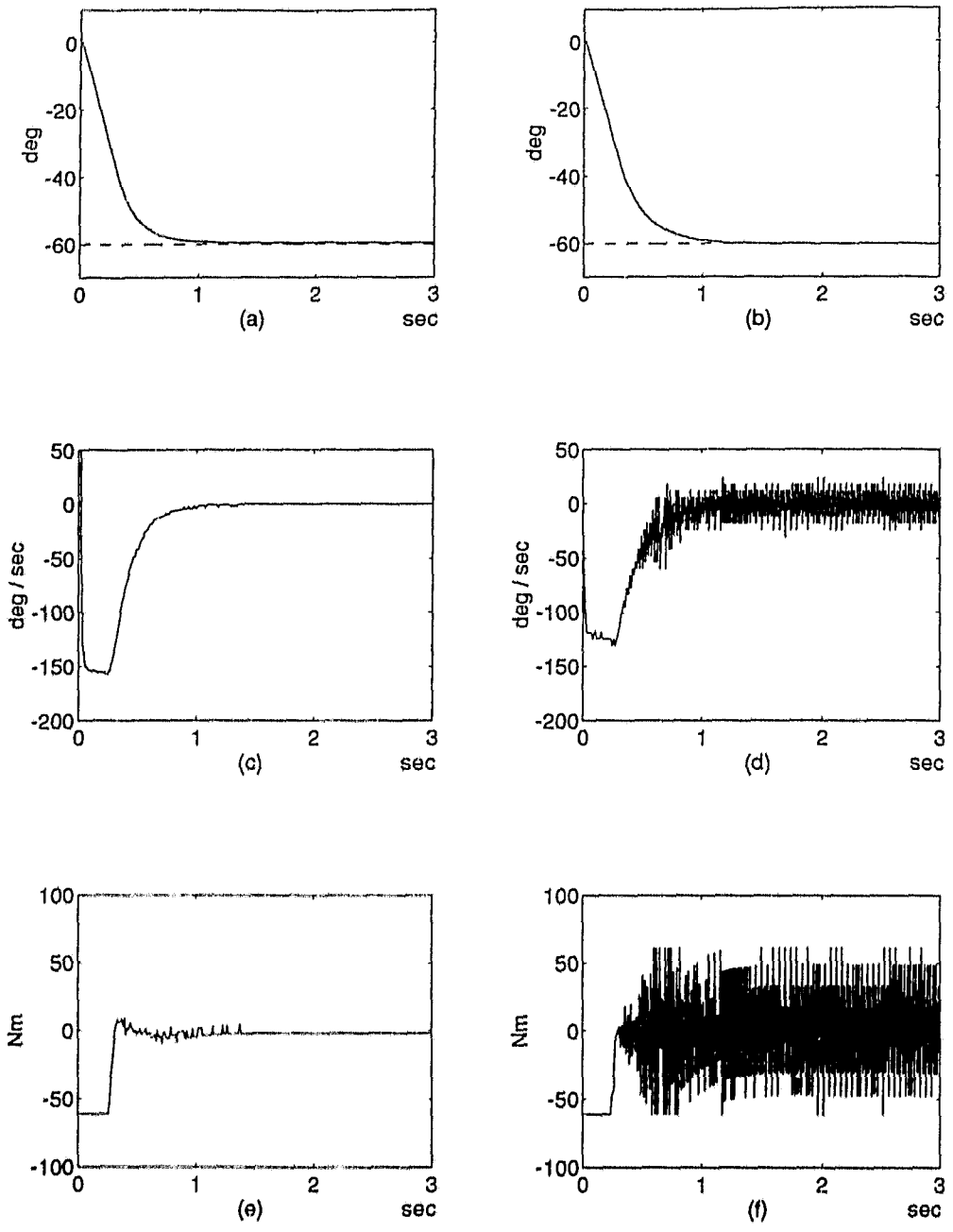

Fig. 3.14: Experiment: joint two step response (a) position response, using observer, (b) position response, using differentiation, (c) velocity response, using observer, (d) velocity response, using differentiation, (e) applied torque, using observer, (f) applied torque, using differentiation.

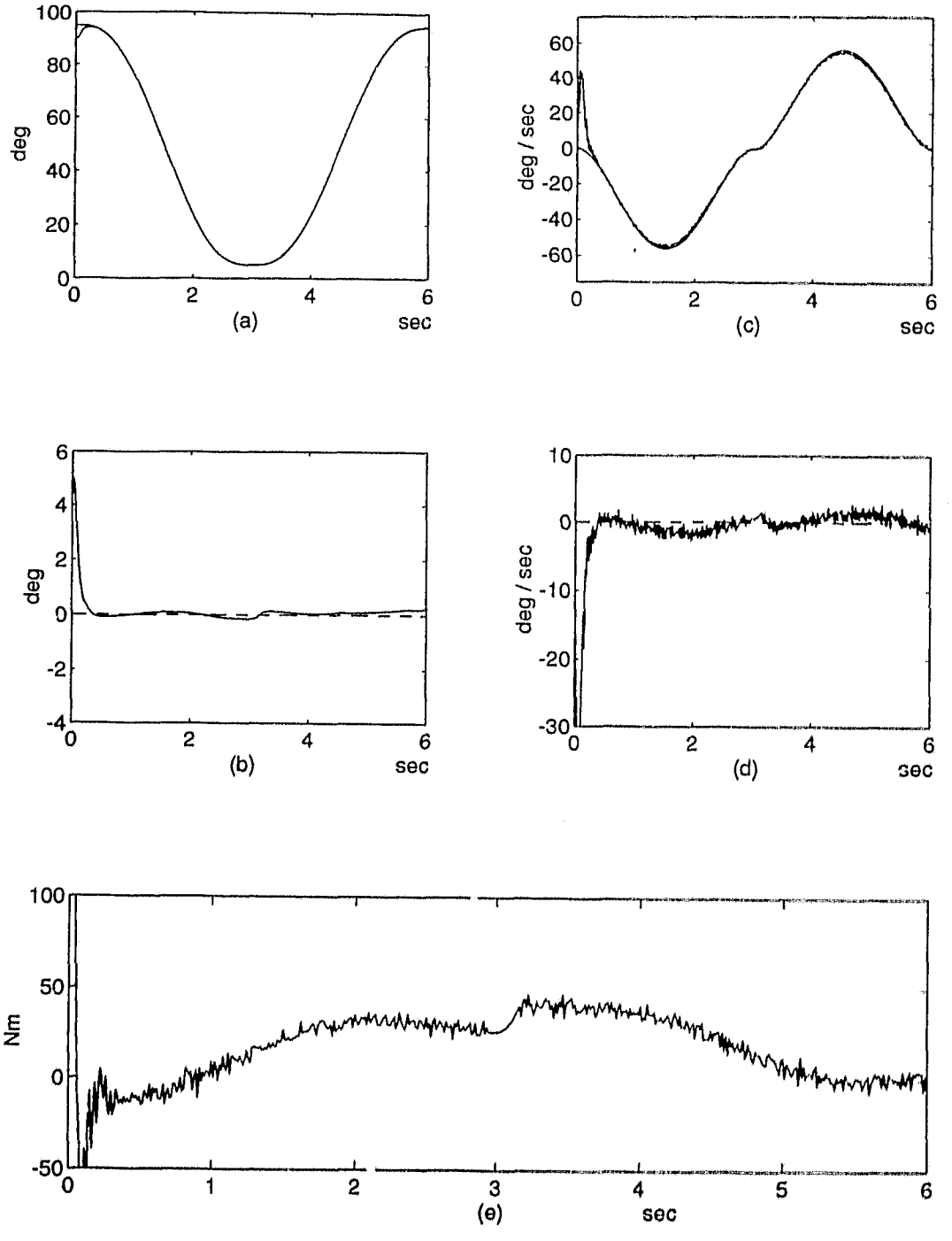

Fig. 3.15: Experiment: joint one using the observer-controller (a) desired versus actual position, (b) position error, (c) desired versus actual velocity, (d) velocity error, (e) applied torque.

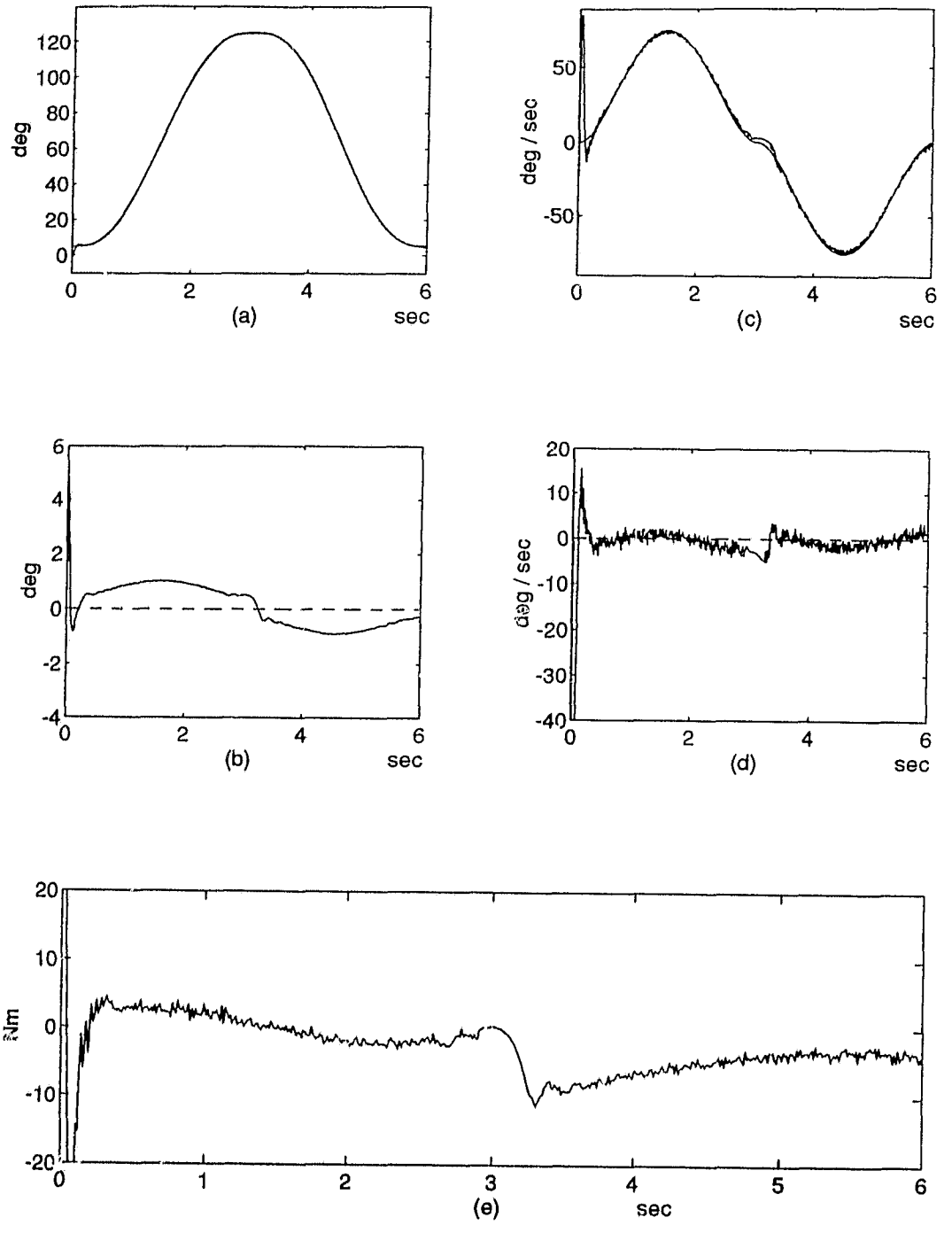

Fig. 3.16: Experiment: joint two using the observer-controller (a) desired versus actual position, (b) position error, (c) desired versus actual velocity, (d) velocity error, (e) applied torque.

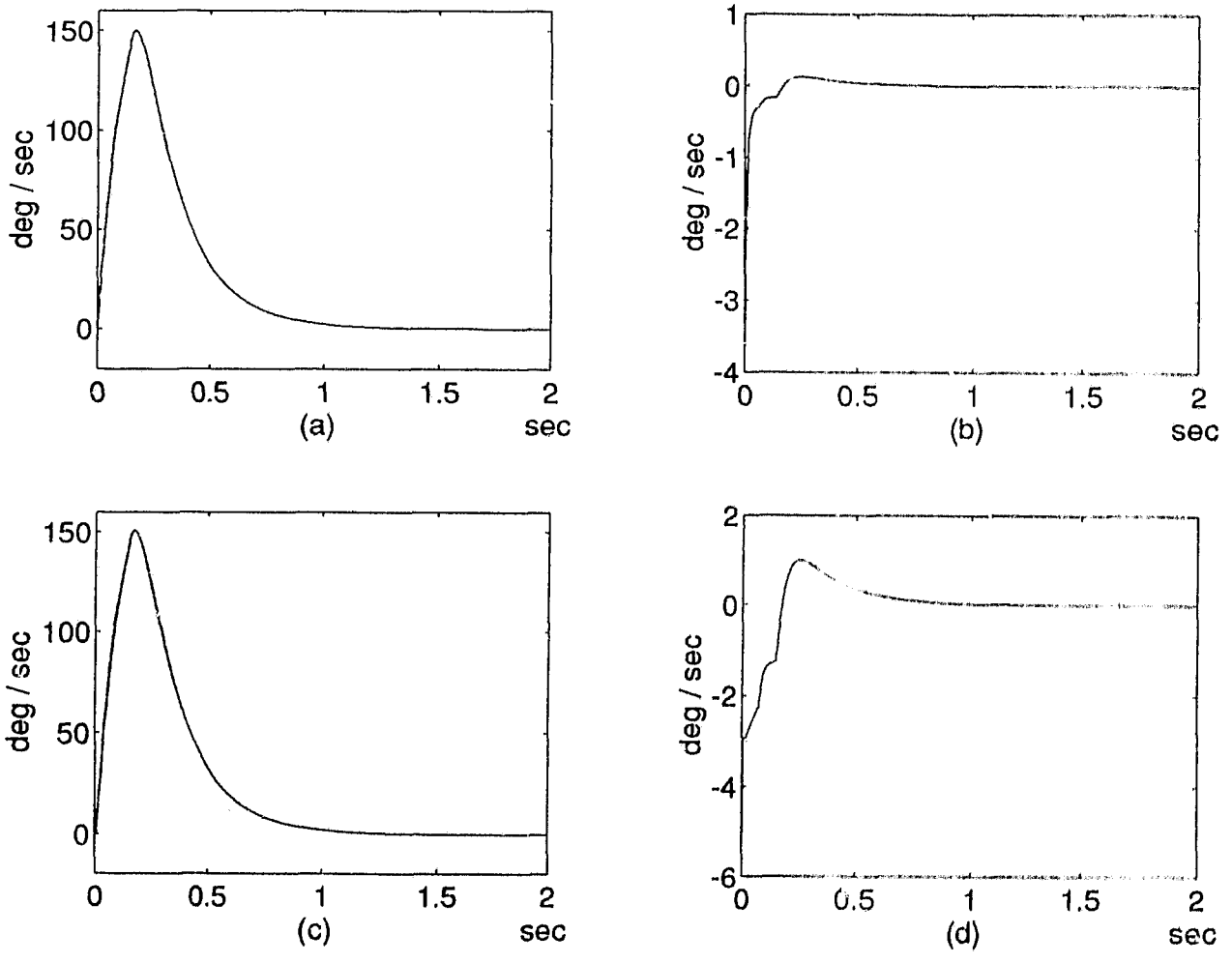

Fig. 3.17: Simulation of the velocity observer (a) actual versus observed velocity, $\Delta = 0.25$ ms. (b) observer error, $\Delta = 0.25$ ms. (c) actual versus observed velocity, $\Delta = 4$ ms. (d) observer error, $\Delta = 4$ ms.

3.A Proof of Theorem 1

Consider the Lyapunov function

$$v(t) = \frac{1}{2}\tilde{x}^T(t)H(q)\tilde{x}(t) \tag{A.1}$$

Note that by property 1, $v(t)$ satisfies

$$\frac{1}{2}m_l\|\tilde{x}(t)\|^2 \le v(t) \le \frac{1}{2}m_u\|\tilde{x}(t)\|^2, \quad m_l, m_u > 0 \tag{A.2}$$

where $m_l = \lambda_{\min}(H(q))$ and $m_u = \lambda_{\max}(H(q))$. The time derivative of (A.1) is given by

$$\dot{v} = \tilde{x}^T H(q)\dot{\tilde{x}} + \frac{1}{2}\tilde{x}^T\dot{H}(q)\tilde{x} \tag{A.3}$$

Substituting the observer error dynamics (3.5) into (A.3) and applying property 4 yields

$$\dot{v} = -\tilde{x}^T\left(C(q,\hat{x}) + H(q)K + F\right)\tilde{x} \tag{A.4}$$

We can now substitute $\hat{x} = x - \tilde{x}$ into (A.4) and use property 3 to give

$$\dot{v} = -\tilde{x}^T H(q)K\tilde{x} - \tilde{x}^T F\tilde{x} - \tilde{x}^T C(q,x)\tilde{x} + \tilde{x}^T C(q,x)\tilde{x}$$

Then the 2-norm of (A.4) gives us

$$\dot{v}(t) \le -\left(\underline{\sigma} + m_f - m_c m_v - m_c\|\tilde{x}(t)\|\right)\|\tilde{x}(t)\|^2 \tag{A.5}$$

where m_v is the assumed bound on $x = \dot{q}$. The non-positiveness of $\dot{v}(t)$ is guaranteed if

$$\|\tilde{x}(t)\| \leq \frac{1}{m_c}\left(\underline{\sigma} + m_f\right) - m_v \tag{A.6}$$

From (A.2), (A.5) and (A.6) we can deduce that if

$$\|\tilde{x}(0)\| \leq \sqrt{\frac{m_l}{m_u}}\left[\frac{1}{mc}\left(\underline{\sigma} + m_f\right) - m_v\right]$$

then

$$\dot{v}(t) \leq -\beta\|\tilde{x}(t)\|^2 \qquad \forall t \geq 0 \tag{A.7}$$

From (A.2) we have that

$$\frac{2}{m_u} v(t) \leq \|\tilde{x}(t)\|^2 \tag{A.8}$$

Substituting (A.8) into (A.7) gives us

$$\dot{v}(t) \leq -\frac{2\beta}{m_u} v(t)$$

So, using the Bellman-Gronwall inequality [54, pp. 23] leads to

$$\|\tilde{x}(t)\| \leq \sqrt{\frac{m_u}{m_l}}\|\tilde{x}(0)\| e^{-\frac{\beta}{m_u}t}$$

which determines the exponential stability of the observer error. □

3.B Proof of Theorem 2

Consider the Lyapunov function:

$$v(t) = \frac{1}{2} e(t)^T P(q) e(t)$$

where $P(q) = \mathrm{diag}\left(H(q), H(q), K_p\right)$, $K_p > 0$ and $e(t)^T = \left[\tilde{x}(t)^T \quad \dot{\tilde{q}}(t)^T \quad \tilde{q}(t)^T\right]$. By using property 1 we can conclude that $v(t)$ satisfies

$$\frac{1}{2} p_l \|e(t)\|^2 \le v(t) \le \frac{1}{2} p_u \|e(t)\|^2 \tag{B.1}$$

where $p_l = \lambda_{\min}\left(P(q)\right)$ and $p_u = \lambda_{\max}\left(P(q)\right)$. The time derivative of $v(t)$ along all trajectories is given by

$$\dot{v}(t) = \tilde{x}^T \left(H(q)\dot{\tilde{x}} + \frac{1}{2}\dot{H}(q)\tilde{x} \right) + \dot{\tilde{q}}^T \left(H(q)\ddot{\tilde{q}} + \frac{1}{2}\dot{H}(q)\dot{\tilde{q}} + K_p \tilde{q} \right) \tag{B.2}$$

Substituting observer and point-to-point control error equations (3.5) and (3.7) respectively into (B.2) and using property 4 yields the expression

$$\dot{v} = -\tilde{x}^T \left(C(q,\hat{x}) + F + H(q)K \right)\tilde{x} - \dot{\tilde{q}}^T \left(F + K_d \right)\dot{\tilde{q}} + \dot{\tilde{q}}^T K_d \tilde{x} \tag{B.3}$$

By taking the 2-norm of (B.3) and observing $\hat{x} = \dot{\tilde{q}} - \tilde{x}$, we obtain

$$\dot{v} \le -\left(\underline{\sigma} + m_f - m_c \left(\|\tilde{x}\| + \|\dot{\tilde{q}}\| \right) \right) \|\tilde{x}\|^2 - \left(k_d + m_f \right) \|\dot{\tilde{q}}\|^2 + k_d \|\tilde{x}\| \|\dot{\tilde{q}}\| \tag{B.4}$$

where $m_f = \lambda_{\min}(F)$. Equation (B.4), which is a quadratic form, can be expressed in matrix notation as

$$\dot{v}(t) \le -\begin{bmatrix} \|\tilde{\dot{q}}\| \\ \|\tilde{x}\| \end{bmatrix}^T \begin{bmatrix} k_d + m_f & -\frac{1}{2}k_d \\ -\frac{1}{2}k_d & \underline{\sigma} + m_f - m_c\left(\|\tilde{x}\| + \|\tilde{\dot{q}}\|\right) \end{bmatrix} \begin{bmatrix} \|\tilde{\dot{q}}\| \\ \|\tilde{x}\| \end{bmatrix} \tag{B.5}$$

To guarantee that $\dot{v}(t)$ remain negative, the principal minors of the matrix in (B.5) must all be positive. From the first principal minor we obtain

$$k_d + m_f > 0$$

Positivity of the second principal minor requires

$$\left[\underline{\sigma} + m_f - m_c\left(\|\tilde{x}\| + \|\tilde{\dot{q}}\|\right)\right]\left(k_d + m_f\right) - \frac{k_d^2}{4} > 0$$

which is equivalent to

$$\underline{\sigma} + m_f > \frac{k_d^2}{4\left(k_d + m_f\right)} + m_c\left(\|\tilde{x}\| + \|\tilde{\dot{q}}\|\right) \tag{B.6}$$

But $\sqrt{3}\|e\| > \|\tilde{x}\| + \|\tilde{\dot{q}}\|$, so (B.6) is certainly valid if

$$\underline{\sigma} + m_f > \frac{k_d^2}{4\left(k_d + m_f\right)} + \sqrt{3}m_c\|e\| \tag{B.7}$$

From (B.7) we obtain that for given $\underline{\sigma}$ and k_d, (B.5) will be negative if

$$\|e(t)\| < \frac{1}{\sqrt{3}m_c}\left(\underline{\sigma} + m_f - \frac{k_d^2}{4(k_d + m_f)}\right)$$

But in order that $\dot{v}$ remain negative for all time, the error vector at time $t = 0$ must satisfy

$$\|e(0)\| < \frac{1}{m_c}\sqrt{\frac{p_l}{3p_u}}\left(\underline{\sigma} + m_f - \frac{k_d^2}{4(k_d + m_f)}\right)$$

by virtue of (B.1). Then

$$\dot{v}(t) \le -\beta\begin{bmatrix}\|\dot{\tilde{q}}\| \\ \|\tilde{x}\|\end{bmatrix}^2 \qquad \forall t \ge 0 \tag{B.8}$$

where $\beta > 0$ is the infimum of the smallest eigenvalue of the matrix in (B.5).

Note that (B.1) and (B.8) imply $\tilde{x}(t), \dot{\tilde{q}}(t) \in L_2$ and $\tilde{x}(t), \dot{\tilde{q}}(t), \tilde{q}(t) \in L_\infty$, respectively. Furthermore, for the observer we have $\dot{\hat{x}} \in L_\infty$ by virtue of (3.5), i.e.

$$\dot{\hat{x}} = -H^{-1}(q)\left[C(q,x)\tilde{x} + C(q,\hat{x})\tilde{x} + F\tilde{x}\right] - K\tilde{x}$$

which is equivalent to

$$\dot{\hat{x}} = -H^{-1}(q)\left[2C\left(q,\dot{\tilde{q}}\right)\tilde{x} - C(q,\tilde{x})\tilde{x} + F\tilde{x}\right] - K\tilde{x}$$

Hence $\tilde{x}, \dot{\hat{x}} \in L_\infty$ and $\tilde{x} \in L_2$. Then Barbalat's Lemma [54, p. 25] tells us that $\tilde{x}(t) \to 0$ as $t \to \infty$. Similarly, we have $\ddot{\tilde{q}} \in L_\infty$ by virtue of (3.7), i.e.

$$\ddot{\tilde{q}} = -H^{-1}(q)\left[C\left(q,\dot{\tilde{q}}\right)\dot{\tilde{q}} + F\dot{\tilde{q}} + K_d\dot{\tilde{q}} - K_d\tilde{x} + K_p\tilde{q}\right]$$

So Barbalat's lemma uses $\dot{\tilde{q}}, \ddot{\tilde{q}} \in L_\infty$ and $\dot{\tilde{q}} \in L_2$ to conclude $\dot{\tilde{q}}(t) \to 0$ as $t \to \infty$.

Now it is left to show that $\tilde{q} = 0$ as $t \to \infty$. In other words, we must show that the system does not settle at a non-zero $\tilde{q}$. To do this we study all system trajectories for which $\dot{\tilde{q}} = \tilde{x} \equiv 0$. Such system equations can be derived from (3.7), i.e. $\ddot{\tilde{q}} = -H^{-1}(q)K_p\tilde{q} = 0$. The only invariant set is $\tilde{q} \equiv 0$, hence by Lasalle's theorem $\tilde{q} \to 0$ as $t \to \infty$ [18, p. 110]. □

3.C Proof of Theorem 3

Consider the Lyapunov function

$$v(t) = \frac{1}{2} e(t)^T P(q) e(t)$$

where $P(q) = \mathrm{diag}\left(H(q), H(q), K_p\right)$, $K_p > 0$ and $e(t)^T = \left[\tilde{x}(t)^T \quad \dot{\tilde{q}}(t)^T \quad \tilde{q}(t)^T\right]$. By using property 1 we can conclude that $v(t)$ satisfies

$$\frac{1}{2} p_l \|e(t)\|^2 \leq v(t) \leq \frac{1}{2} p_u \|e(t)\|^2$$

where $p_l = \lambda_{\min}\left(P(q)\right)$ and $p_u = \lambda_{\max}\left(P(q)\right)$. The time derivative of $v(t)$ along all trajectories is given by

$$\dot{v}(t) = \tilde{x}^T \left(H(q)\dot{\tilde{x}} + \frac{1}{2}\dot{H}(q)\tilde{x} \right) + \dot{\tilde{q}}^T \left(H(q)\ddot{\tilde{q}} + \frac{1}{2}\dot{H}(q)\dot{\tilde{q}} + K_p \tilde{q} \right) \qquad \text{(C.1)}$$

Substituting observer and trajectory tracking control error equations (3.5) and (3.9) respectively into (C.1) and using property 4 yields the expression

$$\dot{v} = -\tilde{x}^T \left(C(q,\hat{x}) + F + H(q)K \right)\tilde{x} - \dot{\tilde{q}}^T \left(F + K_d \right)\dot{\tilde{q}} + \dot{\tilde{q}}^T K_d \tilde{x} - \dot{\tilde{q}}^T C(q, \dot{q}_d)\tilde{x} \qquad \text{(C.2)}$$

By taking the 2-norm of (C.2) and observing $\hat{x} = \dot{q}_d + \dot{\tilde{q}} - \tilde{x}$, we obtain

$$\dot{v} \leq -\left(\underline{\sigma} + m_f - m_c \left(m_d + \|\tilde{x}\| + \|\dot{\tilde{q}}\| \right) \right) \|\tilde{x}\|^2 - \left(k_d + m_f \right) \|\dot{\tilde{q}}\|^2 + \left(k_d + m_c m_d \right) \|\tilde{x}\| \|\dot{\tilde{q}}\| \qquad \text{(C.3)}$$

where $\|\dot{q}_d\| \le m_d$ and $m_f = \lambda_{\min}(F)$. Arguments analogous to those in Appendix 3.B can be used to show that $\dot{v}(t)$ remains negative for all time if $k_d + m_f$ and the initial conditions on the error vector $e^T(t) = \begin{bmatrix} \dot{\tilde{q}}^T & \tilde{x}^T & \tilde{q}^T \end{bmatrix}$ satisfy

$$\|e(0)\| < \frac{1}{m_c}\sqrt{\frac{p_l}{3p_u}}\left(\underline{\sigma} + m_f - m_c m_d - \frac{\left(k_d + m_c m_d\right)^2}{4\left(k_d + m_f\right)}\right)$$

Then

$$\dot{v}(t) \le -\beta\begin{bmatrix}\|\dot{\tilde{q}}\| \\ \|\tilde{x}\|\end{bmatrix}^2 \qquad \forall t \ge 0$$

Barbalat's Lemma and Lasalle's theorem can be used as in Appendix 3.B to show $\tilde{x}(t) \to 0$, $\dot{\tilde{q}}(t) \to 0$ and $\tilde{q}(t) \to 0$ as $t \to \infty$. □

Chapter 4

An Adaptive Velocity Observer

4.1 Introduction

The non-adaptive observer of Chapter 3 can be applied effectively when the dynamic parameters of a robot manipulator and its payload are well known. However, in situations where a manipulator handles many different tools and payloads it is reasonable to consider adaptive control techniques to improve performance. In this chapter an observer-controller is designed whose parameters adaptive to a changing manipulator payload.

This Chapter considers the stability of the adaptive observer-controller and a digital implementation of the observer-controller is formulated. The usefulness and practicality of the adaptive observer-controller is shown through simulations and experiments where comparisons are made with other more traditional control techniques.

4.2 Formulation of the Adaptive Observer

The formulation of the adaptive observer uses the structure of the manipulator dynamics given in (2.8). The dynamics can be solved explicitly for acceleration as

follows

$$\dot{x} = H^{-1}(q)\left[\tau - C(q,x)x - Fx - g(q)\right] \tag{4.1}$$

where the joint velocities are denoted by $x = \dot{q}$. The principal part of the proposed observer has a structure similar to (4.1) and is given by

$$\dot{\hat{x}} = \psi(q,\hat{x},\tau,\hat{a}) + K\tilde{x} \tag{4.2a}$$

$$\psi(q,\hat{x},\tau,\hat{a}) = \hat{H}^{-1}(q)\left[\tau - \hat{C}(q,\hat{x})\hat{x} - \hat{F}\hat{x} - \hat{g}(q)\right] \tag{4.2b}$$

where $\hat{x}$ is the *observed* velocity estimate, $\tilde{x} = x - \hat{x}$ is the observation error, $K > 0$ is a diagonal gain matrix, and $\left(\hat{*}\right)$ denotes the term (*) where the dynamic parameters have been replaced by their estimates. Now let $a \in \Re^p$ be the vector that collects the unknown parameters of the manipulator dynamics. The estimated parameters used in (4.2) are obtained with the following adaptation law

$$\dot{\hat{a}} = -\Gamma Y^T(q,\hat{x},\psi)\tilde{x} \tag{4.3}$$

where $Y(q,\hat{x},\psi)$ is the regressor determined by (2.12) and $\Gamma > 0$ is a diagonal gain matrix. If the manipulator starts from rest, one can take $\hat{x}(t_0) = 0$ where t_0 denotes the moment when the robot motion begins. Otherwise one has to make a guess for $x(t_0)$ and denote it by $\hat{x}(t_0)$. Similarly, one has to make an initial guess for the unknown parameter vector $\hat{a}(t_0)$ at $t = t_0$. Although it is very likely that these initial estimates are not accurate, it will be shown in Section 4.2.2 that the observer being developed here is locally asymptotically stable as long as the norm of the initial estimate errors lie within a region of attraction.

Integrating (4.2a) and (4.3) over the time interval $[t_0, t]$ and using the estimated initial conditions $\hat{x}(t_0)$ and $\hat{a}(t_0)$, we obtain

$$\hat{x}(t) = y(t) + \int_{t_0}^{t} \left[\psi(q, \hat{x}, \tau, \hat{a}) - K\hat{x} \right] dt \tag{4.4a}$$

where

$$y(t) = \hat{x}(t_0) + K\left[q(t) - q(t_0)\right] \tag{4.4b}$$

is known, and

$$\hat{a}(t) = \hat{a}(t_0) - \Gamma \int_{t_0}^{t} Y^T(q, \hat{x}, \psi)\, \tilde{x}\, dt \tag{4.5}$$

Using $\tilde{x} = x - \hat{x}$ with $x = dq/dt$, (4.5) becomes

$$\hat{a}(t) = \hat{a}(t_0) - \Gamma \int_{q(t_0)}^{q(t)} Y^T(q, \hat{x}, \psi)\, dq + \Gamma \int_{t_0}^{t} Y^T(q, \hat{x}, \psi)\, \hat{x}\, dt \tag{4.6}$$

where the first integral is carried out with respect to joint position q. The system of integral equations (4.4a) and (4.6), which are equivalent to (4.2) and (4.3) together with initial conditions $\hat{x}(t_0)$ and $\hat{a}(t_0)$, define the adaptive observer to be further studied in this paper. The signal $\hat{x}(t)$, which is a part of the solution to this system of integral equations, is called the output of the observer.

It is important to stress that the observer (4.2), (4.3) is *not* implementable in cases where the velocity measurements are not available. This is because both (4.2a) and (4.3) involve the use of $x = x - \hat{x}$. Likewise, the observer characterized equivalently by (4.4) and (4.6) is also *not* implementable since the evaluation of $\hat{a}(t)$ using (4.6) (and therefore the evaluation of $\hat{x}(t)$ using (4.4a)) involves the differentiation of the joint position $q(t)$. As will be seen in the next subsection, however, an implementable approximation of the proposed observer does exists.

4.2.1 An Implementable Approximation of the Observer

From (4.4) and (4.6), it follows that for an arbitrary fixed time interval $\Delta > 0$,

$$\hat{x}(t) = \hat{x}(t-\Delta) + K[q(t) - q(t-\Delta)] + \int_{t-\Delta}^{t} [\psi(q, \hat{x}, \tau, \hat{a}) - K\hat{x}]dt \tag{4.7}$$

and

$$\hat{a}(t) = \hat{a}(t-\Delta) - \Gamma \int_{q(t-\Delta)}^{q(t)} Y^T(q, \hat{x}, \psi)dq + \Gamma \int_{t-\Delta}^{t} Y^T(q, \hat{x}, \psi)\hat{x}\,dt \tag{4.8}$$

Assuming that $Y(q, \hat{x}, \psi)$, $\psi(q, \hat{x}, \tau, \hat{a})$ and the joint position $q(t)$ as time functions are continuous and that Δ is sufficiently small, (4.7) and (4.8) suggest a discrete implementation of the proposed observer as follows

$$\hat{x}(i) = (I - \Delta K)\hat{x}(i-1) + \Delta\psi(i-1) + K[q(i) - q(i-1)] \tag{4.9}$$

$$\hat{a}(i) = \hat{a}(i-1) + \Gamma Y^T(i-1)[\Delta\hat{x}(i-1) - q(i) + q(i-1)] \tag{4.10}$$

Remarks

1. Obviously, (4.9) and (4.10) represent only an approximation of the observer proposed in (4.4) and (4.6). They are however implementable, and they approach to (4.7) and (4.8) (and therefore (4.4) and (4.6)) as Δ approaches to zero. In other words, (4.9) and (4.10) stand for a good representative of the observer if the sampling interval Δ is sufficiently small.
2. A problem with the continuity of ψ in (4.9) and (4.10) could develop if the adaptation of $\hat{a}$ causes an ill conditioned $\hat{H}$. To remedy this, a reset condition given in [17, pp. 192] can be used to guarantee $\hat{H} > 0$.

4.2.2 Stability of the Adaptive Observer

If the proposed adaptive observer is not used in control, the local asymptotic stability of the observation error is assumed by Theorem 4 which is stated below. For the sake of simplicity, in the rest of the chapter we have taken $t_0 = 0$.

Theorem 4: For a given $K > 0$, $\tilde{x}(t) \to 0$ as $t \to \infty$ if $\|\tau(t)\|$ is bounded, $\|x(t)\| \le m_v$,

$$\underline{\sigma} > m_c m_v + \beta - m_f$$

where $\underline{\sigma} = \lambda_{\min}\left(KH(q) + H(q)K\right)/2$, $\beta > 0$ is a fixed constant, $m_f = \lambda_{\min}(F)$, m_c is given in (2.13), and the initial estimation error $e(0) = \left[\tilde{x}^T(0) \quad \tilde{a}^T(0)\right]^T$ belongs to the ball B_v defined by

$$B_v = \left\{ e(0) \in \Re^{n+p} : \|e(0)\| < \sqrt{\frac{p_l}{p_u}} \left(\frac{1}{m_c}\left(\underline{\sigma} + m_f - \beta\right) - m_v \right) \right\}$$

where $p_l = \lambda_{\min}(P)$ and $p_u = \lambda_{\max}(P)$ with $P = \mathrm{diag}\left\{H(q), \Gamma^{-1}\right\}$.

A proof of Theorem 4 is given in Appendix 4.A. The main assumptions made in Theorem 4 are that joint velocities and joint torques are bounded and the bound of $x(t)$ is known. Although these assumptions appear to be restrictive, the result of Theorem 4 can be interpreted as a quantitative relation of the region of attraction to the magnitude of joint velocity (among other things). In some circumstances the robot is controlled to move along a given trajectory so a reasonable upper bound of $\|x\|$ may be obtained by adding a sufficient tolerance to the desired joint velocity trajectory $\|\dot{q}_d\|$. More importantly, these assumptions will be eliminated when the proposed observer is

combined with an adaptive controller in a feedback loop for robot motion control. Finally, Theorem 4 also quantifies the relation of observer gain K to the region of attraction, indicating how a gain matrix K is selected to make the observer work for a given $e(0)$.

4.3 Control using the Adaptive Observer

4.3.1 The Controller

The adaptive observer presented above can be combined with an adaptive controller to realize a manipulator observer-controller system which exhibits locally asymptotically stable trajectory tracking and locally asymptotically stable velocity *observation.*

The trajectory tracking controller proposed in this thesis has characteristics similar to that of [58]. However, an adaptive observer (4.2) is used to provide velocity estimates to it. The adaptive controller considered here is defined by

$$\tau = \hat{H}(q)\left[\dot{x}_d - (\hat{x}_a - x_d)\right] + \hat{C}(q,\hat{x}_a)x_r + \hat{F}x_r + \hat{g}(q) - K_d\hat{s} - K_p\tilde{q} \tag{4.11}$$

where $\hat{s} = \hat{x} - x_r$; the reference velocity is given by $x_r = x_d - \tilde{q}$ where $x_d(t)$ is the desired velocity trajectory; and the position tracking error is given by $\tilde{q} = q - q_d$ where $q_d(t)$ is the desired joint displacement trajectory. The proportional and derivative gain matrices are $K_p > 0$ and $K_d > 0$ respectively.

The adaptation rule employed to update the estimated dynamic parameters is given by

$$\dot{\hat{a}} = -\Gamma\left[Y^T(q,\hat{x},x_r,\dot{x}_d)s + Y^T(q,\hat{x},\psi)\tilde{x}\right] \tag{4.12}$$

where $s = \tilde{q} + \dot{\tilde{q}}$ contains an unknown quantity x. Integrating (4.12) over $[0,t]$, we obtain

an equivalent version of (4.12) where x is eliminated.

$$\hat{a}(t) = \hat{a}(t_0) - \Gamma \int_{q(0)}^{q(t)} (Y_{obs} + Y_{ctr})^T dq - \Gamma \int_0^t \left[Y_{obs}^T \hat{x} + Y_{ctr}^T (\tilde{q} - x_d) \right] dt \qquad (4.13)$$

where $Y_{obs} = Y(q, \hat{x}, \psi)$ and $Y_{ctr} = Y(q, \hat{x}, x_r, \dot{x}_d)$. The estimated parameters obtained from (4.13) are used both in the observer (4.2) and in the controller (4.11).

An implementation of controller (4.11) involves simply the calculation of $\tau(t)$ at time instant $t = i\Delta$. For the implementation of the parameter estimator, it follows from (4.13) that

$$\hat{a}(t) = \hat{a}(t-\Delta) - \Gamma \int_{q(t-\Delta)}^{q(t)} (Y_{obs} + Y_{ctr})^T dq - \Gamma \int_{t-\Delta}^{t} \left[Y_{obs}^T \hat{x} + Y_{ctr}^T (\tilde{q} - x_d) \right] dt$$

which suggests a digital implementation of (4.13) as follows

$$\begin{aligned} \hat{a}(i) = \hat{a}(i-1) &- \Gamma \left[Y_{obs}(i-1) + Y_{ctr}(i-1) \right]^T \left[q(i) - q(i-1) \right] \\ &- \Delta\Gamma \left[Y_{obs}^T(i-1)\hat{x}(i-1) + Y_{ctr}(i-1)\left(q(i-1) - q_d(i-1) - x_d(i-1) \right) \right] \end{aligned}$$

4.3.2 Stability of the Adaptive Observer-Controller

When the proposed adaptive observer is employed to provide a velocity signal which is used by the trajectory tracking controller given in (4.11), it can be shown that the position and velocity tracking errors as well as the *observed* velocity errors exhibit local asymptotic stability. This is established in Theorem 5 whose proof can be found in Appendix 4.B.

Theorem 5: For given $K>0$, $K_p=K_p^T>0$, $K_d=k_dI>0$ and $\Gamma>0$, $\tilde{x}(t),\tilde{q}(t),\dot{\tilde{q}}(t)\to 0$ as $t\to\infty$ if

$$\underline{\sigma}>c-\frac{b^2}{4a}-m_f+\beta \tag{4.14a}$$

and the initial estimate error $e(0)^T=\left[s^T(0)\quad \tilde{x}_a^T(0)\quad \tilde{q}^T(0)\quad \tilde{a}^T(0)\right]$ belongs to the ball B defined by

$$B=\left\{e(0)\in\Re^{3n+p}:\|e(0)\|<\sqrt{\frac{p_l}{p_u}}\left[\frac{\sqrt{4a\left(\underline{\sigma}+m_f-\beta\right)+b^2-4ac}-b}{2a}\right]\right\}$$

where $\beta>0$ is a fixed constant, $p_l=\lambda_{\min}(P)$, $p_u=\lambda_{\max}(P)$ with $P=\mathrm{diag}\left(H(q),H(q),K_p,\Gamma^{-1}\right)$, $\underline{\sigma}=\lambda_{\min}\left(KH(q)+H(q)K\right)/2$ and

$$a=\frac{m_c^2}{\left(k_d+m_f\right)} \tag{4.14b}$$

$$b=\left\{\frac{1}{\left(k_d+m_f\right)}\left[2m_c^2+m_d+2m_c\left(k_d+m_u\right)\right]+2m_c\right\} \tag{4.14c}$$

$$c=\frac{1}{\left(k_d+m_f\right)}\left\{\frac{1}{4}\left(k_d+m_u\right)^2+m_c^2m_d^2+2m_cm_d\left(k_d+m_u\right)\right\}+m_cm_d \tag{4.14d}$$

4.4 Simulation of the Proposed Adaptive Observer-Controller and a Well-Know Adaptive Controller

4.4.1 The Model

The second and third links of the PUMA-560 were used to demonstrate the performance of the proposed observer-controller in the presence of position measurement noise. In order to approximate continuous control more accurately PUMA's Mark II

controller was modified [20], making a sampling frequency of 250Hz possible. In this section, the second PUMA-560 link angle is considered joint angle one and the third link angle is considered joint angle two. The fourth, fifth and sixth links of the PUMA-560 were fixed. As such they constituted the third link of the robot; the mass of this last link was denoted by m_3. In the experiments it was assumed that m_3 was an unknown quantity, even though it had been accurately determined in [6]. The relevant robot model is given by

$$H(q)=\begin{bmatrix} a_1+2a_2c_2+(p_1+2p_2c_2)a_9 & (a_3+a_2c_2)+(p_3+p_2c_2)a_9 \\ (a_3+a_2c_2)+(p_3+p_2c_2)a_9 & a_7+p_3a_9 \end{bmatrix}$$

$$C(q,\dot{q})=s_2(a_2+p_2a_9)\begin{bmatrix} -\dot{q}_2 & -(\dot{q}_1+\dot{q}_2) \\ \dot{q}_1 & 0 \end{bmatrix}$$

$$F=\begin{bmatrix} a_4 & 0 \\ 0 & a_8 \end{bmatrix}, \quad g(q)=\begin{bmatrix} a_5c_1+a_6c_{12}+(p_4c_1+p_5c_{12})a_9 \\ a_6c_{12}+(p_5c_{12})a_9 \end{bmatrix}$$

where $a_1=6.33\ Kgm^2$, $a_2=0.14\ Kgm^2$, $a_3=0.11\ Kgm^2$, $a_4=27.6\ Kgm/s$, $a_5=31.9\ Nm$, $a_6=3.30\ Nm$, $a_7=0.94\ Kgm^2$, $a_8=4.54\ Kgm/s$, $a_9=1.25\ Kg$ and $p_1=0.37\ m^2$, $p_2=0.18\ m^2$, $p_3=0.18\ m^2$, $p_4=4.23\ m/s^2$, and $p_5=4.15\ m/s^2$. Note the use of the short notation $c_i=\cos(q_i)$, $s_i=\sin(q_i)$, and $c_{ij}=\cos(q_i+q_j)$ for the trigonometric functions. In the regressor formulation, the manipulator model is given by $Y_k a_k + Y_u a_u = \tau$ where

$$Y_k=\begin{bmatrix} \dot{x}_1 & 2c_2\dot{x}_1+c_2\dot{x}_2-2s_2x_1x_2-s_2x_2^2 & \dot{x}_2 & x_1 & c_2 & c_{12} & 0 & 0 \\ 0 & c_2\dot{x}_1+s_2x_1^2 & \dot{x}_1 & 0 & 0 & c_{12} & \dot{x}_2 & x_2 \end{bmatrix}$$

is the regressor associated with the known parameters $a_k = [a_1 \ldots a_8]^T$, $p = [p_1 \ldots p_5]^T$ and

$$Y_u = \begin{bmatrix} (p_1 + 2p_2c_2)\dot{x}_1 + (p_3 + p_2c_2)\dot{x}_2 - 2p_2s_2x_1x_2 - p_2s_2x_2^2 + p_4c_1 + p_5c_{12} \\ (p_3 + p_2c_2)\dot{x}_1 + p_3\dot{x}_2 + p_2s_2x_1^2 + p_5c_{12} \end{bmatrix}$$

is the regressor associated with the unknown parameter $a_9 = m_3$. The velocities of joint angles one and two are denoted by x_1 and x_2 respectively. The implementation of the observer will be detailed presently.

4.4.2 Implementation of The Observer

The velocity estimate provided by the reduced-order adaptive velocity observer at the i-th time instant was calculated with

$$\hat{x}(i) = \hat{x}(i-1) + \Delta\psi(i-1) + K(q(i) - q(i-1)) - \Delta K\hat{x}(i-1)$$

where

$$\psi(i-1) = \hat{H}^{-1}(q(i-1))\left[\tau - \hat{C}(q(i-1), \hat{x}(i-1))\hat{x}(i-1) - F\hat{x}(i-1) - \hat{g}(\hat{x}(i-1))\right]$$

The estimates of $H(q)$, $C(q,x)$ and $g(q)$ used in the above are given by

$$\hat{H}(q) = \begin{bmatrix} a_1 + 2a_2c_2 + (p_1 + 2p_2c_2)\hat{a}_9 & (a_3 + a_2c_2) + (p_3 + p_2c_2)\hat{a}_9 \\ (a_3 + a_2c_2) + (p_3 + p_2c_2)\hat{a}_9 & a_7 + p_3\hat{a}_9 \end{bmatrix}$$

$$\hat{C}(q,\hat{x}) = s_2(a_2 + p_2\hat{a}_9)\begin{bmatrix} -\hat{x}_2 & -(\hat{x}_1 + \hat{x}_2) \\ \hat{x}_1 & 0 \end{bmatrix}, \quad \hat{g}(q) = \begin{bmatrix} a_5c_1 + a_6c_{12} + (p_4c_1 + p_5c_{12})\hat{a}_9 \\ a_6c_{12} + (p_5c_{12})\hat{a}_9 \end{bmatrix}$$

These were created by replacing the third link's mass $a_9 = m_3$ with estimate $\hat{a}_9 = \hat{m}_3$. The initial estimate chosen for m_3 was $\hat{a}_9(0) = 0$. The initial velocity estimate was purposefully set at $\hat{x}(0) = [10 \quad -10]^T$ degrees per second, even though the trajectory starts from rest. This was done to show the robustness of the observer response to incorrect initial conditions.

The i-th torque signal was calculated with

$$\tau(i) = Y_{kctr}\left(q(i), \hat{x}(i), x_r(i), \dot{x}_d(i)\right)a_k(i) + Y_{uctr}\left(q(i), \hat{x}(i), x_r(i), \dot{x}_d(i)\right)\hat{a}_9(i) - K_d\hat{s}(i) - K_p\left(q(i) - q_d(i)\right)$$

where

$$Y_{kctr} = \begin{bmatrix} \dot{x}_{d1} & 2c_2\dot{x}_{d1} + c_2\dot{x}_{d2} - s_2\hat{x}_2x_{r1} - s_2\hat{x}_1x_{r2} - s_2\hat{x}_2x_{r2} & \dot{x}_{d2} & \hat{x}_1 & c_2 & c_{12} & 0 & 0 \\ 0 & c_2\dot{x}_{d1} + s_2\hat{x}_1x_{r1} & \dot{x}_{d1} & 0 & 0 & c_{12} & \dot{x}_{d2} & \hat{x}_2 \end{bmatrix}$$

was the regressor used in control associated with the known dynamic parameters and

$$Y_{uctr} = \begin{bmatrix} \left(p_1 + 2p_2c_2\right)\dot{x}_{d1} + \left(p_3 + p_2c_2\right)\dot{x}_{d2} - p_2s_2\hat{x}_1x_{r2} - p_2s_2x_{r1}\hat{x}_2 - p_2s_2\hat{x}_2x_{r2} + p_4c_1 + p_5c_{12} \\ \left(p_3 + p_2c_2\right)\dot{x}_{d1} + p_3\dot{x}_{d2} + p_2s_2\hat{x}_1x_{r1} + p_5c_{12} \end{bmatrix}$$

was the regressor used in control associated with the unknown dynamic parameter.

4.4.3 Parameter Adaptation

The i-th parameter estimate $\hat{a}_9(i)$ was calculated with

$$\hat{a}_9(i) = \hat{a}_9(i-1) - \gamma\left[Y_{uobs}(i-1) + Y_{uctr}(i-1)\right]^T\left[q(i) - q(i-1)\right] - \gamma\Delta\left[Y_{uobs}^T(i-1)\hat{x}(i-1) + Y_{uctr}^T(i-1)\left(q(i-1) - q_d(i-1) - x_d(i-1)\right)\right]$$

where $\Gamma = \gamma I$ was used for the adaptation gain, Y_{uctr} was defined as above and

$$Y_{uobs} = \begin{bmatrix} (p_1 + 2p_2c_2)\psi_1 + (p_3 + p_2c_2)\psi_2 - 2p_2s_2\hat{x}_1\hat{x}_2 - p_2s_2\hat{x}_2^2 + p_4c_1 + p_5c_{12} \\ (p_3 + p_2c_2)\psi_1 + p_3\psi_2 + p_2s_2\hat{x}_1^2 + p_5c_{12} \end{bmatrix}$$

4.4.4 The Joint Trajectory and Sampling Rates

In order to test the trajectory tracking capability of the proposed adaptive observer-controller and compare results to those obtained for the well-known Slotine-Li adaptive controller, fifth order polynomial trajectories were designed for both the first and second joints of the robot manipulator (see Fig. 3.1). A set of 500 points on the trajectory were provided to the controller every 12 ms. producing a trajectory duration of 6 seconds. The control update period was $\Delta = 4$ ms.

4.4.5 Simulation Results

This section compares the proposed observer-controller with Slotine-Li's adaptive controller [58]. Slotine-Li's method is assumed to use differentiated filtered position signals to obtain velocity estimates. The comparison of the two schemes is based on computer simulation.

The fifth order polynomials described in Section 3.5.2 were used as the desired trajectory. The position measurements were assumed to have zero-mean Gaussian noise with standard deviation $\sigma_n = 0.0818$ degrees. This noise statistic was derived from experiments conducted on a General Electric hydraulic robot arm located at International Submarine Engineering Ltd. of Port Coquitlam British Columbia (see Appendix A). The General Electric arm had rotary potentiometers to obtain position measurements.

The observer gains for the proposed method were $K = \text{diag}(30,20)$. The position and

derivative gains were taken as $K_p = \text{diag}(500,500)$ and $K_d = \text{diag}(50,50)$, respectively. These gains were selected to reduce tracking error while keeping the control torque chatter small.

For Slotine-Li's controller, which used differentiated position signals to obtain velocities, first-order filters were used to reduce noise in the velocity signal. These filters are described in (3.11a) where the selected filter gains are given by $K_f = \text{diag}(30,20)$. The position and derivative gains used for Slotine-Li's controller were equivalent to those used for the proposed method.

The position and velocity tracking results for the proposed method are shown in Figs. 4.1 and 4.2. Results for Slotine-Li's method are shown in Figs. 4.3 and 4.4, where the joint velocities were obtained using numerical differentiation of filtered position data. Comparison of the position tracking shows substantial difference, where due to the delays introduced with the position filter, control with Slotine-Li's method leads to larger errors. The maximum tracking errors for joints one and two after the first one second of motion using our method were found to be 0.3 deg and 0.4 deg respectively. Using Slotine-Li's method, these errors were found to be 1.8 deg and 3.4 deg for joints one and two respectively. The velocity tracking for the two methods also differed. For the proposed method, these errors were found to be 0.63 deg/sec and 1.7 deg/sec for joints one and two after the first one second of motion and for Slotine-Li's method these were determined as 2.5 deg/sec and 5.2 deg/sec.

It must be stressed that the improved tracking results were achieved with the proposed method while the magnitude in the applied control torque is reduced. The torque required to achieve these results was less than Slotine-Li's method, see Fig. 4.5. The 1-norm was used to quantify the average torque applied in achieving the results described above. For our scheme, the average torques applied at joints one and two were calculated as 27 N

and 6.4 N. For Slotine-Li's control scheme, the torques were 29 N and 6.5 N for joints one and two respectively. These results are summarized in Table 4.1 below.

	$\|\tilde{q}_1\|_\infty$ (deg)	$\|\tilde{q}_2\|_\infty$ (deg)	$\|\dot{\tilde{q}}_1\|_\infty$ (deg/s)	$\|\dot{\tilde{q}}_2\|_\infty$ (deg/s)	$\|\tau_1\|_1$ (Nm)	$\|\tau_2\|_1$ (Nm)
Proposed Method	0.3	0.4	0.63	1.7	27	6.4
Slotine Li's Method	1.8	3.4	2.5	5.2	29	6.5

Table 4.1: Summary of performance results for Slotine-Li's Method and for the Proposed Observer-Controller.

The adaptation of the unknown parameter $\hat{a}_9(t)$ for both methods is shown in Fig. 4.6. The adaptive gain used in both techniques was taken as $\gamma = 5$. The dashed lines in Figs. 4.6(a) and 4.6(b) represent the actual value of the "unknown" parameter. The dynamics of parameter adaptation for the proposed method drifts less than that for Slotine-Li's method. The reason for this may be that since a simple lowpass filter is used with Slotine-Li's method, their regressor formulation requires an additional filter model.

4.5 Experiments with the Observer-Controller

Experimental testing was carried out on PUMA-560. The observer gain used was $K = \text{diag}(100,100)$, the adaptation gain was selected as $\gamma = 1.5$ and the controller gains were taken as $K_p = \text{diag}(500,500)$ and $K_d = \text{diag}(50,50)$. The results of the experiment are shown in Figs. 4.7, 4.8 and 4.9. Figures 4.7(a-b) and 4.8(a-b) show that after the initial transient, the maximum position tracking error does not exceed 1 degree for both the first and second joints over the entire six second trajectory. The velocity tracking

results are shown in Figs. 4.7(c-d) and 4.8(c-d). The torques applied to the joints and parameter adaptation are shown in Fig. 4.9. Note the lower level of chattering in the torque signals as well as the smooth adaptation of the unknown parameter to its actual value. The mass of the end-effector was known to be $m_3 = 1.25$ Kg from [6].

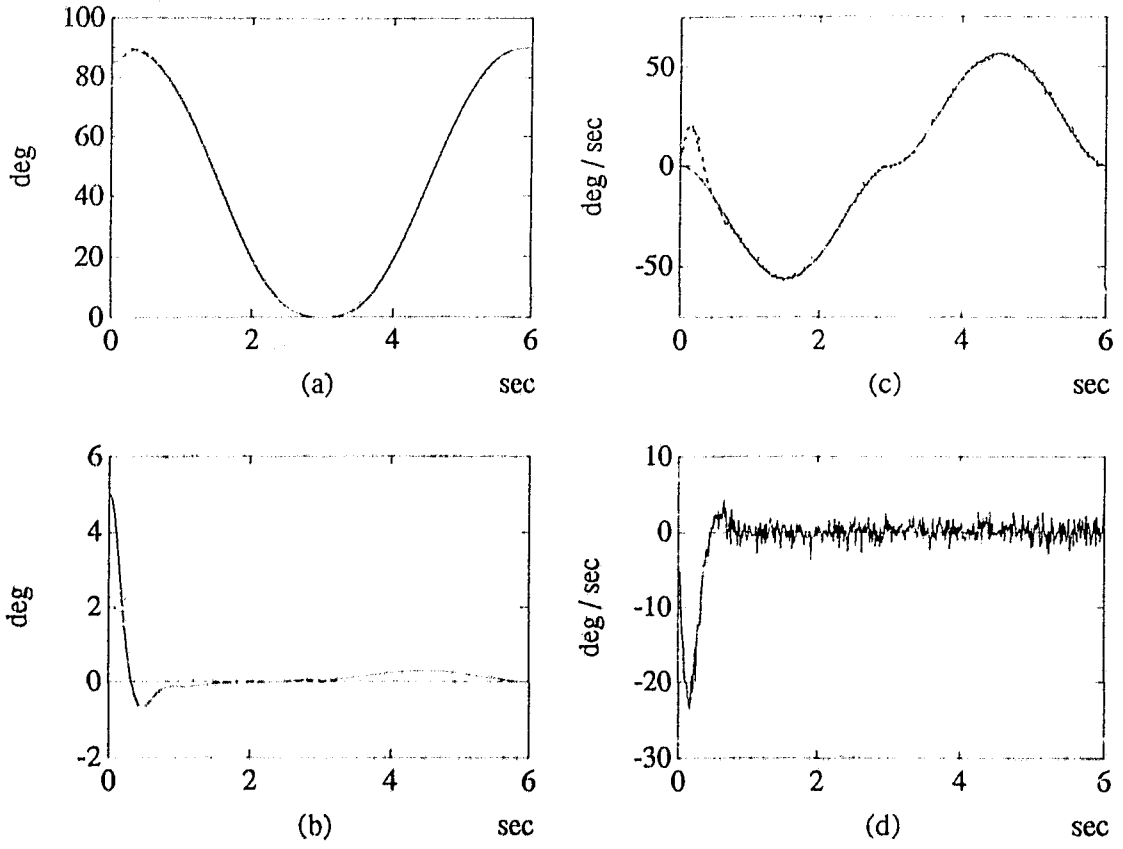

Fig. 4.1: Simulation results for the first link using the adaptive observer (a) desired versus actual position, (b) position error, (c) desired versus actual velocity, (d) velocity error.

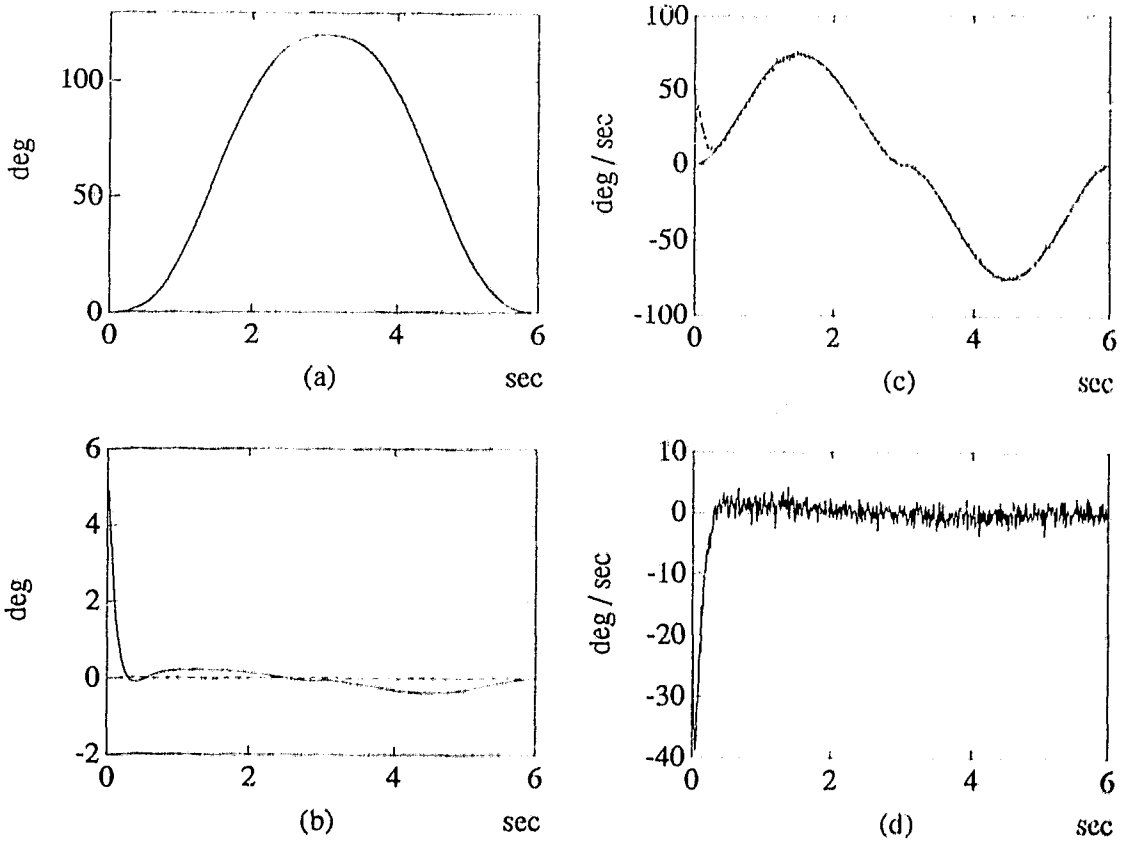

Fig. 4.2: Simulation results for the second link using the adaptive observer (a) desired versus actual position, (b) position error, (c) desired versus actual velocity, (d) velocity error.

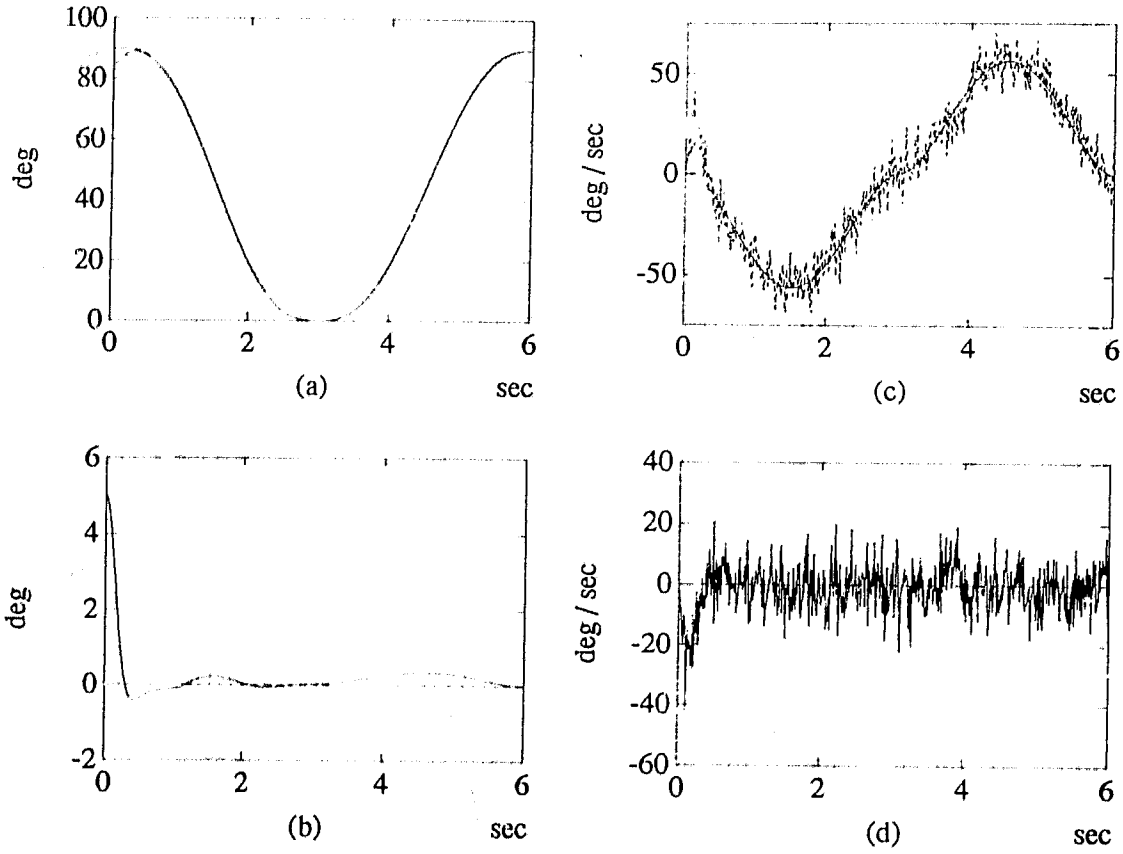

Fig. 4.3: Simulation results for the first link using Slotine-Li method with differentiation (a) desired versus actual position, (b) position error, (c) desired versus actual velocity, (d) velocity error.

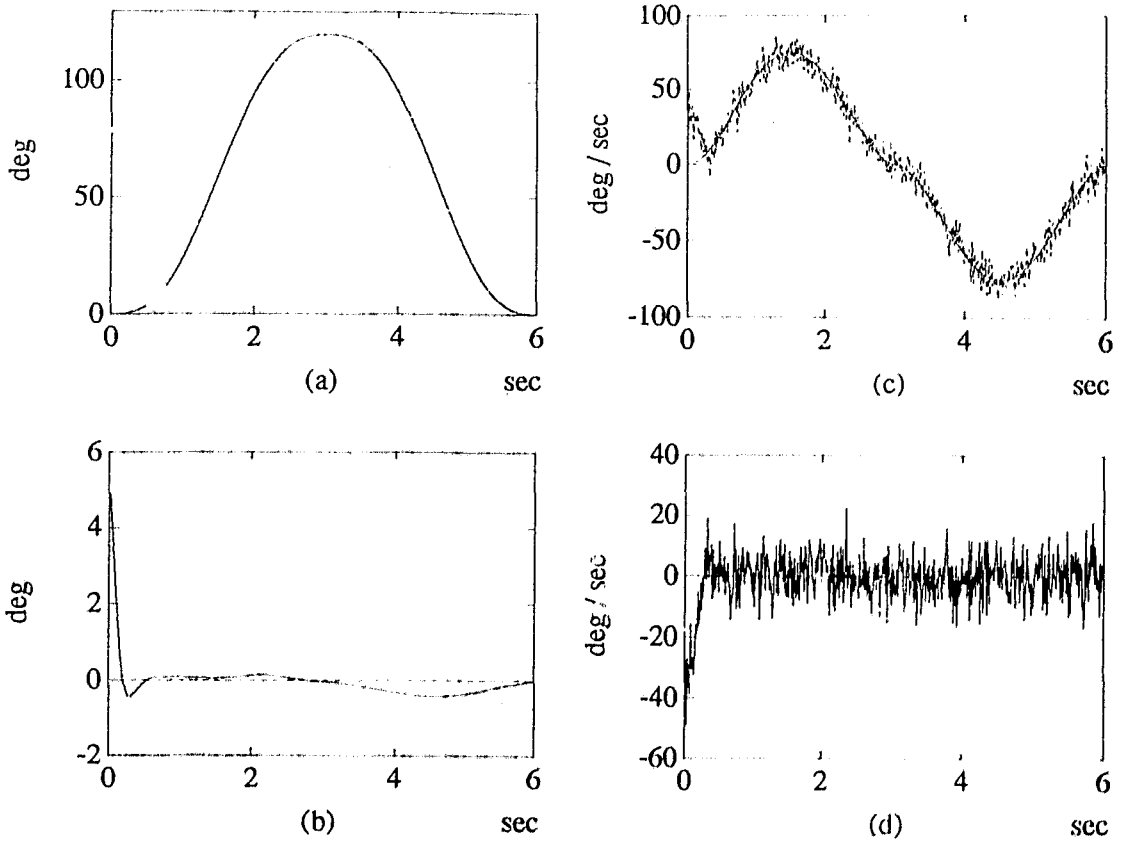

Fig. 4.4: Simulation results for the second link using Slotine-Li method with differentiation (a) desired versus actual position, (b) position error, (c) desired versus actual velocity, (d) velocity error.

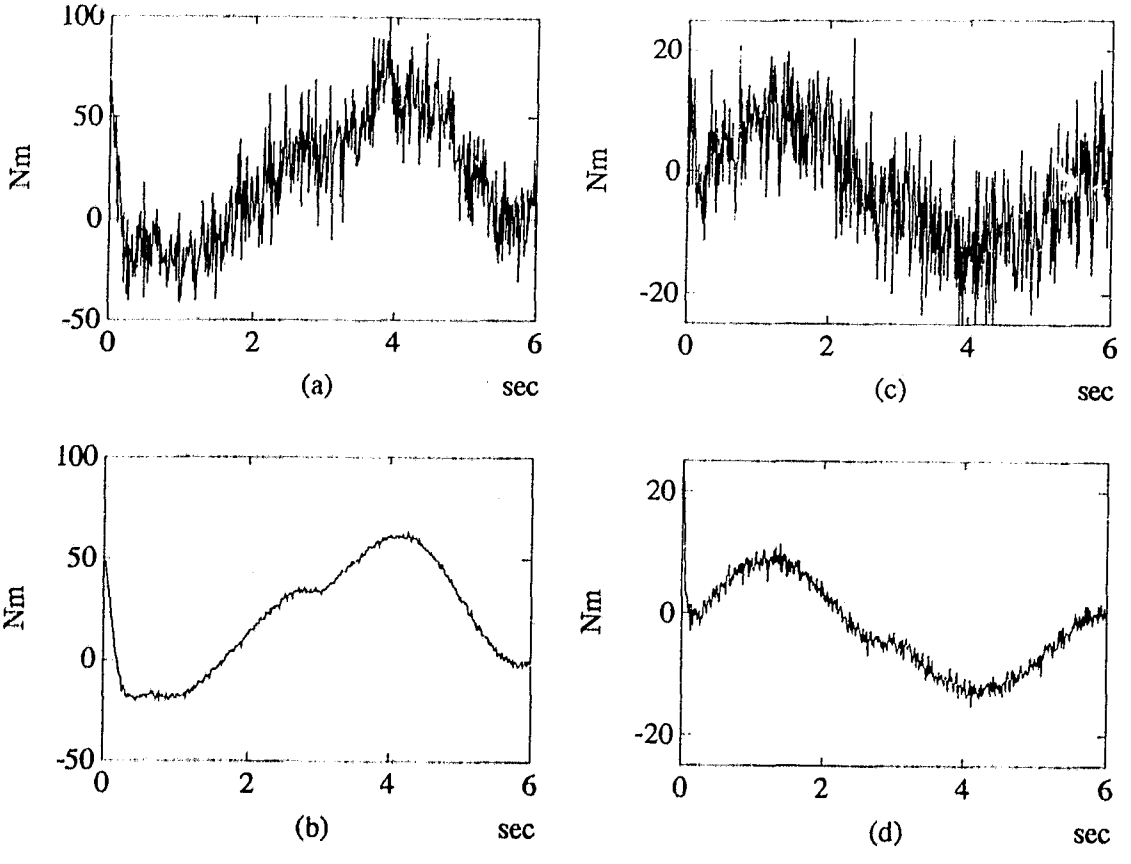

Fig. 4.5: Simulation: comparison of joint torques (a) Slotine-Li method with differentiation, joint 1, (b) adaptive observer method, joint 1, (c) Slotine-Li method with differentiation, joint 2, (d) adaptive observer method, joint 2.

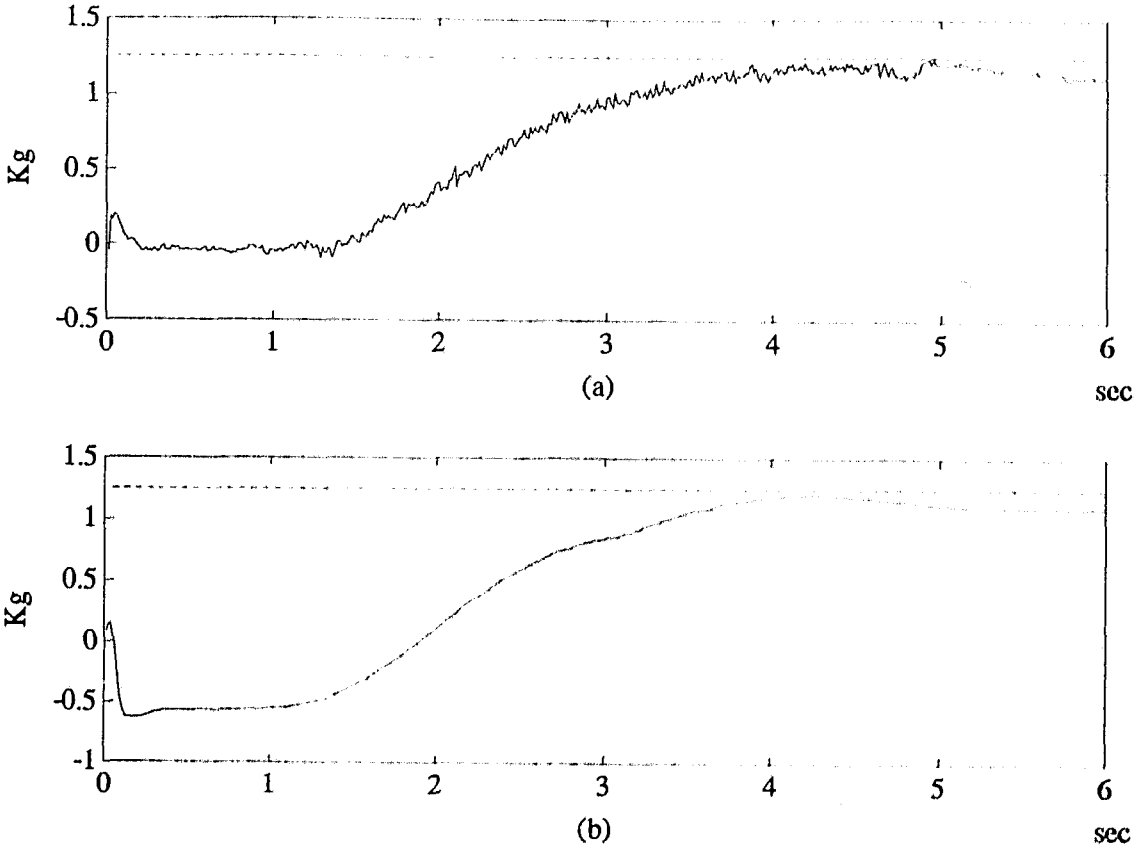

Fig. 4.6: Simulation: comparison of parameter adaptation (a) adaptive observer method, (b) Slotine-Li method with differentiation .

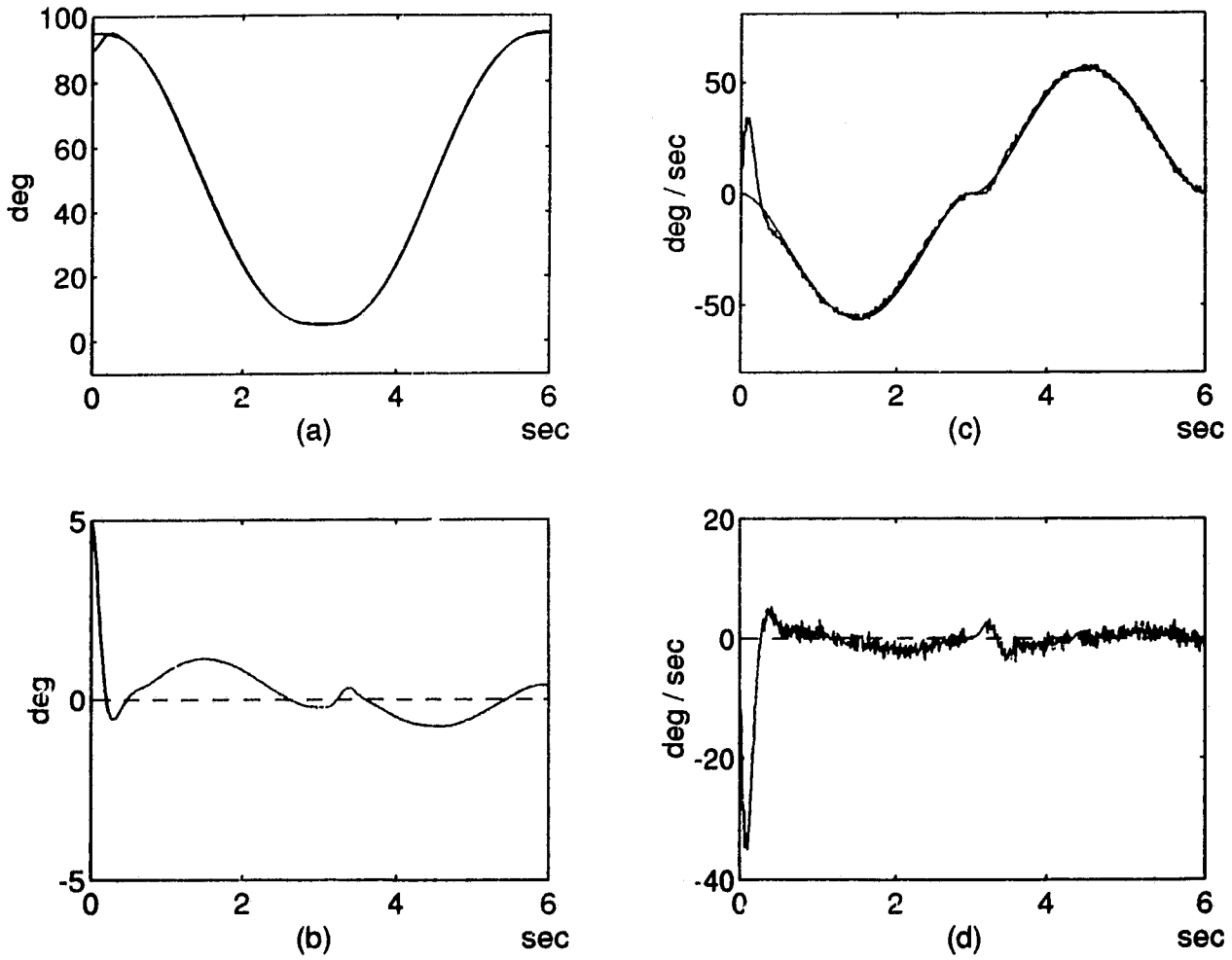

Fig. 4.7: Experimental results for the first link using the adaptive observer (a) desired versus measured position, (b) position error, (c) desired versus measured velocity, (d) velocity error.

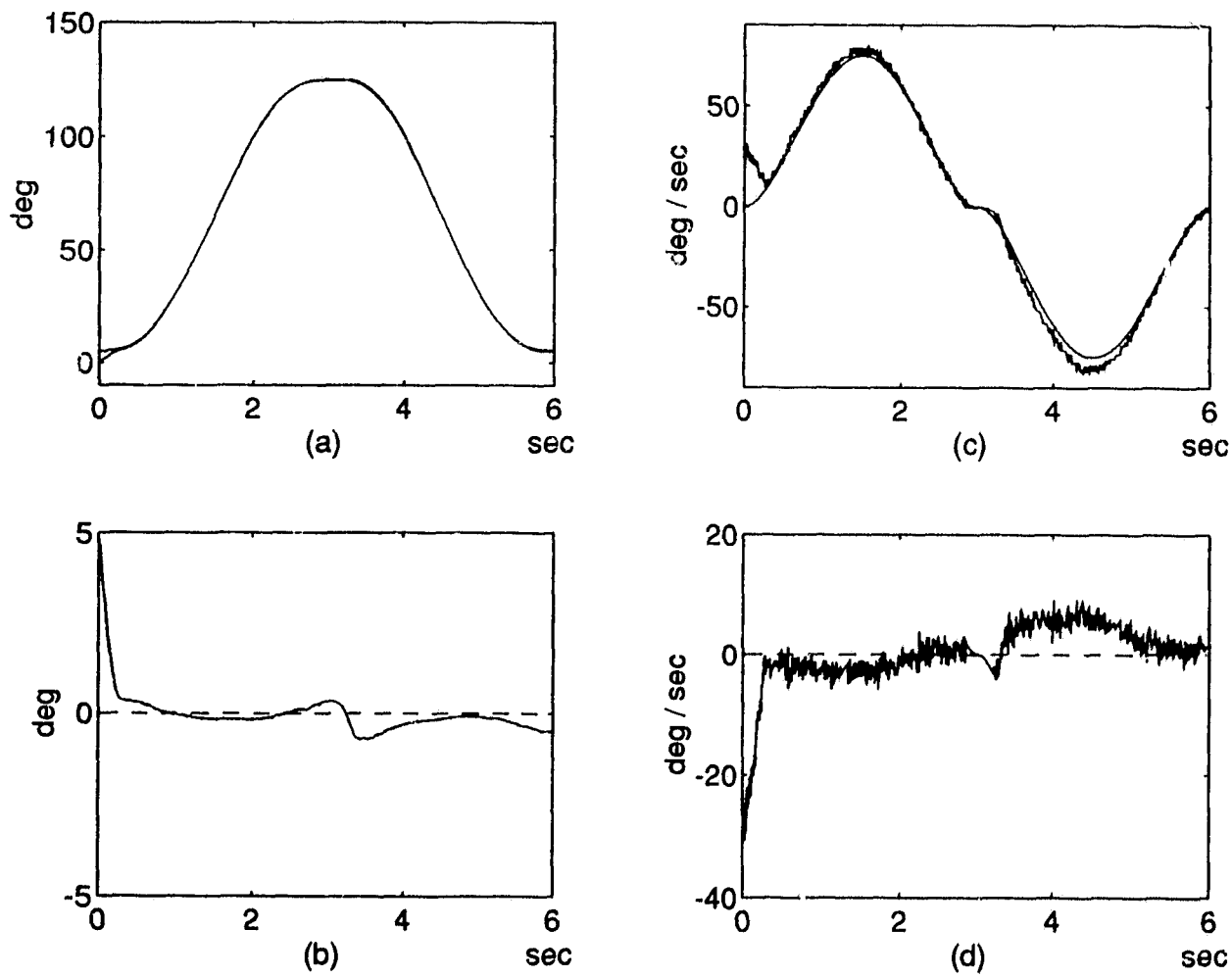

Fig. 4.8: Experimental results for the second link using the adaptive observer (a) desired versus measured position, (b) position error, (c) desired versus measured velocity, (d) velocity error.

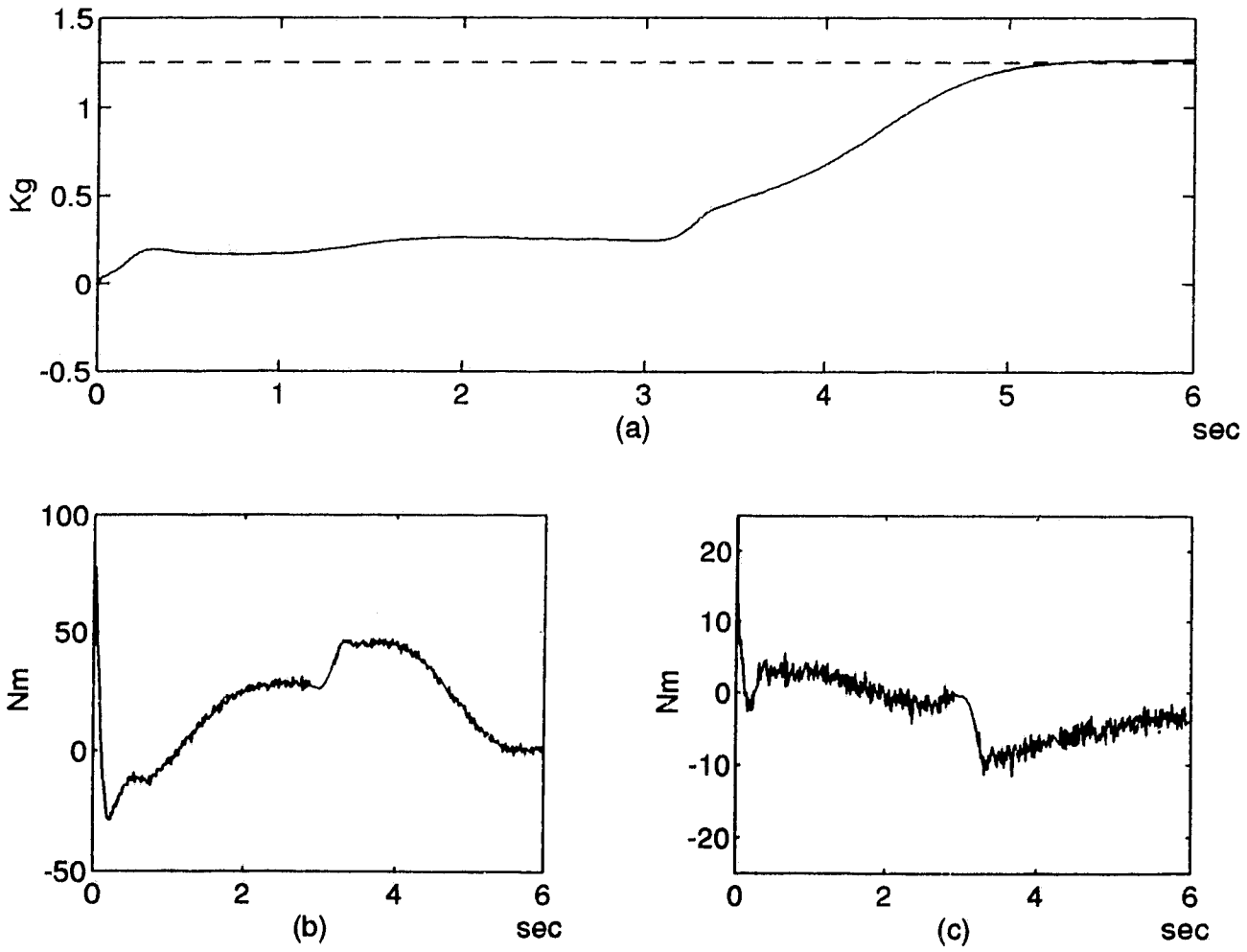

Fig. 4.9: Experimental results using the adaptive observer (a) parameter adaptation, (b) joint torque 1, (c) joint torque 2.

4.A Proof of Theorem 4

Consider the Lyapunov function

$$v(t) = \frac{1}{2} e(t)^T P e(t)$$

where $e^T = \begin{bmatrix} \tilde{x}^T & \tilde{a}^T \end{bmatrix}$ and $P = \text{diag}\left(H(q), \Gamma^{-1}\right)$ with $\Gamma > 0$. Function $v(t)$ is upper and lower bounded, i.e.

$$\frac{1}{2} p_l \|e(t)\|^2 \le v(t) \le \frac{1}{2} p_u \|e(t)\|^2 \tag{A.1}$$

The time derivative of $v(t)$ along trajectories of $\tilde{x}$ and $\tilde{a}$ is computed as

$$\dot{v} = \tilde{x}^T \left(H(q)\dot{\tilde{x}} + \frac{1}{2}\dot{H}(q)\tilde{x} \right) + \tilde{a}^T \Gamma^{-1} \dot{\tilde{a}} \tag{A.2}$$

Subtracting (4.2) from (4.1), we have

$$H(q)\dot{\tilde{x}} = -C(q,\hat{x})\tilde{x} - C(q,x)\tilde{x} - F\tilde{x} - H(q)K\tilde{x} + \Theta$$

where

$$\begin{aligned} \Theta &= \tau - C(q,\hat{x})\hat{x} - F\hat{x} - g(q) - H(q)\hat{H}^{-1}(q)\left[\tau - \hat{C}(q,\hat{x})\hat{x} - \hat{F}\hat{x} - \hat{g}(q)\right] \\ &\quad - \left[\tau - \hat{C}(q,\hat{x})\hat{x} - \hat{F}\hat{x} - \hat{g}(q)\right] + \left[\tau - \hat{C}(q,\hat{x})\hat{x} - \hat{F}\hat{x} - \hat{g}(q)\right] \\ &= \tilde{H}(q)\psi + \tilde{C}(q,\hat{x})\hat{x} + \tilde{F}\hat{x} + \tilde{g}(q) \end{aligned}$$

Hence

$$H(q)\dot{\tilde{x}} = -C(q,\hat{x})\tilde{x} - C(q,x)\tilde{x} - F\tilde{x} - H(q)K\tilde{x} + \tilde{H}(q)\psi + \tilde{C}(q,\hat{x})\hat{x} + \tilde{F}\hat{x} + \tilde{g}(q) \tag{A.3}$$

where $\tilde{H} = \hat{H} - H$, $\tilde{C} = \hat{C} - C$, $\tilde{F} = \hat{F} - F$, and $\tilde{g} = \hat{g} - g$. By applying property 5, (A.3) becomes

$$H(q)\dot{\tilde{x}} = -C(q,\hat{x})\tilde{x} - C(q,x)\tilde{x} - F\tilde{x} - H(q)K\tilde{x} + Y(q,\hat{x},\psi)\tilde{a} \tag{A.4}$$

Now, substituting (A.4) into (A.2) and using properties 3 and 4 leads to

$$\dot{v} = -\tilde{x}^T\big(H(q)K + F + C(q,\hat{x})\big)\tilde{x} + \tilde{a}^T\left[\Gamma^{-1}\dot{\hat{a}} + Y^T(q,\hat{x},\psi)\tilde{x}\right] \tag{A.5}$$

Further, (A.5) in conjunction with (4.3) and properties 1 and 2 gives

$$\dot{v} \le -\big(\underline{\sigma} + m_f - m_c m_v - m_c\|\tilde{x}\|\big)\|\tilde{x}\|^2 \tag{A.6}$$

where m_v denotes the upper bound of $\|x(t)\|$. Equation (A.6) remains negative semidefinite if

$$\underline{\sigma} > m_c\|\tilde{x}\| + m_c m_v - m_f \tag{A.7}$$

But $\|e\| > \|\tilde{x}\|$, so (A.7) holds if $\underline{\sigma} > m_c\|e\| + m_c m_v - m_f$ is satisfied which is equivalent to

$$\|e\| < \frac{1}{m_c}\big(\underline{\sigma} + m_f\big) - m_v \tag{A.8}$$

From (A.6), (A.8) and (A.1), we obtain that if

$$\|e(0)\| < \sqrt{\frac{p_l}{p_u}}\left[\frac{1}{m_c}\left(\underline{\sigma} + m_f\right) - m_v\right]$$

then

$$\dot{v}(t) \le -\beta\|\tilde{x}(t)\|^2 \qquad \forall t \ge 0 \tag{A.9}$$

Note that (A.1) and (A.9) mean that $\tilde{x}(t) \in L_\infty$ and $\tilde{x}(t) \in L_2$, respectively. Furthermore, (A.1) and $\dot{v}(t) < 0$ implies that $\tilde{a}(t) \in L_\infty$, thus $\hat{a}(t) = \tilde{a}(t) + a \in L_\infty$. So $\psi(q, \hat{x}, \tau, \hat{a})$ as a time function belongs to L_∞ if $\|\tau\|$ is bounded, i.e.

$$\dot{\tilde{x}} = -H(q)\left[C(q,\hat{x})\tilde{x} + C(q,x)\dot{\tilde{x}} + F\tilde{x} + H(q)K\tilde{x} - Y(q,\hat{x},\psi)\tilde{a}\right]$$

where

$$\psi(q,\hat{x},\tau,\hat{a}) = \hat{H}^{-1}(q)\left[\tau - \hat{C}(q,\hat{x})\hat{x} - \hat{F}\hat{x} - \hat{g}(q)\right]$$

or equivalently

$$\psi(q,\hat{x},\tau,\hat{a}) = \hat{H}^{-1}(q)\left[\tau - \hat{C}(q,x-\tilde{x})(x-\tilde{x}) - \hat{F}(x-\tilde{x}) - \hat{g}(q)\right]$$

Leading to $\dot{\tilde{x}}(t) \in L_\infty$. In summary, we have $\tilde{x}, \dot{\tilde{x}} \in L_\infty$ and $\tilde{x} \in L_2$, thus Barbalat's lemma [54, pp. 25] implies that $\tilde{x}(t) \to 0$ as $t \to \infty$ □

4.B Proof of Theorem 5

Define

$$v(t) = \frac{1}{2} e(t)^T P e(t)$$

where $e^T = \begin{bmatrix} s^T & \tilde{x}^T & \tilde{q}^T & \tilde{a}^T \end{bmatrix}$ and $P = \text{diag}\left(H(q), H(q), K_p, \Gamma^{-1}\right)$ with $K_p = K_p^T > 0$ and $\Gamma > 0$. Then $v(t)$ satisfies

$$\frac{1}{2} p_l \|e(t)\|^2 \leq v(t) \leq \frac{1}{2} p_u \|e(t)\|^2 \tag{B.1}$$

The time derivative of $v(t)$ along trajectories of $e(t)$ is given by

$$\dot{v} = s^T \left(H(q)\dot{s} + \frac{\dot{H}(q)}{2} s \right) + \dot{\tilde{q}}^T K_p \tilde{q} + \tilde{x}^T \left(H(q)\dot{\tilde{x}} + \frac{\dot{H}(q)}{2} \tilde{x} \right) + \tilde{a}^T \Gamma^{-1} \dot{\tilde{a}} \tag{B.2}$$

As $\dot{\tilde{a}} = \dot{\hat{a}}$ and $\dot{\tilde{q}} = s - \tilde{q}$, (B.2) becomes

$$\dot{v} = s^T \left(H(q)\dot{s} + K_p \tilde{q} + \frac{\dot{H}(q)}{2} s \right) - \tilde{q}^T K_p \tilde{q} + \tilde{x}^T \left(H(q)\dot{\tilde{x}} + \frac{\dot{H}(q)}{2} \tilde{x} \right) + \tilde{a}^T \Gamma^{-1} \dot{\hat{a}} \tag{B.3}$$

The controller's error dynamics is found by equating (2.8) and (4.11) and applying properties 3, 4 and 5 along with the result

$$
\begin{aligned}
&H(q)\dot{x} - \hat{H}(q)[\dot{x}_r + \tilde{x}] \\
&\quad = H(q)\dot{x} - H(q)\dot{x}_r + H(q)\dot{x}_r - \hat{H}(q)\dot{x}_r - \hat{H}(q)\tilde{x} \\
&\quad = H(q)\dot{s} + H(q)(\dot{x}_r + x - \hat{x}) - H(q)x + H(q)\hat{x} - \hat{H}(q)\dot{x}_r - \hat{H}(q)x + \hat{H}(q)\hat{x} \\
&\quad = H(q)\dot{s} - \tilde{H}(q)(\dot{x}_r + x - \hat{x}) + \hat{H}(q)\dot{x}_r + \hat{H}(q)x - \hat{H}(q)\hat{x} - H(q)x + H(q)\hat{x} \\
&\quad -\hat{H}(q)\dot{x}_r - \hat{H}(q)x + \hat{H}(q)\hat{x} \\
&\quad = H(q)\dot{s} - \tilde{H}(q)\big(\dot{x}_d - (\hat{x} - x_d)\big) - H(q)\tilde{x}
\end{aligned}
$$

to obtain

$$
H(q)\dot{s} = -C(q,x)s - (K_d + F)s - K_p\tilde{q} + K_d\tilde{x} + H(q)\tilde{x} - C(q,x_r)\tilde{x} + Y(q,\hat{x},x_r,\dot{x}_d)\tilde{a} \tag{B.4}
$$

where $s = x - x_r = \dot{\tilde{q}} + \tilde{q}$. The observer error dynamics was developed in Appendix A and is given by

$$
H(q)\dot{\tilde{x}} = -C(q,\hat{x})\tilde{x} - C(q,x)\tilde{x} - F\tilde{x} - H(q)K\tilde{x} + Y(q,\hat{x},\psi)\tilde{a} \tag{B.5}
$$

Substituting observer and controller error dynamics (B.4) and (B.5) into (B.3) and using property 4 gives

$$
\begin{aligned}
\dot{v} = &-s^T(K_d + F)s - \tilde{q}^T K_p\tilde{q} - \tilde{x}^T\big(H(q)K + F + C(q,\hat{x})\big)\tilde{x} \\
&+s^T\big(K_d + H(q) - C(q,x_r)\big)\tilde{x} + s^T Y(q,\hat{x},x_r,\dot{x}_d)\tilde{a} \\
&+\tilde{x}^T Y(q,\hat{x},\psi)\tilde{a} + \tilde{a}^T\Gamma^{-1}\dot{\hat{a}}
\end{aligned}
$$

If the parameter adaptation law is selected in (4.12) then

$$
\dot{v} = -s^T(K_d + F)s - \tilde{q}^T K_p\tilde{q} - \tilde{x}^T\big(H(q)K + F + C(q,\hat{x})\big)\tilde{x} + s^T\big(K_d + H(q) - C(q,x_r)\big)\tilde{x}
$$

As $x_r = x_d - \tilde{q}$ and $\hat{x} = x_d + s - \tilde{x} - \tilde{q}$ we obtain

$$\begin{aligned}\dot{v} \le & -\left(k_d + m_f\right)\|s\|^2 - \left(\underline{\sigma} + m_f - m_c m_d - m_c\left(\|\tilde{x}\| + \|s\| + \|\tilde{q}\|\right)\right)\|\tilde{x}\|^2 \\ & -k_p\|\tilde{q}\|^2 + \left(k_d + m_u + m_c\left(m_d + \|\tilde{q}\|\right)\right)\|\tilde{x}\|\|s\|\end{aligned} \tag{B.6}$$

where $\|x_d\| \le m_d$, $K_d = k_d I$, $k_p = \lambda_{\min}\left(K_p\right)$ and $m_f = \lambda_{\min}(F)$. Equation (B.6) can be reformulated using matrix notation to give

$$\dot{v} = -\begin{bmatrix}\|s\| & \|\tilde{x}\| & \|\tilde{q}\|\end{bmatrix}^T B\left(\|s\|, \|\tilde{x}\|, \|\tilde{q}\|\right)\begin{bmatrix}\|s\| \\ \|\tilde{x}\| \\ \|\tilde{q}\|\end{bmatrix} \tag{B.7}$$

where

$$B\left(\|s\|, \|\tilde{x}\|, \|\tilde{q}\|\right) = \begin{bmatrix} k_d + m_f & -\frac{1}{2}\left[k_d + m_u + m_c\left(m_d + \|\tilde{q}\|\right)\right] & 0 \\ -\frac{1}{2}\left[k_d + m_u + m_c\left(m_d + \|\tilde{q}\|\right)\right] & \left[\underline{\sigma} + m_f - m_c md - m_c\left(\|x\| + \|\tilde{s}\| + \|\tilde{q}\|\right)\right] & 0 \\ 0 & 0 & k_p \end{bmatrix}$$

To guarantee that (B.7) remains negative, matrix $B\left(\|s\|, \|\tilde{x}\|, \|\tilde{q}\|\right) \in \Re^{3\times 3}$ must be positive definite which is true if the leading principal minors of $B\left(\|s\|, \|\tilde{x}\|, \|\tilde{q}\|\right)$ are all positive. The first condition is given by

$$k_d + m_f > 0$$

The second condition is given by the following

$$\left(k_d + m_f\right)\left[\underline{\sigma} + m_f - m_c m_d - m_c\left(\|\tilde{x}\| + \|s\| + \|\tilde{q}\|\right)\right]$$
$$-\frac{1}{4}\left[\left(k_d + m_u\right)^2 + m_c^2\left(m_d + \|\tilde{q}\|\right)^2 + 2m_c\left(k_d + m_u\right)\left(m_d + \|\tilde{q}\|\right)\right] > 0$$

which is equivalent to

$$\underline{\sigma} + m_f > \frac{1}{\left(k_d + m_f\right)}\left\{\frac{1}{4}\left(k_d + m_u\right)^2 + m_c^2 m_d^2 + 2m_c^2 m_d\|\tilde{q}\| + m_c^2\|\tilde{q}\|^2\right\}$$
$$\frac{1}{\left(k_d + m_f\right)}\left\{2m_c m_d\left(k_d + m_u\right) + 2m_c\left(k_d + m_u\right)\|\tilde{q}\|\right\} + m_c\left(m_d + \|\tilde{x}\| + \|s\| + \|\tilde{q}\|\right) \tag{B.8}$$

But $2\|e\| > \|\tilde{x}\| + \|s\| + \|\tilde{q}\|$, $\|e\| > \|\tilde{q}\|$ and $\|e\|^2 > \|\tilde{q}\|^2$ so (B.8) can be rewritten as

$$\underline{\sigma} + m_f > \frac{1}{\left(k_d + m_f\right)}\left\{\frac{1}{4}\left(k_d + m_u\right)^2 + m_c^2 m_d^2 + 2m_c m_d\left(k_d + m_u\right)\right\} + m_c m_d$$
$$+\left\{\frac{1}{\left(k_d + m_f\right)}\left[2m_c^2 + m_d + 2m_c\left(k_d + m_u\right)\right] + 2m_c\right\}\|e\|$$
$$+\frac{m_c^2}{\left(k_d + m_f\right)}\|e\|^2$$

or

$$\underline{\sigma} + m_f > a\|e\|^2 + b\|e\| + c'$$

where

$$a = \frac{m_c^2}{\left(k_d + m_f\right)} \tag{B.9a}$$

$$b = \left\{\frac{1}{\left(k_d + m_f\right)}\left[2m_c^2 + m_d + 2m_c\left(k_d + m_u\right)\right] + 2m_c\right\} \tag{B.9b}$$

$$c' = \frac{1}{\left(k_d + m_f\right)}\left\{\frac{1}{4}\left(k_d + m_u\right)^2 + m_c^2 m_d^2 + 2m_c m_d\left(k_d + m_u\right)\right\} + m_c m_d \tag{B.9c}$$

so

$$a\|e(t)\|^2 + b\|e(t)\| + c' - \left(\underline{\sigma} + m_f\right) < 0 \tag{B.10}$$

The roots of (B.10) are given by

$$\|e\| = \frac{-b \pm \sqrt{b^2 - 4ac' + 4a\left(\underline{\sigma} + m_f\right)}}{2a}$$

The roots of (B.10) are real if

$$\underline{\sigma} > c' - \frac{b^2}{4a} - m_f \tag{B.11}$$

Then equation (B.10) can be written as

$$\left[\|e\| - \frac{\left(\sqrt{b^2 - 4ac' + 4a\left(\underline{\sigma} + m_f\right)} - b\right)}{2a}\right]\left[\|e\| + \frac{\left(\sqrt{b^2 - 4ac' + 4a\left(\underline{\sigma} + m_f\right)} + b\right)}{2a}\right] < 0 \tag{B.12}$$

Since the second term in (B.12) is always positive by virtue of (B.11), we are interested in placing a condition on the first term to satisfy the inequality of (B.12). This condition leads to

$$\|e(t)\| < \frac{\sqrt{4a\left(\underline{\sigma} + m_f\right) + b^2 - 4ac'} - b}{2a}$$

The third principal minor of $B\left(\|s\|, \|\tilde{x}\|, \|\tilde{q}\|\right)$ in equation (B.7) must also be positive to assure $\dot{v}$ remains negative. This third condition is met if $k_p > 0$.

But, in order that $\dot{v}$ remain negative for all time, the initial condition on the error vector $e(0)$ must satisfy the following condition, namely

$$\|e(0)\| < \sqrt{\frac{p_l}{p_u}}\left[\frac{\sqrt{4a(\underline{\sigma}+m_f)+b^2-4ac'}-b}{2a}\right]$$

then

$$\dot{v}(t) \le -\beta\left\|\begin{bmatrix} s \\ \tilde{x} \\ \tilde{q} \end{bmatrix}\right\|^2 \qquad \forall t \ge 0 \tag{B.13}$$

where β is a constant equal to the smallest eigenvalue of the positive definite matrix $B(\|s\|,\|\tilde{x}\|,\|\tilde{q}\|)$.

Regarding stability, we note from (B.1) and (B.13) that s, $\tilde{x}$, $\tilde{q}$, $\tilde{a} \in L_\infty$. In addition, from (B.13) we conclude s, $\tilde{x}$, $\tilde{q} \in L_2$. To show $\dot{s}, \dot{\tilde{x}} \in L_\infty$, express (B.4) and (B.5) explicitly for $\dot{s}$ and $\dot{\tilde{x}}$. For $\dot{s}(t)$ we have

$$\dot{s} = H^{-1}(q)\left[-C(q,x)s-(K_d+F)s-K_p\tilde{q}+K_d\tilde{x}+H(q)\tilde{x}-C(q,x_r)\tilde{x}+Y(q,\hat{x},x_r,\dot{x}_d)\tilde{a}\right]$$

Here, all terms on the right hand side are bounded since, $x = x_d + s - \tilde{q} \in L_\infty$, $x_r = x_d - \tilde{q} \in L_\infty$ and $\hat{x} = x_d + s - \tilde{x} - \tilde{q} \in L_\infty$. For $\dot{\tilde{x}}$ we have

$$\begin{aligned}\dot{\tilde{x}} = {} & H^{-1}(q)\left[-C(q,\hat{x})\tilde{x}-C(q,x)\tilde{x}-F\tilde{x}-H(q)K\tilde{x}\right] \\ & +H^{-1}(q)\left[\tilde{H}(q)\psi+\tilde{C}(q,\hat{x})\hat{x}+\tilde{F}\hat{x}+\tilde{g}(q)\right]\end{aligned}$$

Since x, $\hat{x} \in L_\infty$ we need only show $\psi \in L_\infty$. Furthermore, since

$$\psi(q,\hat{x},\tau,\hat{a}) = \hat{H}^{-1}(q)\left[\tau - \hat{C}(q,\hat{x})\hat{x} - \hat{F}\hat{x} - \hat{g}(q)\right]$$

we need only show $\tau \in L_\infty$. To do this we recognize that all signals in controller (6) belong to L_∞. Now we can state $\dot{s}$, $\dot{\tilde{x}} \in L_\infty$.

For the observer we have $\tilde{x}, \dot{\tilde{x}} \in L_\infty$ and $\tilde{x} \in L_2$. Proceeding with Barbalat's lemma we conclude $\tilde{x} \to 0$ as $t \to \infty$. Similarly, for the controller we have $s, \dot{s} \in L_\infty$ and $s \in L_2$ which implies $s \to 0$ as $t \to \infty$. Finally, since $s = \dot{\tilde{q}} + \tilde{q}$ is a stable filter $s \to 0$ implies that both $\tilde{q} \to 0$ and $\dot{\tilde{q}} \to 0$ as $t \to \infty$. □

Chapter 5

Force Control Using the Velocity Observer

5.1 Introduction

In previous chapters we have applied the observer-controller to tasks in which contact is not made between a robot and its environment. Yet, many important manipulator tasks require interaction with the environment. In this chapter, force control and the adaptation of the velocity observer to the force control problem is considered. The reduced-order observer-controller of Chapter 3 is adjusted to compensate for end-effector contact forces. It is shown that the proposed force controller and observer form a system which results in stable manipulator behaviour. In particular the observer-controller is shown to be asymptotically stable. Simulations verify that the observer should be able to be used successfully in manipulator contact force tasks.

5.2 A Reduced-Order Observer Modified for Force Control

In the formulation of the velocity observer for force control it is useful to rearrange the dynamic equation which contains a term incorporating end-effector contact forces (2.9) to give

$$\dot{y} = H^{-1}(q)\left[\tau - C(q,y)y - Fy - g(q) - J^T F_{ext}\right] \tag{5.1}$$

where $y = \dot{q}$. The proposed observer has a structure similar to (5.1) and is given by

$$\dot{\hat{y}} = H^{-1}(q)\left[\tau - C(q,\hat{y})\hat{y} - F\hat{y} - g(q) - J^T F_{ext}\right] + K\tilde{y} \tag{5.2}$$

where $\hat{y}$ is the observed velocity estimate, $\tilde{y} = y - \hat{y}$ is the observer error and $K > 0$ is a diagonal gain matrix. By subtracting (5.2) from (5.1), and applying the results of Appendix 5.B, the observer error dynamics can be expressed in Cartesian coordinates as

$$H_x(q)\ddot{\tilde{x}} = -C_x(q,\dot{q})\dot{\tilde{x}} - J^{-T}C(q,\hat{y})J^{-1}\dot{\tilde{x}} - F_x(q)\dot{\tilde{x}} - J^{-T}H(q)KJ^{-1}\dot{\tilde{x}} \tag{5.3}$$

where $\dot{\tilde{x}} = Jy - J\hat{y} = J\tilde{y}$. Equation (5.3) describes the error dynamics of the observer and will be invoked in the stability analysis. It has been assumed that the external forces are exactly canceled by digital computation. Further theoretical work would be required if this assumption were to be relaxed.

5.2.1 Implementation of the Observer

In order to implement the observer we integrate (5.2) with respect to time which leads

to

$$\begin{aligned}\hat{y}(t) &= \hat{y}(t-\Delta) + K\left[q(t) - q(t-\Delta)\right] \\ &\quad + \int_{t-\Delta}^{t} \left\{ H^{-1}(q)\left[\tau - C(q,\hat{y})\hat{y} - F\hat{y} - g(q) - J^T F_{ext}\right] - K\hat{y} \right\} dt\end{aligned} \tag{5.4}$$

where $\hat{y}(0)$ is a reasonable initial guess of $\dot{q}(0)$ and Δ is the integration interval. The implementation of the velocity observer (5.4) on a digital computer requires discretization. Let Δ be the sampling interval over which a velocity estimation is made, then use of Euler's first method of integration of (5.4) leads to

$$\begin{aligned}\hat{y}(t) &= \hat{y}(t-\Delta) + K\left[q(t) - q(t-\Delta)\right] \\ &\quad + \Delta H^{-1}(q)\left[\tau - C(q,\hat{y})\hat{y} - F\hat{y} - g(q) - J^T F_{ext}\right] - \Delta K\hat{y}\end{aligned} \tag{5.5}$$

where i represents the time at $t = i\Delta$.

5.3 Contact Force Control Using the Observer

The proposed observer can be used to provide a velocity signal to the contact force controller. This leads to locally asymptotically stable tracking and observation errors. The proposed contact force controller is given by

$$\begin{aligned}\tau &= J^T F_c \\ F_c &= F_{ext} + H_x \ddot{x}_v + C_x(q,\hat{y})\dot{x}_v + F_x \dot{x}_v + g_x(q) - B\left(\dot{\hat{x}} - \dot{x}_v\right) - Ge\end{aligned} \tag{5.6}$$

where $\dot{\hat{x}} = J(q)\hat{y}$ is the observed end-effector Cartesian velocity and the Cartesian position tracking error is given by $e = x - x_v$ where $x_v(t)$ is the virtual or desired end-

effector pose trajectory. The proportional and derivative gain matrices are G and B respectively. The controller's error dynamics are found by substituting controller (5.6) into (5.1) and invoking the results obtained in Appendix 5.B. The error expression for the trajectory tracking dynamics is

$$H_x(q)\ddot{e} = -C_x(q,\dot{q})\dot{e} - F_x\dot{e} - B\dot{e} - Ge - J^{-T}C\left(q, J^{-1}\dot{x}_v\right)J^{-1}\dot{\tilde{x}} + H_x(q)\dot{\tilde{J}}J^{-1}\dot{x}_v + B\dot{\tilde{x}} \tag{5.7}$$

where

$$\dot{\tilde{J}} = \dot{J} - \dot{\hat{J}} = \dot{J}(q,y) - \dot{J}(q,\hat{y})$$

5.3.1 Stability of the Observer Plus Impedance Controller

Theorem 6. For given $K > 0$ and $B > 0$, $\dot{\tilde{x}}, \dot{e}, e \to 0$ as $t \to \infty$ as long as the initial conditions for the state vector $\xi^T = \left[\dot{e}^T \quad e^T \quad \dot{\tilde{x}}^T\right]$ satisfy

$$\Omega = \left\{ \xi(0) \in \Re^5 : \|\xi(0)\| < \frac{1}{m_c}\sqrt{\frac{p_l}{2p_u}}\left[\underline{\sigma} + m_f - \frac{\left(k_b + m_x + m_c m_d\right)^2}{4\left(k_b + m_f\right)} - m_c m_d\right]\right\}$$

where $\underline{\sigma} = \lambda_{\min}\left(J^{T}KH(q)J^{-1} + J^{-T}H(q)KJ^{-1}\right)/2$, $B = k_b I$ and $p_l = \lambda_{\min}(P)$, $p_u = \lambda_{\max}(P)$ with $P = \mathrm{diag}\left(H_x, G, H_x\right)$.

The proof of theorem 6 can be found in Section 5.A.

5.4 Simulation of the Proposed Observer-Controller

5.4.1 The Model

The manipulator considered for simulation of the observer plus force controller is a three degree of freedom planar manipulator based on a PUMA-560 subset. In particular,

the second link of the PUMA-560 was chosen to be our first link, the third and fourth links of the PUMA-560 were chosen as a group to be our second link and the fifth and sixth PUMA links with force sensor and end-effector were chosen as a group to be our third link. The kinematic and dynamic parameters of the manipulator considered here were obtained from [6]. The dynamic equation based on (2.6) for our three degree of freedom manipulator will be given presently. The inertia matrix is defined by

$$
\begin{aligned}
H_{11} &= I_{m1} + I_{zz1} + I_{zz2} + I_{zz3} + m_1\left(r_{x1}^2 + r_{y1}^2\right) + m_2\left(a_1^2 + r_{x2}^2 + 2a_1 r_{x2} c_2\right) \\
&\quad + m_3\left(a_1^2 + a_2^2 + r_{x3}^2 + 2a_1 a_2 c_2 + 2a_1 r_{x3} c_{23} + 2a_2 r_{x3} c_3\right) \\
H_{12} &= I_{zz2} + I_{zz3} + m_2\left(r_{x2}^2 + a_1 r_{x2} c_2\right) + m_3\left(a_2^2 + r_{x3}^2 + a_1 a_2 c_2 + a_1 r_{x3} c_{23} + 2a_2 r_{x3} c_3\right) \\
H_{13} &= I_{zz3} + m_3\left(r_{x3}^2 + a_1 r_{x3} c_{23} + a_2 r_{x3} c_3\right) \\
H_{22} &= I_{m1} + I_{zz2} + I_{zz3} + m_2 r_{x2}^2 + m_3\left(a_2^2 + r_{x3}^2 + 2a_2 r_{x3} c_3\right) \\
H_{23} &= I_{zz3} + m_3\left(r_{x3}^2 + a_2 r_{x3} c_3\right) \\
H_{33} &= I_{m1} + I_{zz3} + m_3 r_{x3}^2
\end{aligned}
$$

where symmetry defines the lower diagonal terms and the short form for trigonometric functions is given by $c_2 = \cos(q_2)$ and $c_{23} = \cos(q_2 + q_3)$. The matrix of Christoffel coefficient symbols is given by

$$
\begin{aligned}
C_{11} &= -m_2 a_1 r_{x2} \dot{q}_1 s_2 - m_3\left[a_1 a_2 \dot{q}_2 s_2 + a_1 r_{x3}\left(\dot{q}_1 + \dot{q}_2\right) s_{23} + a_2 r_{x3} \dot{q}_3 s_3\right] \\
C_{12} &= -m_2\left[a_1 r_{x2}\left(\dot{q}_1 + \dot{q}_2\right) s_2\right] - m_3\left[a_1 a_2\left(\dot{q}_1 + \dot{q}_2\right) s_2 + a_1 r_{x3}\left(\dot{q}_1 + \dot{q}_2 + \dot{q}_3\right) s_{23} + a_2 r_{x3} \dot{q}_3 s_3\right] \\
C_{13} &= -m_3\left[a_1 r_{x3}\left(\dot{q}_1 + \dot{q}_2 + \dot{q}_3\right) s_{23} + a_2 r_{x3}\left(\dot{q}_1 + \dot{q}_2 + \dot{q}_3\right) s_3\right] \\
C_{21} &= m_2 a_1 r_{x2} \dot{q}_1 s_2 + m_3\left[a_1 a_2 \dot{q}_1 s_2 + a_1 r_{x3} \dot{q}_1 s_{23} - a_2 r_{x3} \dot{q}_3 s_3\right] \\
C_{22} &= -m_3 a_2 r_{x3} \dot{q}_3 s_3 \\
C_{23} &= -m_3 a_2 r_{x3}\left(\dot{q}_1 + \dot{q}_2 + \dot{q}_3\right) s_3 \\
C_{31} &= m_3\left(a_1 r_{x3} \dot{q}_1 s_{23} + a_2 r_{x3}\left(\dot{q}_1 + \dot{q}_2\right) s_3\right)
\end{aligned}
$$

$$C_{32} = m_3 a_2 r_{x3}(\dot{q}_1 + \dot{q}_2)s_3$$
$$C_{33} = 0$$

where $s_2 = \sin(q_2)$ and $s_{23} = \sin(q_2 + q_3)$. The torques generated at the three joints due to gravitational forces are given by

$$g_1 = m_1 g(r_{x1}c_1 - r_{y1}s_1) + m_2 g(a_1 c_1 + r_{x2}c_{12}) + m_3 g(a_1 c_1 + a_2 c_{12} + r_{x3}c_{123})$$
$$g_2 = m_2 g r_{x2} c_{12} + m_3 g(a_2 c_{12} + r_{x3}c_{123})$$
$$g_3 = m_3 g r_{x3} c_{123}$$

and the matrix of damping coefficients is defined by $F = \text{diag}(f_1, f_2, f_3)$. The Cartesian force/torque vector applied at the manipulator's end-effector is given by $F_{ext} = \begin{bmatrix} f_x & f_y & n_z \end{bmatrix}$. The transpose of the Jacobian matrix is used to map the force/torque applied at the end-effector to torques applied at the joints. The Jacobian matrix is given by

$$J_{11} = -(a_1 s_1 + a_2 s_{12} + a_3 s_{123}) \qquad J_{12} = -(a_2 s_{12} + a_3 s_{123}) \qquad J_{13} = -a_3 s_{123}$$
$$J_{11} = a_1 c_1 + a_2 c_{12} + a_3 c_{123} \qquad J_{12} = a_2 c_{12} + a_3 c_{123} \qquad J_{13} = a_3 c_{123}$$
$$J_{31} = 1 \qquad J_{32} = 1 \qquad J_{33} = 1$$

The change of coordinates from generalized joint space to end-effector Cartesian space requires the derivative of the Jacobian matrix. This is easily accomplished and the result will not be presented here. These relationships complete the requirements for the description of the manipulator dynamic equation where interaction with the environment is considered.

The kinematic and dynamic parameters of the manipulator will now be given. The kinematic parameters are the link lengths. Their values are $a_1 = 0.432$ m, $a_2 = 0.433$ m and $a_3 = 0.15$ m. The dynamic parameters consist of the link and motor inertias, link masses, link mass centers and dissipative coefficients. These are: $I_{zz1} = 0.539\ \text{kg m}^2$, $I_{zz2} = 0.212\ \text{kg m}^2$, $I_{zz3} = 0.006\ \text{kg m}^2$, $I_{m1} = 4.71\ \text{kg m}^2$, $I_{m2} = 0.830\ \text{kg m}^2$, $I_{m3} = 0.179\ \text{kg m}^2$, $m_1 = 17.4$ kg, $m_2 = 5.62$ kg, $m_3 = 1.00$ kg, $r_{x1} = 0.068$ m, $r_{y1} = 0.006$ m, $r_{x2} = 0.070$ m, $r_{x3} = -0.010$ m, $f_1 = 27.4$ kg/s, $f_2 = 4.54$ kg/s, $f_3 = 5.0$ kg/s where most have been obtained from [6].

5.4.2 Test Trajectory, Contact Surface and Joint Position Noise

The desired Cartesian trajectory specified for the end-effector consists of unconstrained and constrained motion parts. The unconstrained motion trajectory is described by the following truncated ellipse

$$x_v(t) = \begin{bmatrix} 0.5 + 0.2\sin\left(2\pi ft - \pi/2\right)\text{ m} \\ 0.5\cos\left(2\pi ft - \pi/2\right)\text{ m} \\ 0.0\text{ rad} \end{bmatrix}, \qquad x_{v1} < 0.65\text{ m}$$

where $f = 0.1$ Hz. Contact with the environment occurs when $x_{v1} \geq 0.65$ m and it is at contact that the desired or virtual trajectory switches to

$$x_v(t) = \begin{bmatrix} 0.65196\text{ m} \\ 0.5\cos\left(2\pi ft - \pi/2\right)\text{ m} \\ 0.0\text{ rad} \end{bmatrix}, \qquad x_{v1} \geq 0.65\text{ m}$$

Note that the virtual trajectory lies 0.00196 m inside the contact material. The desired or

virtual trajectory is depicted in Fig. 5.1a.

For the simulations carried out in this section it is assumed that the joint position measurements are contaminated by noise. The assumed noise is quantified in Appendix A. The joint position noise is zero mean with standard deviation $\sigma_n = 0.082$ deg. Another assumption made is with regard to the environment with which the robot comes into contact. It is assumed that the stiffness of the environment is 10^4 N/ m; i.e., a deflection of 0.00196 m creates a contact force equal to 19.6 N. This is equivalent to the weight that a 2 kg mass would make under the influence of gravity.

5.4.3 Simulation of the Proposed Observer-Controller

The simulation results for the proposed observer and force controller are outlined in this section. The observer used is given in (5.5) and the controller is given in (5.6). The gains implemented were as follows: for the observer $K = \text{diag}(2,2,2)$ was used and for the controller position gain $G = \text{diag}(500,500,100)$ and velocity gain $B = \text{diag}(50,50,20)$ were used. These gains were obtained by a trial-and-error tuning process which optimized performance. The controller and observer update frequency was chosen as 400 Hz. The results of the simulation are shown in Figs. 5.1-5.4.

Fig. 5.1a shows the desired Cartesian trajectory versus the actual Cartesian trajectory. The initial position of the end-effector was located at the coordinates $(0.3,0.0)$ m. Note the tracking error decreases as the control maneuver proceeds in the positive xy-direction. When the end-effector comes into contact with the environmental barrier at $x = 0.65$ m, there is a tracking overshoot which can be observed in more detail in Fig. 5.1c. Here the bottom horizontal line represents the boundary of the material, the middle line represents the virtual trajectory and the dash-dot line represents actual motion of the end-effector. The desired orientation of the end-effector is constant and normal to the contact surface.

In Fig. 5.1b the desired end-effector orientation is shown as 0 deg. The end-effector is originally misaligned by 4 deg, but the controller makes the necessary compensation and the error is quickly reduced to zero. The orientational velocity of the end-effector is given in Fig. 5.1d.

To observe the contact force as a function of time see Fig. 5.2a. The desired contact force is achieved within approximately 1.5 sec. The applied joint torques for the trajectory are given in Figs. 5.1b-1d respectively for joints 1 through 3. The joint torques shown are well within the capability of the PUMA-560, see [6].

The velocity tracking results are shown in Fig. 5.3. The desired x-velocity versus the actual x-velocity is shown in Fig. 5.3a and the velocity tracking error for this motion is shown in Fig. 5.3c. The differences between the desired and actual trajectory are due to initial controller startup. Errors are also due to the interaction of the end-effector with the contact surface. The motion trajectory of the end-effector in the y-direction is shown in Fig. 5.3b. The motion error in the y-direction is shown in 5.3d.

The observed versus actual Cartesian velocities are shown in Fig. 5.4. The actual x-velocity versus the observed x-velocity is shown in Fig. 5.4a The observer error for this direction is shown in Fig. 5.2c. The same graphics are shown for the y-direction in Figs. 5.2b and 5.2d.

5.4.4 Simulation of Hogan's Impedance Controller

The same motion trajectory, environmental stiffens and position measurement noise were assumed for simulations using Hogan's impedance controller. The impedance controller is given by

$$\tau = J^T F_c$$

$$F_c = F_{ext} + C_x\left(q_n, \dot{q}_f\right)\dot{x}_f + F_x\dot{x}_f + g_x\left(q_n\right) + H_x\left\{\ddot{x}_v - M^{-1}\left[B\left(\dot{x}_f - \dot{x}_v\right) + G\left(x_n - x_v\right)\right]\right\}$$

where it has been assumed that the first-order position filter given in (3.11a) has been employed with filter gains $K_f = \text{diag}(100, 100, 100)$. A backwards difference was then used on the resulting filtered position signal to obtain velocity estimates. A Jacobian transformation mapped the joint space velocity estimate into end-effector Cartesian coordinates.

The effective mass, viscous and stiffness gain matrices for the impedance controller were set respectively to $M = \text{diag}(0.15, 0.15, 0.15)$, $B = \text{diag}(2, 12, 38)$, and G=diag(1, 35, 350). These gains were tuned to provide stable position and force tracking. It was difficult to tune the impedance controller plus filter to provide good performance in the presence of the measurement noise. Reduction of the filter bandwidth to deal effectively with the noise in the estimated velocity signal leads quickly to instability. The results of the simulation are shown in Figs. 5.5-5.8.

Fig. 5.1a shows the same desired Cartesian trajectory versus the actual Cartesian trajectory as for the simulation of the proposed observer plus controller. When the end-effector contacts the environment at $x = 0.65$ m, overshoot results as shown in Fig. 5.5c. The desired orientation of the end-effector is constant and normal to the contact surface. In Fig. 5.5b the desired end-effector orientation is shown as 0 deg. Note that the impedance controller stabilizes the orientational error more quickly than the proposed method; however, more noise is present in the orientational velocity of the end-effector as shown in Fig. 5.5d.

To observe the contact force as a function of time see Fig. 5.6a. The desired contact force is not achieved since higher control gains are not possible due to the large amount of noise in the velocity estimate. The applied joint torques for the trajectory are given in

Figs. 5.5b-5d respectively for joints 1 through 3. The joint torques contain a considerable amount of chatter.

The desired versus actual velocity graphs are shown in Fig. 5.7. and the difference between the estimated velocities and the actual velocities are shown in Fig. 5.8. The velocity estimates obtained by numerical differentiation combined with filtering leads to greater noise than the proposed reduced-order observer plus force controller. This leads to smoother tracking and as well as a larger stability margin.

In order to quantify the tracking performance for both the proposed observer-controller and Hogan's modified Impedance controller, computations were conducted using the 1-norm to provide the results in Table 5.1. The proposed method had smaller position tracking errors $\|\tilde{x}\|_1$, whereas Hogan's method resulted in smaller velocity tracking errors $\|\dot{\tilde{x}}\|_1$. The better performer with respect to contact force tracking $\|f - f_d\|_1$ was the proposed method. The applied joint torques were smaller and contained less chatter for the proposed method.

	$\|\tilde{x}\|_1$ (mm)	$\|\dot{\tilde{x}}\|_1$ (mm/s)	$\|f - f_d\|_1$ (N)	$\|\tau_1\|_1$ (Nm)	$\|\tau_2\|_1$ (Nm)	$\|\tau_3\|_1$ (Nm)
Hogan's Method	7.0	3.0	56.3	30.6	7.9	3.4
Proposed Method	1.4	4.4	21.2	17.3	4.3	2.4

Table 5.1: Summary of performance results for Hogan's Method and for the Proposed Observer-Force Controller.

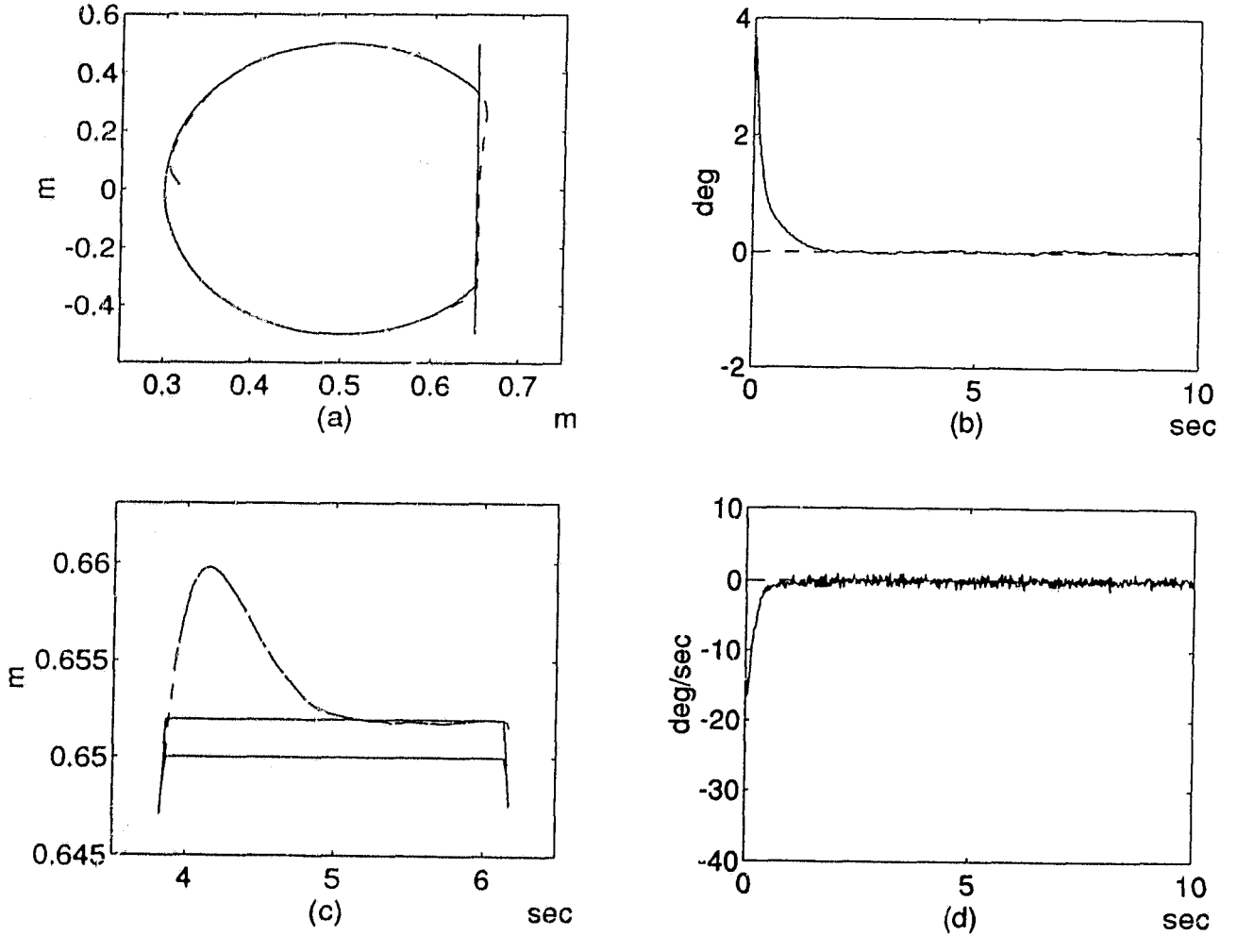

Fig. 5.1: Simulation results for proposed observer and force controller (a) desired versus actual Cartesian end-effector position, (b) desired vs. actual end-effector orientation (c) Cartesian end-effector contact error, (d) end-effector orientational error.

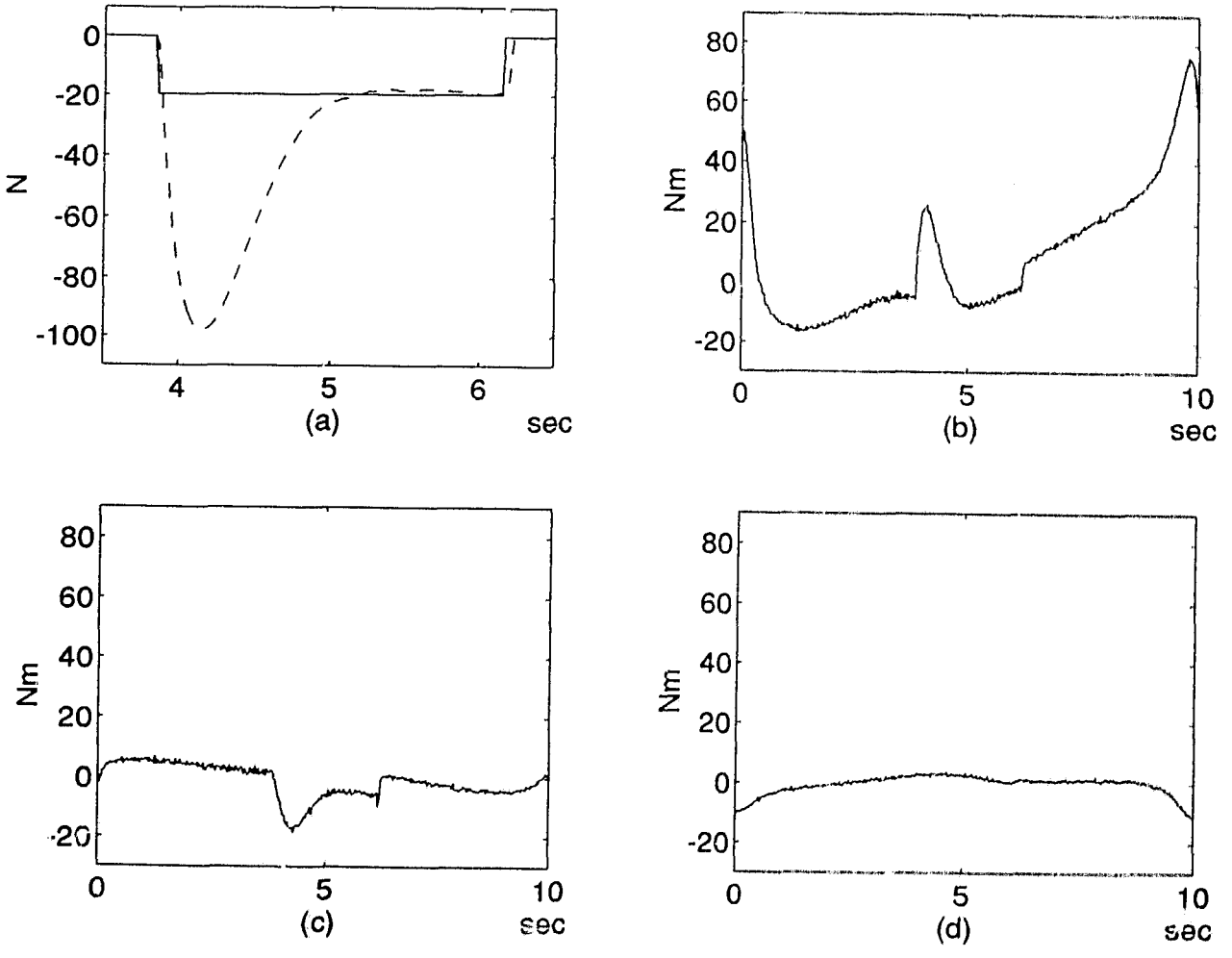

Fig. 5.2: Simulation results for proposed observer and force controller (a) desired versus actual contact force, (b) joint-1 torque (c) joint-2 torque, (d) joint-3 torque.

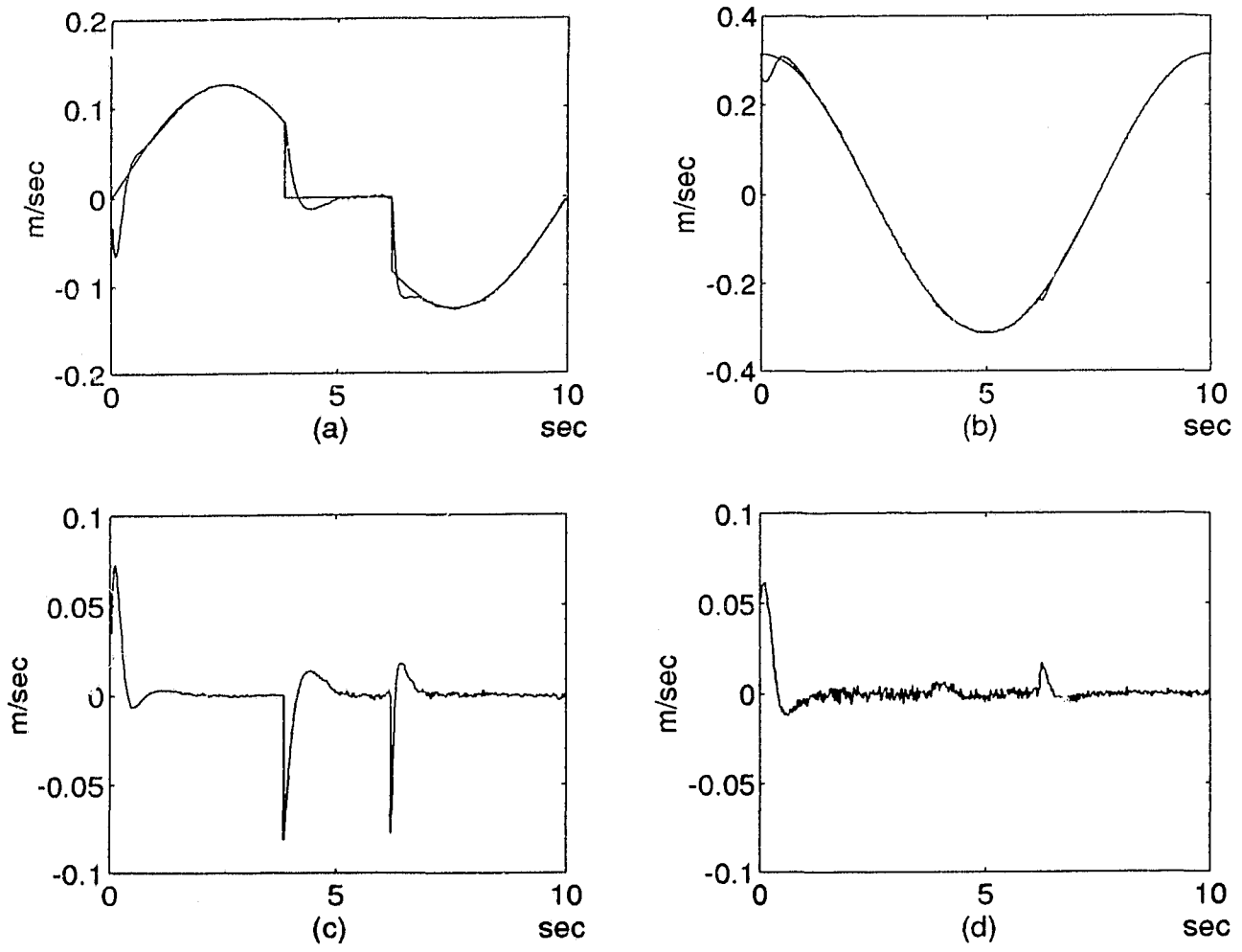

Fig. 5.3: Simulation results for proposed observer and force controller (a) desired vs. actual x-velocity, (b) desired vs. actual y-velocity (c) x-velocity error, (d) y-velocity error.

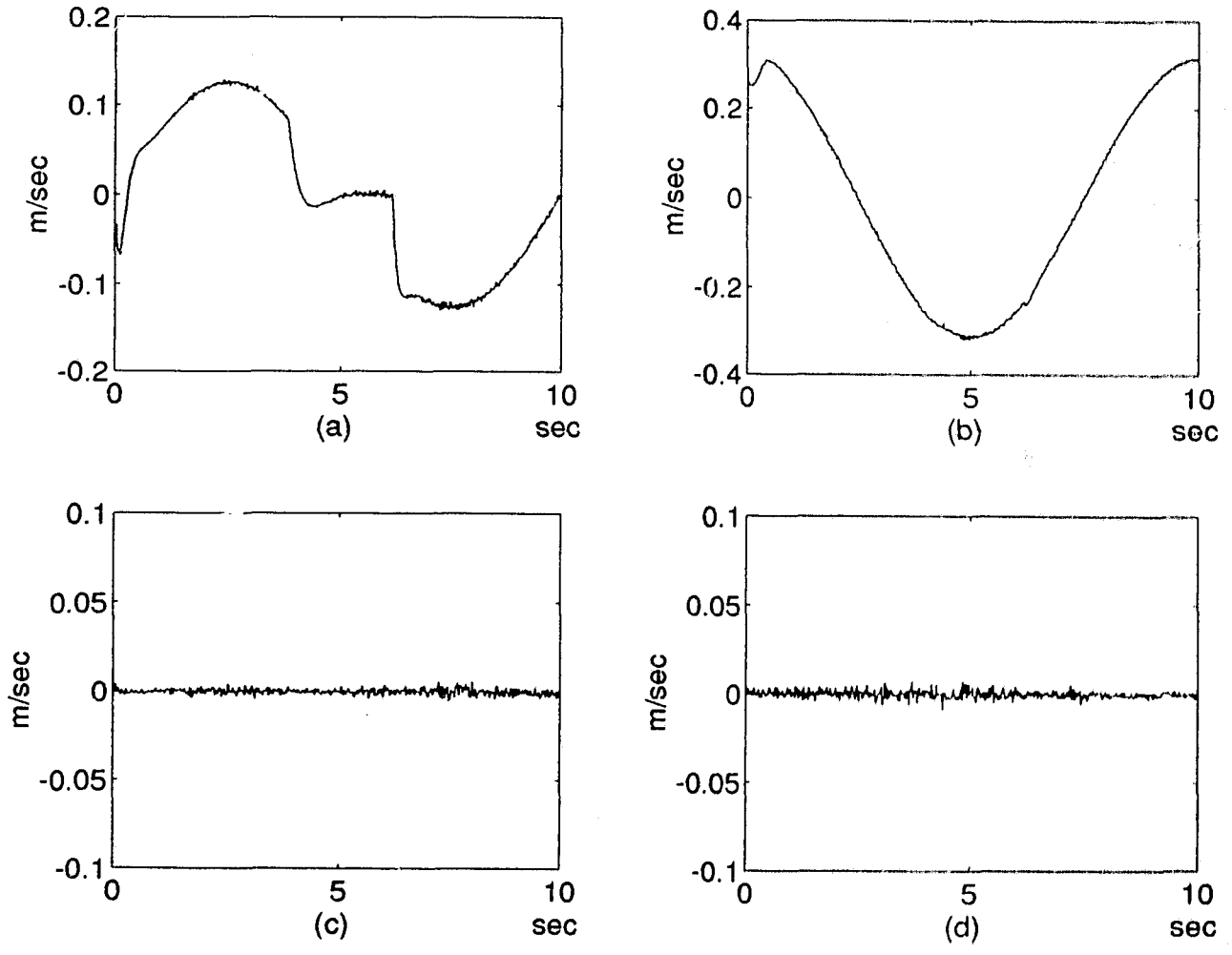

Fig. 5.4: Simulation results for proposed observer and force controller (a) actual vs. observed x-velocity, (b) actual vs. observed y-velocity (c) x-velocity observer error, (d) y-velocity observer error.

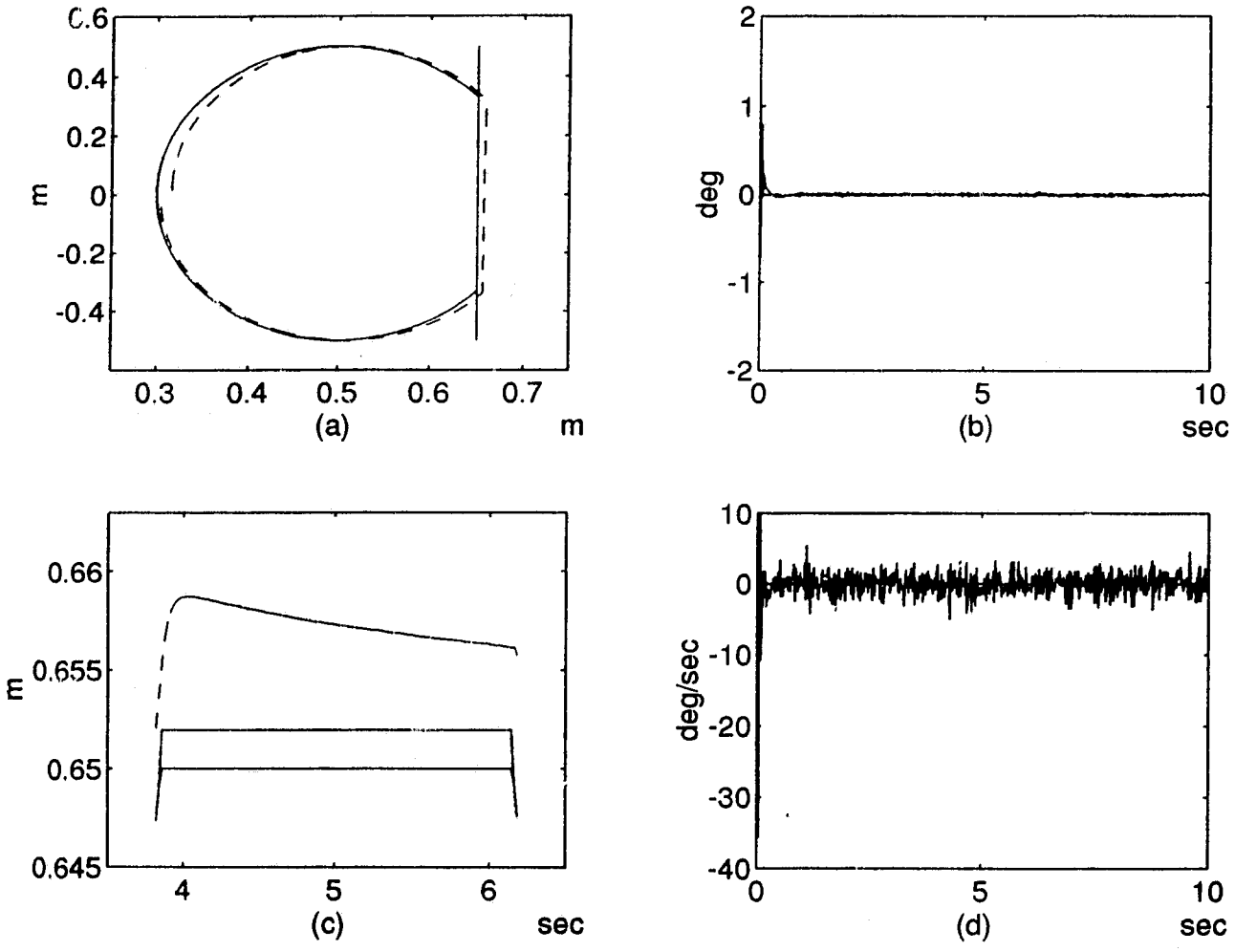

Fig. 5.5: Simulation results for Hogan's force controller (a) desired versus actual Cartesian end-effector position, (b) desired vs. actual end-effector orientation (c) Cartesian end-effector contact error, (d) end-effector orientational error.

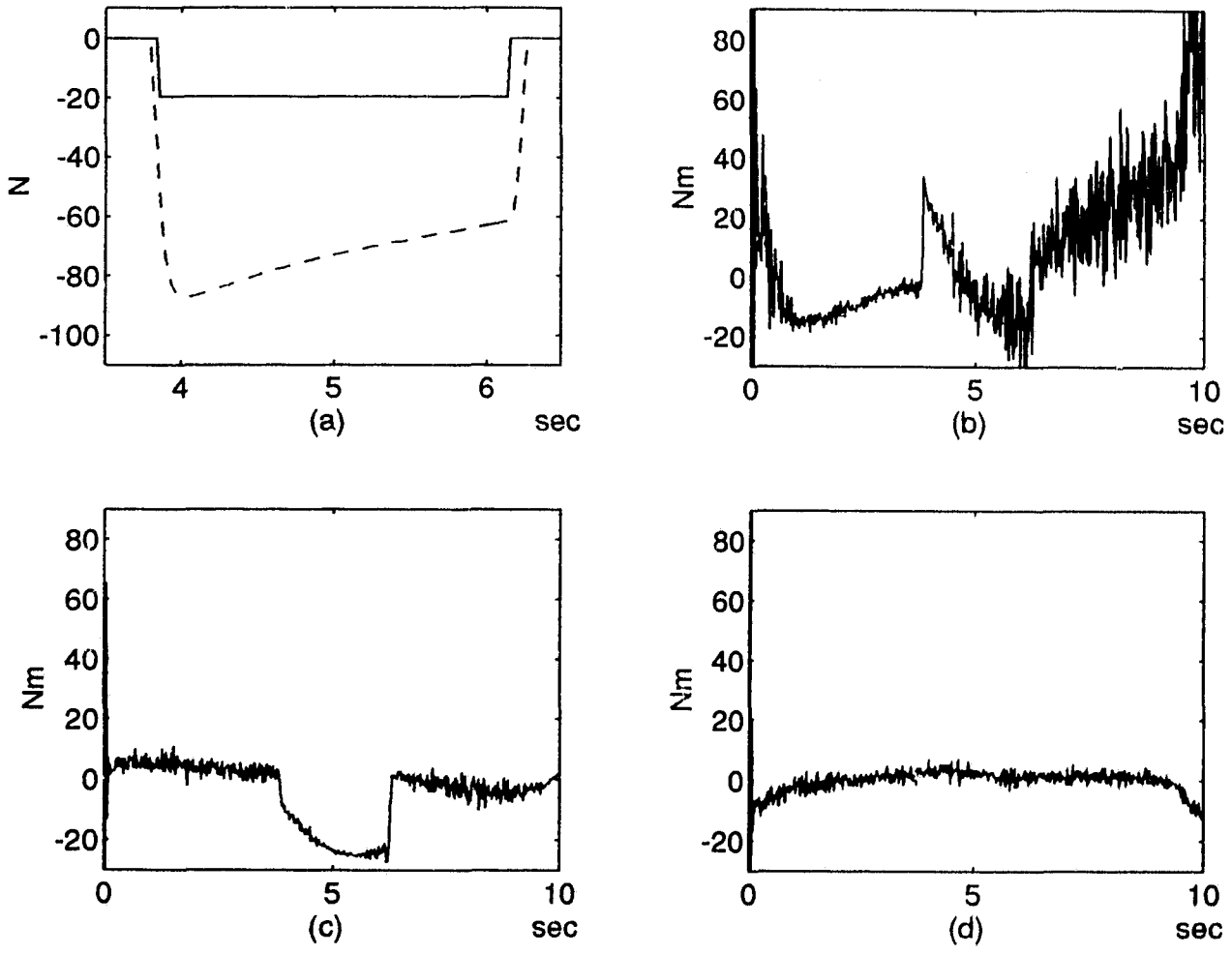

Fig. 5.6: Simulation results for Hogan's force controller (a) desired versus actual contact force, (b) joint-1 torque (c) joint-2 torque, (d) joint-3 torque.

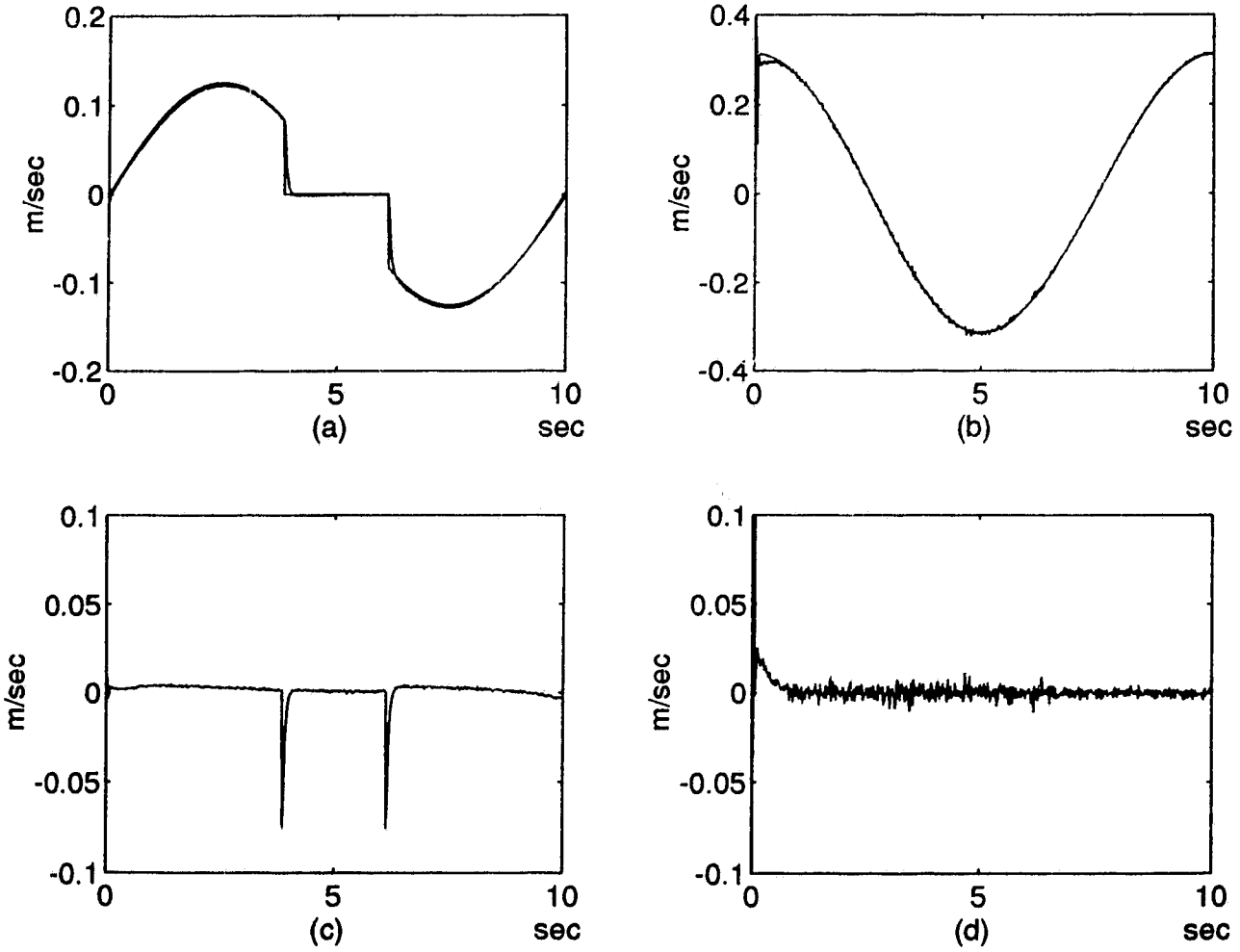

Fig. 5.7: Simulation results for Hogan's force controller (a) desired vs. actual x-velocity, (b) desired vs. actual y-velocity (c) x-velocity error, (d) y-velocity error.

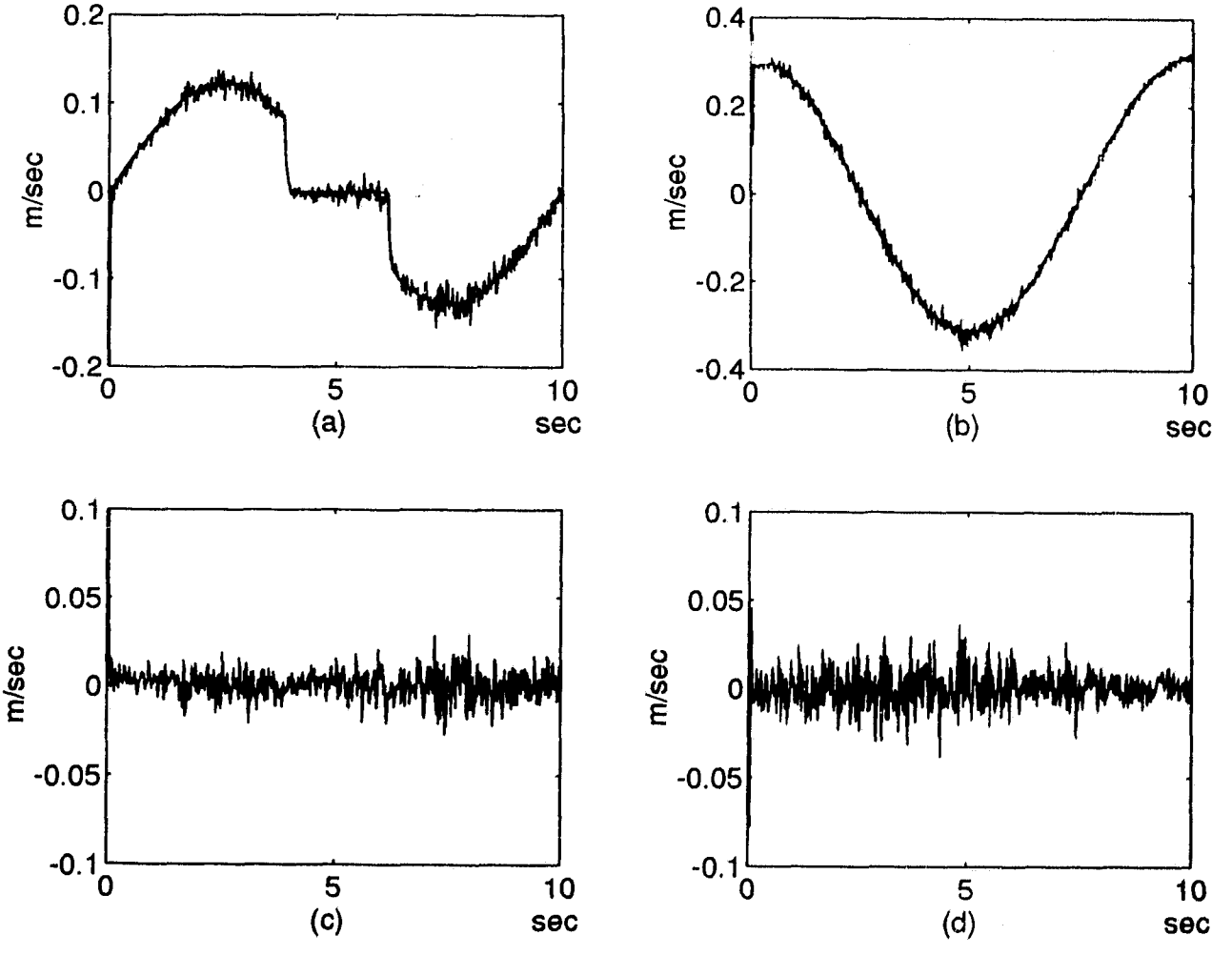

Fig. 5.8: Simulation results for Hogan's force controller (a) actual vs. estimated x-velocity, (b) actual vs. estimated y-velocity (c) x-velocity estimation error, (d) y-velocity estimation error.

5.A Proof of Theorem 6

Consider the Lyapunov function

$$v(t) = \frac{1}{2}\xi(t)^T P(q)\xi(t) \tag{A.1}$$

where $\xi^T(t) = \begin{bmatrix} \dot{e}^T(t) & e^T(t) & \dot{\tilde{x}}^T(t) \end{bmatrix}$ and $P = \mathrm{diag}\left(H_x(q), G, H_x(q)\right)$ with $G = G^T > 0$. Then (A.1) satisfies

$$\frac{1}{2}p_l\|\xi(t)\|^2 \le v(t) \le \frac{1}{2}p_u\|\xi(t)\|^2 \tag{A.2}$$

where $p_l = \lambda_{\min}(P)$ and $p_u = \lambda_{\max}(P)$. The time derivative of $v(t)$ along all trajectories of $\xi(t)$ is given by

$$\dot{v} = \dot{e}^T\left(H_x(q)\ddot{e} + \frac{1}{2}\dot{H}_x(q)\dot{e} + Ge\right) + \dot{\tilde{x}}^T\left(H_x(q)\ddot{\tilde{x}} + \frac{1}{2}\dot{H}_x(q)\dot{\tilde{x}}\right) \tag{A.3}$$

Substituting observer and controller error dynamics (5.3) and (5.7) into (A.3) and using property 8 yields

$$\begin{aligned}\dot{v} = &-\dot{e}^T\left(F_x + B\right)\dot{e} - \dot{\tilde{x}}^T\left(F_x + J^{-T}H(q)KJ^{-1}\right)\dot{\tilde{x}} \\ &+\dot{e}^T B\dot{\tilde{x}} + \dot{e}^T H_x\dot{\tilde{J}}J^{-1}\dot{x}_v - \dot{e}^T J^{-T}C\left(q, J^{-1}\dot{x}_v\right)J^{-1}\dot{\tilde{x}} \\ &-\dot{\tilde{x}}J^{-T}C\left(q, J^{-1}\left(\dot{e} - \dot{\tilde{x}} + \dot{x}_v\right)\right)J^{-1}\dot{\tilde{x}}\end{aligned} \tag{A.4}$$

By applying properties 6, 7, and $\left\|\dot{\tilde{J}}\right\| = \left\|\dot{J}(q,y) - \dot{J}(q,\hat{y})\right\| = \left\|\dot{J}(q,\tilde{y})\right\| = \left\|\dot{J}\left(q, J^{-1}\dot{\tilde{x}}\right)\right\| \le m_2\left\|\dot{\tilde{x}}\right\|$ we can write (A.4) as

$$\dot{v} \le -\left[k_b + m_f\right]\|\dot{e}\|^2 - \left[\underline{\sigma} + m_f - m_c m_d - m_c\left(\|\dot{\tilde{x}}\| + \|\dot{e}\|\right)\right]\|\dot{\tilde{x}}\|^2 + \left[k_b + m_x + m_c m_d\right]\|\dot{e}\|\|\dot{\tilde{x}}\| \quad \text{(A.5)}$$

where $m_f = \lambda_{\min}(F_x)$, $\|\dot{x}_v\| \le m_d$ and $\|\ddot{H}_x(q)\|\|J^{-1}\|\|\dot{x}_v\| \le m_x$. Equation (A.5) can then be rewritten to obtain

$$\dot{v}(t) \le -\begin{bmatrix}\|\dot{e}\| & \|\dot{\tilde{x}}\|\end{bmatrix}\begin{bmatrix} k_b + m_f & -\frac{1}{2}\left(k_b + m_x + m_c m_d\right) \\ -\frac{1}{2}\left(k_b + m_x + m_c m_d\right) & \underline{\sigma} + m_f - m_c m_d - m_c\left(\|\dot{\tilde{x}}\| + \|\dot{e}\|\right)\end{bmatrix}\begin{bmatrix}\|\dot{e}\| \\ \|\dot{\tilde{x}}\|\end{bmatrix} \quad \text{(A.6)}$$

The negativity of $\dot{v}(t)$ in (A.6) is guaranteed if the principal minors of the matrix in (A.6) are all positive. The first principal minor is positive if

$$k_b + m_f > 0$$

and for the second principal minor positivity is guaranteed if

$$\underline{\sigma} + m_f > m_c\left(\|\dot{\tilde{x}}(t)\| + \|\dot{e}(t)\|\right) + m_c m_d + \frac{\left(k_b + m_x + m_c m_d\right)^2}{4\left(k_b + m_f\right)} \quad \text{(A.7)}$$

Since $\sqrt{3}\|\xi(t)\| \ge \|\dot{e}(t)\| + \|\dot{\tilde{x}}(t)\|$, it is evident that (A.7) definitely holds if

$$\underline{\sigma} + m_f > \sqrt{3} m_c\|\xi(t)\| + m_c m_d + \frac{\left(k_b + m_x + m_c m_d\right)^2}{4\left(k_b + m_f\right)} \quad \text{(A.8)}$$

is satisfied. Then, (A.8) certainly holds if

$$\underline{\sigma} > \frac{\left(k_b + m_x + m_c m_d\right)^2}{4\left(k_b + m_f\right)} - m_f + m_c m_d + m_c \sqrt{\frac{2p_u}{p_l}} \left\| \xi(0) \right\| \tag{A.9}$$

Condition (A.9) is equivalent to

$$\left\| \xi(t) \right\| < \frac{1}{\sqrt{3} m_c} \left(\underline{\sigma} + m_f - m_c m_d + \frac{\left(k_b + m_x + m_c m_d\right)^2}{4\left(k_b + m_f\right)} \right)$$

where $\underline{\sigma}$ and k_b have been fixed. However, in order to guarantee the negativity of $\dot{v}(t)$ for all time, the error vector $\xi(t)$ at time $t = 0$ must belong to

$$\left\| \xi(0) \right\| < \frac{1}{m_c} \sqrt{\frac{p_l}{3p_u}} \left(\underline{\sigma} + m_f - m_c m_d + \frac{\left(k_b + m_x + m_c m_d\right)^2}{4\left(k_b + m_f\right)} \right)$$

by virtue of (A.2) Therefore, we have

$$\dot{v}(t) \leq -\beta \left\| \begin{bmatrix} \|\dot{e}(t)\| \\ \|\dot{\tilde{x}}(t)\| \end{bmatrix} \right\|^2 \quad , \qquad \forall t \geq 0 \tag{A.10}$$

where $\beta > 0$ is the infimum of the matrix in (A.6).

Regarding stability, we note from (A.2) and (A.10) that $\dot{e}$, e , $\dot{\tilde{x}} \in L_\infty$ as long as the initial conditions $\xi(0)$ lie within Ω. If this is the case, it follows that $\ddot{e}$, $\ddot{\tilde{x}} \in L_\infty$ by virtue of (5.3) and (5.7). Integration and re-ordering of (A.10) yields

$$\int_0^\infty \left\| \begin{bmatrix} \|\dot{e}(t)\| \\ \|\dot{\tilde{x}}(t)\| \end{bmatrix} \right\|^2 dt = \frac{1}{\beta} \left(v(0) - v(\infty) \right) < \infty$$

which implies $\dot{e}$, $\dot{\tilde{x}} \in L_2$. We can now apply Barbalat's Lemma to conclude that $\dot{e} \to 0$ and $\dot{\tilde{x}} \to 0$ as $t \to \infty$. The stability of $e(t)$ is obtained by invoking Lasalle's theorem. Consider (5.7); here we note that the largest invariant set is $e = 0$ since $\dot{e} \to 0$ and $\dot{\tilde{x}} \to 0$ as $t \to \infty$. □

5.B Error Dynamics of the Observer

Combine the expression for the manipulator observer (5.2) and the manipulator dynamic equation (5.1) to give the following

$$H(q)\dot{y} + C(q,y)y + Fy = H(q)\dot{\hat{y}} + C(q,\hat{y})\hat{y} + F\hat{y} - H(q)K\tilde{y} \tag{B.1}$$

where $\tilde{y} = y - \hat{y}$. Some reorganization of (B.1) yields

$$H(q)\dot{\tilde{y}} + C(q,y)y - C(q,\hat{y})\hat{y} + F\tilde{y} + H(q)K\tilde{y} = 0 \tag{B.2}$$

but by Property 3

$$\begin{aligned} C(q,y)y - C(q,\hat{y})\hat{y} &= C(q,y)y - C(q,y)\hat{y} \\ &\quad + C(q,\hat{y})y - C(q,\hat{y})\hat{y} \\ &= C(q,y)\tilde{y} + C(q,\hat{y})\tilde{y} \end{aligned}$$

so (B.2) becomes

$$H(q)\dot{\tilde{y}} = -C(q,y)\tilde{y} - C(q,\hat{y})\tilde{y} - F\tilde{y} - H(q)K\tilde{y} \tag{B.3}$$

Now, using the relationships given in (2.6) and (2.5), we apply the change of coordinates

$$\tilde{y} = J^{-1}\dot{\tilde{x}}$$
$$\dot{\tilde{y}} = J^{-1}\left[\ddot{\tilde{x}} - \dot{J}J^{-1}\dot{\tilde{x}}\right]$$

to equation (B.3) to yield

$$H(q)J^{-1}\left[\ddot{\tilde{x}} - \dot{J}J^{-1}\dot{\tilde{x}}\right] = -C(q,y)J^{-1}\dot{\tilde{x}} - C(q,\hat{y})J^{-1}\dot{\tilde{x}} - FJ^{-1}\dot{\tilde{x}} - H(q)KJ^{-1}\dot{\tilde{x}}$$

rearranging and pre-multiplying this last expression by J^{-T} gives us

$$H_x(q)\ddot{\tilde{x}} = -C_x(q,\dot{q})\dot{\tilde{x}} - J^{-T}C(q,\hat{y})J^{-1}\dot{\tilde{x}} - F_x(q)\dot{\tilde{x}} - J^{-T}H(q)KJ^{-1}\dot{\tilde{x}}$$

This is the observer error equation expressed in the Cartesian coordinates.

5.C Error Dynamics of the Controller

The controller error equation is obtained by substituting the controller given in (5.6) into (5.2). As a preliminary result we obtain

$$H_x(q)\ddot{x} + C_x(q,y)\dot{x} + F_x\dot{x} = H_x(q)\ddot{x}_v + C_x(q,\hat{y})\dot{x}_v + F_x\dot{x}_v - B\left(\dot{\hat{x}} - \dot{x}_v\right) - G\left(x - x_v\right) \qquad \text{(C.1)}$$

Noting $\dot{\hat{x}} = \dot{x} - \dot{\tilde{x}}$ and re-ordering (C.1) we get

$$H_x(q)\ddot{e} + C_x(q,y)\dot{x} - C_x(q,\hat{y})\dot{x}_v + F_x\dot{e} + B\dot{e} + Ge - B\dot{\tilde{x}} = 0 \qquad \text{(C.2)}$$

But

$$
\begin{aligned}
&C_x(q,y)\dot{x} - C_x(q,\hat{y})\dot{x}_v \\
&\qquad = J^{-T}\left[C(q,y) - H(q)J^{-1}\dot{J}\right]J^{-1}\dot{x} \\
&\qquad J^{-T}\left[C(q,\hat{y}) - H(q)J^{-1}\dot{\hat{J}}\right]J^{-1}\dot{x}_v \\
&\qquad = J^{-T}\left[C(q,\dot{q})\dot{q} - C(q,\dot{q})\dot{q}_v + C(q,\dot{q}_v)y - C(q,\dot{q}_v)\hat{y}\right]J^{-1}\dot{x} \\
&\qquad H_x(q)\left[\dot{\hat{J}}\dot{q}_v - \dot{J}\dot{q} + \dot{J}\dot{q}_v - \dot{J}\dot{q}_v\right] \\
&\qquad = J^{-T}\left[C(q,\dot{q})\dot{\tilde{q}} + C(q,\dot{q}_v)\tilde{y}\right] \\
&\qquad + J^{-T}H(q)J^{-1}\left[-\dot{J}\dot{\tilde{q}} + \left(\dot{\hat{J}} - \dot{J}\right)\dot{q}_v\right] \\
&\qquad = J^{-T}\left[C(q,\dot{q}) - H(q)J^{-1}\dot{J}\right]J^{-1}\dot{e} \\
&\qquad + J^{-T}\left[C(q,\dot{q}_v)J^{-1}\dot{\tilde{x}} - H(q)J^{-1}\left(\dot{\hat{J}} - \dot{J}\right)J^{-1}\dot{x}_v\right]
\end{aligned}
$$

from which we obtain

$$
\begin{aligned}
&C_x(q,y)\dot{x} - C_x(q,\hat{y})\dot{x}_v \\
&= C_x(q,\dot{q})\dot{e} + J^{-T}C\left(q,J^{-1}\dot{x}_v\right)J^{-1}\dot{\tilde{x}} - H_x(q)\dot{\tilde{J}}J^{-1}\dot{x}_v
\end{aligned}
\qquad \text{(C.3)}
$$

where $\dot{\tilde{J}} = \dot{J} - \dot{\hat{J}} = \dot{J}(q,y) - \dot{J}(q,\hat{y})$. Substituting (C.3) into (C.2) finalizes the expression for the controller error which is given by

$$
H_x(q)\ddot{e} + C_x(q,\dot{q})\dot{e} + J^{-T}C\left(q,J^{-1}\dot{x}_v\right)J^{-1}\dot{\tilde{x}} - H_x(q)\dot{\tilde{J}}J^{-1}\dot{x}_v + F_x\dot{e} + B\dot{e} + Ge - B\dot{\tilde{x}} = 0
$$

Chapter 6

Conclusions and Recommendations for Future Work

In this thesis, nonlinear model-based observers have been proposed which allow for the estimation of a robot manipulator's joint velocities. The output of the observers, i.e. the velocity estimates, were used in manipulator position and force control. For position control an adaptive observer and a non-adaptive observer have been developed. In force control, an additional force compensating term was added to the observer's analytical description.

It has been shown that the observer together with a proportional-derivative controller leads to asymptotically stable observers and position errors. Stable control is also achieved when the observer is used with a model-based controller for the tracking of time varying trajectories. An adaptive version of the velocity observer was developed to accommodate situations where the dynamic parameters of a manipulator's links or end-effector load vary. Theoretical analysis shows that the adaptive observer plus adaptive

controller leads to the asymptotic stable behaviour of the observer errors as well as the asymptotic behaviour of the position and velocity errors. The parameter estimates are shown to remain bounded. Asymptotic stability results were also shown for the observer used in contact force control, whereby stable position and force control have been achieved.

The three observer-controller constructions described above have been extensively simulated and compared to existing velocity estimation and control techniques used in robotics. Some advantages of the proposed schemes over other methods are (i) the reduction of the observer order from two to one, (ii) a smooth velocity estimate and (iii) higher bandwidth compared to velocity estimation techniques using numerical differentiation and filtering.

The advantage of a reduced-order velocity observer over its full-order counterpart lies in the simpler dynamic behaviour of the first-order (reduced) system. In a full order observer there are more dynamic states and more can go wrong especially in gain tuning. As a practical matter, first-order linear systems are easy to tune because all positive gains lead to exponential stability - the speed of error convergence is all that one has to worry about. For a second-order linear system this is not the case. One has to wrestle with underdamped and overdamped responses and suitable choice of gains. In nonlinear systems such as robot dynamics, transient behaviour is more complex. Nevertheless, the tendencies observed in first and second-order linear systems carry over to the nonlinear case. That is, first-order systems are always preferred to second-order systems, due mostly to gain tuning issues.

As for the implementation, a reduced-order observer requires fewer computing resources compared to its full-order counterpart. Less high-speed computer memory is required and a fewer number of floating point operations are needed to obtain a result which is the same or better than that obtained with the full-order observer.

The adaptive and non-adaptive velocity observers and their associated controllers have been implemented on a PUMA-560 robot. The experimental results show good tracking with an improvement in bandwidth and reduction in noise compared to more traditional methods.

Future research in robot velocity estimation will involve several research directions. One direction will be the study of simplified observers. In these, the nonlinear matrices and vectors in the robot dynamics are replaced by constant approximations of these matrices and vectors. For example the inertia matrix is replaced by a positive definite matrix having constant entries and similar norm. An observer with simpler terms would lead to a more economic implementation on computer hardware. Another research direction will be the investigation of optimal differentiators using adaptive filtering and over-sampling.

The implementation of the model and non-model based velocity estimators on digital signal processing (DSP) and programmable gate array (PGA) systems will be investigated - leading potentially to commercial products. Efficient numerical implementations of the velocity estimators will be sought.

Further experimental investigations will be conducted to characterize the position sensing technologies available in the industry. The main technologies used are optical encoders, potentiometer and resolvers. The signal and noise characteristics of these technologies will be determined - aiding in the design of future velocity estimators.

Appendix A

Characteristics of Position Measurement Noise

The experiments were performed on the PUMA-560 manipulator. This manipulator uses optical encoders to obtain joint position measurements. However, in order to investigate the expected performance of the proposed observer for robots which use potentiometers to obtain joint positions, we performed some tests on a General Electric (GE) hydraulic sub-sea arm which was fitted with potentiometers. The arm data was collected at International Submarine Engineering Ltd. (ISE Ltd.) of Port Coquitlam, British Columbia where the arm's old analog controller was being replaced by a new digital controller.

Data logging was made possible with the aid of ISE's real-time system control software, Control System Probe (CSP). The position measurements were taken during unconstrained manipulator motions. A typical position trajectory for joint one of the manipulator is shown in Fig. 3.2a. This trajectory was obtained during teleoperation.

Twenty ensemble sets of data were logged during the tests. A sampling frequency of 150 Hz was used for a duration of 11 seconds leading to more than 1600 samples per set of data. The sampling of the potentiometer signal was accomplished with a 12 bit analog to digital converter board connected to the PC-Bus of a 80386 IBM-PC compatible computer.

The measurement noise was separated from the signal with a 256th order off-line low pass filter with cutoff frequency 30 Hz. A plot of one ensemble set of measurement noise is given in Fig. 3.2c. Although the position trajectory in Fig. 3.2a seems smooth, numerical differentiation of the position signal yields a noisy velocity estimate which is shown in Fig. 3.2b. It is obvious that this velocity estimate could not be used in control. The distribution density of the position measurement noise is shown in Fig. 3.2d as the dashed curve. For comparison, a normal distribution density is shown by the solid curve.

The average noise power spectrum for the twenty ensemble sets of noise data is shown in Fig 3.2e. Note the flat spectrum above the filter cutoff frequency of 30 Hz. The standard deviation for the measurement noise in the 30Hz-75Hz band was found to be $\sigma_n = 0.0818$ degrees.

In light of the previous characterization, a model of the measurement noise was approximated as zero mean, normally distributed noise with standard deviation $\sigma_n = 0.0818$ degrees. With this noise model in consideration, simulations of point-to-point control and trajectory tracking control were made. Their results will be described in Sec. VI.C.

Appendix B

Lyapunov Stability

(i) Let $v(x):\Re^n \rightarrow R$ be a continuous function with continuous first partial derivatives. If $v(x)$ is positive definite, i.e. $v(0)=0$ and $v(x)>0$ for $x \neq 0$ then $v(x)$ is a Lyapunov function candidate.

(ii) Consider the nonlinear system

$$\dot{x} = f(x) \tag{B.1}$$

where $x \in \Re^n$ and suppose $f(0)=0$. Then the origin of $\Re^n$ is said to be the equilibrium point of (B.1). The null solution of (B.1) is asymptotically stable if there exists a Lyapunov function candidate $v(x)$ such that $\dot{v}(x)$ is strictly negative definite along solutions of (B.1), i.e.

$$\dot{v}(x) < 0 \quad , \quad \dot{v}(x) = 0 \quad at \quad x = 0 \tag{B.2}$$

The strict inequality of (B.2) implies that $v(x)$ is decreasing along all solutions of (B.1) leading all trajectories to the equilibrium.

(iii) Local asymptotic stability occurs when a Lyapunov function candidate is found for (B.1) and $\dot{v}(x) < 0$ holds as long as $\|x(0)\| < B$ where B defines the region of attraction.

(iv) **Lasalle's Theorem**: For the system (B.1) a Lyapunov function candidate is found such that the derivative of $v(x)$ is negative semi-definite for all solution trajectories. Then (B.1) is asymptotically stable if the only invariant set for $\dot{v}(x) \equiv 0$ is $x = 0$.

Barbalat's Lemma

If $h(t)$ is a uniformly continuous function such that $\lim_{t\to\infty} \int_0^t h(t)\,dt < \infty$ then $h(t) \to 0$ as $t \to \infty$. **Corollary:** If $g, \dot{g} \in L_\infty$ and $g \in L_p$ for some $p \in [1, \infty)$ then $g(t) \to 0$ as $t \to \infty$ [54, pp. 19]

References

[1] C. Delepaut, G.B. and Gevers, M., "Stabilization of Nonlinear Systems by Means of State-Estimate Feedback," in *Proc. IEEE Conference on Decision and Control*, 1989, .

[2] Åström, K.J. and Wittenmark, B., *Adaptive Control*, Reading, MA: Addison-Wesley, 1989.

[3] Huang H.-P. and Tseng W.-L., "Asymptotic Observer Design for Constrained Robot Systems," *IEE Proceedings - D*, vol. 138, pp. 211-216, 1991.

[4] An, C.H., Atkeson, C., and Hollerbach, J.M., "Estimation of Parameters of Rigid Body Links of Manipulators," in *Proc. 24th Conference on Decision and Control*, 1985, pp. 990-95.

[5] Arimoto, S. and Miyazaki, F., "Stability and Robustness of P.I.D. Feedback Control for Robot Manipulators of Sensory Capability," in *Proc. 1st International Symposium on Robotics Research*, 1983, pp. 783-799.

[6] Armstrong, B., Khatib, O., and Burdick, J., "The Explicit Dynamic and Inertial Parameters of the PUMA 560 Arm," in *Proc. IEEE International Conference on Robotics and Automation*, 1986, pp. 510-518.

[7] Asada, H. and Slotine, J.-J.E., *Robot Analysis and Control*, Wiley Interscience, 1986.

[8] Bejczy, A.K., "Robot Arm Dynamics and Control," JPL, California Institute of Technology, 1974.

[9] Belanger, P.R., "Estimation of Angular Velocity and Acceleration from Shaft Encoder Measurements," in *Proc. IEEE Conference on Robotics and Automation*, 1992, pp. 585-592.

[10] Bestle, D. and Zeitz, M., "Canonical Form Observer Design for Nonlinear Time-Varying Systems," *International Journal of Control*, vol. 38, pp. 419-431, 1983.

[11] Canudas de Wit, C., Åström, K.J., and Fixot, N., "Computed Torque Control via a Nonlinear Observer," *International Journal of Adaptive Control and Signal Processing*, vol. 4, pp. 443-452, 1990.

[12] Canudas de Wit, C. and Slotine, J.-J.E., "Sliding Observers for Robot Manipulators," *Automatica*, vol. 27, pp. 859-864, 1991.

[13] Canudas de Wit, C. and Fixot, N., "Robot Control via Robust Estimated State Feedback," *IEEE Transactions on Automatic Control*, vol. 36, pp. 1497-1500, 1991.

[14] Canudas de Wit, C. and Fixot, N., "Adaptive Control of Robot Manipulators via Velocity Estimated Feedback," in *Proc. IEEE International Conference on Robotics and Automation*, 1991, pp. 16-21.

[15] Canudas de Wit, C. and Fixot, N., "Adaptive control of robot manipulators via velocity estimated feedback," in *Proc. IEEE International Conference on Robotics and Automation*, 1991, pp. 16-21.

[16] Canudas de Wit, C., Fixot, N., and Åström, K.J., "Trajectory Tracking in Robot Manipulators via Nonlinear Estimated State Feedback," *IEEE Transactions on Robotics and Automation*, vol. 8, pp. 138-144, 1992.

[17] Craig, J.J., Hsu, P., and Sastry, S.S., "Adaptive Control of Mechanical Manipulators," in *Proc. IEEE International Conference on Robotics and Automation*, 1986, pp. 190-95.

[18] Craig, J.J., *Adaptive Control of Mechanical Manipulators*, Addison-Wesley, 1988.

[19] Craig, J.J., *Introduction to Robotics, Mechanics and Control*, Addison Wesley, 1989.

[20] Erlic, M. and Lu, W.-S., "Computer Independent Driver-Sensor Interface for Closed-Loop Control of a Mechanical Manipulator," in *Proc. Canadian Conference on Electrical and Computer Engineering*, 1989, pp. 504-507.

[21] Erlic, M. and Lu, W.-S., "Manipulator Control with an Exponentially Stable Velocity Observer," in *Proc. The American Control Conference*, 1992, pp. 1241-42.

[22] Erlic, M. and Lu, W.-S., "A Reduced-Order Adaptive Velocity Observer for Manipulator Control," in *Proc. IEEE International Conference on Robotics and Automation*, 1993, pp. 328-333.

[23] Erlic, M. and Lu, W.-S., "A Reduced-Order Adaptive Observer for Manipulator Control," *IEEE Transactions on Robotics and Automation*, 1994.

[24] Fisher, W.D. and Mujtaba, M.S., "Hybrid Position/Force Control: A Correct Formulation," *The International Journal of Robotics Research*, vol. 11, pp. 299-311, 1992.

[25] Hogan, N., "Impedance Control: An Approach to Manipulation: Part I - Theory," *Transactions of ASME, Journal of Dynamic Systems, Measurement and Control*, vol. 107, pp. 1-7, 1985.

[26] Hogan, N., "Impedance Control: an Approach to Manipulation: Part II - Implementation," *Transactions of ASME, Journal of Dynamic Systems, Measurement and Control*, vol. 107, pp. 8-16, 1985.

[27] Hogan, N., "Impedance Control: An Approach to Manipulation: part III - Applications," *Transactions of ASME, Journal of Dynamic Systems, Measurement and Control*, vol. 107, pp. 17-24, 1985.

[28] Hogan, N., "Stable Execution of Contact Tasks using Impedance Control," in *Proc. IEEE International Conference on Robotics and Automation*, 1987, pp. 1047-1053.

[29] Hsia, T.C., "Adaptive Control of Robot Manipulators - A Review," in *Proc. IEEE International Conference on Robotics and Automation*, 1986, pp. 183-189.

[30] Hsu, P., Sastry, S., and Paden, B., "Adaptive identification for manipulators without using joint acceleration," in *Proc. IEEE International Conference on Robotics and Automation*, 1987, pp. 1210-1215.

[31] Inigo, R.M. and Kossey, R.M., "Closed-Loop Control of a Manipulator Arm Using a Wrist Force Sensor," *IEEE Transactions on Industrial Electronics*, vol. IE-34, pp. 371-78, 1987.

[32] Johansson, R., "Adaptive Control of Robot Manipulator Motion," *IEEE Transactions on Robotics and Automation*, vol. 6, pp. 483-90, 1990.

[33] Kailath, T., *Linear Systems*, Englewood Cliffs, N.J., 07632: Prentice-Hall, 1980.

[34] Kalman, R.E., "Design of Self-Optimizing Control Systems," *Trans. ASME*, vol. 80, pp. 468-478, 1958.

[35] Kenjo, T. and Nagamori, S., *Permanent-Magnet and Brushless DC Motors*, Oxford University Press, 1985.

[36] Khosla, P.K. and Kanade, T., "Experimental Evaluation of Nonlinear Feedback and Feedforward Control Schemes for Manipulators," *The International Journal of Robotics Research*, vol. 7, pp. 18-28, 1988.

[37] Koditschek, D.E., "Adaptive Techniques for Mechanical Systems," in *Proc. Proceedings of the Fifth Yale Workshop on Adaptive System Theory*, 1987, pp. 259-265.

[38] Koivo, A.J. and Guo, T.H., "Adaptive Linear Controller for Robotic Manipulators," *IEEE Transactions on Automatic Control*, vol. AC-28, pp. 162-171, 1983.

[39] Kou, R., Elliot, D.L., and Tarn, T.J., "Exponential Observers for Nonlinear Dynamical Systems," *Information and Control*, vol. 29, pp. 204-216, 1975.

[40] Krener, A. and Isidori, A., "Linearization by Output Injection and Nonlinear Observers," *System Control Letters*, vol. 3, pp. 47-52, 1983.

[41] Li, W. and Slotine, J.-J.E., "Indirect Adaptive Robot Control," in *Proc. IEEE International Conference on Robotics and Automation*, 1988, pp. 704-709.

[42] Lu, W.-S., "Linear Robust Control of Mechanical Manipulators," in *Proc. International Symposium on Intelligent Control*, 1988, .

[43] Lu, W.-S. and Meng, Q.H., "Impedance Control with Adaptation for Robotic Manipulations," *IEEE Transactions on Robotics and Automation*, vol. 7, pp. 408-15, 1991.

[44] Luenberger, D.G., "Observing the State of Linear Systems," *IEEE Transactions on Military Electronics*, vol. 8, pp. 74-90, 1964.

[45] Luenberger, G.D., "Observers for Multivariable Systems," *IEEE Transactions on Automatic Control*, pp. 190-197, 1966.

[46] Mo, L. and Bayoumi, M.M., "Hybrid Adaptive Control for Robot Manipulators," *System and Control Letters*, pp. 405-409, 1990.

[47] Nicosia, S. and Tomei, P., "Robot Control by Using Only Position measurement," *IEEE Transaction on Automatic Control*, vol. 35, pp. 1058-1061, 1990.

[48] O'Reilly, J., *Observers for Linear Systems*, Academic Press, 1983.

[49] Ortega, R. and Spong, M.W., "Adaptive Motion Control of Rigid Robots: a Tutorial," in *Proc. 27th Conference on Decision and Control*, 1988, pp. 1575-1584.

[50] Paul, R. and Shimano, B., "Compliance and Control," in *Proc. Proceedings of the Joint Control Conference*, 1976, pp. 694-699.

[51] Raibert, M.H. and Craig, J.J., "Hybrid Position/Force Control of Manipulators," *Journal of Dynamic Systems, Measurement and Control*, vol. 102, pp. 126-133, 1981.

[52] Salcudean, S., "A Globally Convergent Angular Velocity Observer for Rigid Body Motion," *IEEE Transactions on Automatic Control*, vol. 36, pp. 1493-1497, 1991.

[53] Salisbury, J.K., "Active Stiffness Control of a Manipulator in Cartesian Coordinates," in *Proc. 19th International Conference on Decision and Control*, 1980, pp. 95-100.

[54] Sastry, S. and Bodson, M., *Adaptive Control, Stability, Convergence, and Robustness*, Englewood Cliffs, N.J: Prentice Hall , 1989.

[55] Seraji, H., "Decentralized Adaptive Control of Manipulators: Theory, Simulation, and Experimentation," *IEEE Transactions on Robotics and Automation*, vol. 5, pp. 183-201, 1989.

[56] Slotine, J.-J. and Sastry, S.S., "Tracking Control of Nonlinear Systems using Sliding Surfaces, with Applications to Robot Manipulators," *International Journal of Control*, vol. 38, pp. 465-492, 1983.

[57] Slotine, J.-J.E., Hedrick, J.K., and Misawa, E.A., "On Sliding Observers for Nonlinear Systems," *Journal of Dynamic Systems, Measurement, and Control*, vol. 109, pp. 245-252, 1987.

[58] Slotine, J.-J.E. and Li, W., "Adaptive Manipulator Control: A Case Study," *IEEE Transactions on Automatic Control*, vol. 33, pp. 995-1003, 1988.

[59] Spong, M.W. and Vidyasagar, M., "Robust linear Compensator Design for Nonlinear Robotic Control," *IEEE Journal of Robotics and Automation*, vol. RA-3, pp. 345-350, 1987.

[60] Spong, M.W. and Vidyasagar, M., *Robot Dynamics and Control*, New York, NY: John Wiley & Sons, 1989.

[61] Thau, F.E., "Observing the State of Nonlinear Dynamic Systems," *International Journal of Control*, vol. 29, pp. 197-216, 1973.

[62] Tornambe, A., "High-Gain Observers for Nonlinear Systems," *International Journal on Systems Science*, vol. 23, pp. 1475-1489, 1992.

[63] Tornambe, A., "Asymptotic Observers for Nonlinear Systems," *International Journal on Systems Science*, vol. 23, pp. 435-442, 1992.

[64] Umeno, T. and Hori, Y., "Two Degrees of Freedom Controllers for Robust Servomechanism," in *Proc. IEEE International Workshop on Advanced Motion Control*, 1990, pp. 47-56.

[65] Van Der Schaft, A.J., "On Nonlinear Observers," *IEEE Transactions on Automatic Control*, vol. AC-30, pp. 1254-1256, 1985.

[66] Waibel, B.J. and Kazerooni, H., "Theory and Experiments on the Stability of Robot Compliance Control," *IEEE Transactions on Robotics and Automation*, vol. 7, pp. 95-104, 1991.

[67] Walcott, B.L. and Zak, S.H., "Combined Observer-Controller Synthesis for Uncertain Dynamical Systems with Applications," *IEEE Transactions on Systems, Man and Cybernetics*, vol. 18, pp. 88-104, 1988.

[68] Wen, J.T. and Murphy, S., "Stability Analysis and Force Control Problems for Robot Arms," in *Proc. IEEE International Conference on Robotics and Automation*, 1990, pp. 252-57.

[69] Whitaker, H.P., "An Adaptive System for Control of the Dynamic Performance of Aircraft and Spacecraft," *Paper no. 59-100, Institute of the Aeronautical Sciences*, 1959.

[70] Whitney, D.E., "Force Feedback Control of Manipulator Fine Motions," *Transactions of ASME, Journal of Dynamic Systems, Measurement and Control*, pp. 91-97, 1977.

[71] Wu, C.H. and Paul, R.P., "Resolved Motion Force Control of Robot Manipulators," *IEEE Transactions on Systems, Man and Cybernetics*, vol. SMC-12, pp. 389-98, 1982.

[72] Xia, X. and Gao, W., "On Exponential Observers for Nonlinear Systems," *System and Control Letters*, vol. 1, pp. 319-325, 1988.

[73] Zeitz, M., "The Extended Luenberger Observer for Nonlinear Systems," *System and Control Letters*, vol. 9, pp. 147-56, 1987.

[74] Zhu, W., Chen, H., and Zhang, Z., "A Variable Structure Robot Control Algorithm with an Observer," *IEEE Transactions on Robotics and Automation*, vol. 8, pp. 486-492, 1992.

VITA

Surname: Erlic Given Names: Mile

Place of Birth: Tinj, Polace, Croatia Date of Birth: April 12, 1963

Educational Institutions Attended:

Queen's University	1981-1985
University of Victoria	1987-1995

Degrees Awarded:

B.A.Sc. (Honours)	Queen's University	1985
M.A.Sc.	University of Victoria	1992

Honours and Awards:

Science Council of British Columbia G.R.E.A.T Award 1989-1992

Publications:

1. Erlic M. and W.–S Lu, "Computer Independent Driver–Sensor Interface (DSI) for Closed Loop Control of a Mechanical Manipulator," in *Proc. Canadian Conference on Electrical and Computer Engineering,* pp. 504-507, Montreal, PQ, Sept. 1989.

2. Lu, W.–S and M. Erlic, "Robust Motion Control of Manipulators: Design and Experimental Evaluation," in *Proc. Canadian Conference on Electrical & Computer Engineering,* pp. 57-60, Montreal, PQ, Sept. 1989.

3. Erlic, M and W.-S. Lu, "A comparative evaluation of adaptive, robust and classical feedback controllers used in unconstrained trajectory tracking for robot manipulators," in *Proc. 33rd Midwest Symposium on Circuits and Systems*, pp. 661-664, Calgary ALTA., Aug. 1990.

4. Erlic M., K. Jones and W.-S. Lu, "Hardware interface configurations for motion control of the PUMA-560 and Mitsubishi RM-501," in *Proc. 1991 IEEE Pacific Rim Conf.*, pp. 506-509, Victoria B.C., May 1991.

5. Erlic M., "Redundant Manipulator Control: An Overview," poster paper at the. *IRIS-PRECARN First Annual Conference*, Vancouver B.C., June 1991

6. Erlic, M. and Lu, W.-S., "Manipulator Control with an Exponentially Stable Velocity Observer," in *Proc. The American Control Conference*, 1992, pp. 1241-42.

7. Erlic, M., and W.-S. Lu, "Impedance Control Without Using Velocity Measurements," in *Proc. 2nd IEEE Conference on Control Applications*, vol. 2, pp. 47-52, Vancouver, B.C., Sept. 1993.

8. Erlic, M., and W.-S. Lu, "A Reduced-Order Observer for Underwater Manipulators Using Potentiometers for Position Measurement," in *Proc. Oceans '93*, vol. 2, pp. 307-312, Victoria, B.C., Oct. 1993.

9. Erlic, M., and W.-S. Lu, "A Reduced-Order Adaptive Velocity Observer for Manipulator Control," *IEEE Transactions on Robotics and Automation*, vol. 11, pp. 293-303, April 1995.

10. Erlic, M. and W.-S. Lu, "A Reduced-Order Velocity Observer Used in Manipulator Control," submitted to *IEEE Transactions on Systems, Man and Cybernetics*.

PARTIAL COPYRIGHT LICENSE

I hereby grant the right to lend my dissertation to users of the University of Victoria Library, and to make single copies only for such users or in response to a request from the Library of any other university, or similar institution, on its behalf or for one of its users. I further agree that permission for extensive copying of this thesis for scholarly purposes may be granted by me or a member of the University designated by me. It is understood that copying or publication of this thesis for financial gain shall not be allowed without my written permission.

Title of Thesis/Dissertation: Manipulator Control Using Reduced Order Velocity Observers

Author: 

MILE ERLIC

April 10, 1995